An Optimization Framework for Elastomer Machine Tools

Love Montan Larsson

DIVISION OF PRODUCT DEVELOPMENT | DEPARTMENT OF DESIGN SCIENCES
FACULTY OF ENGINEERING LTH | LUND UNIVERSITY
2021

MASTER THESIS

ARPACKAGING

An Optimization Framework for Elastomer Machine Tools

Master Thesis

Love Montan Larsson

LUND
UNIVERSITY

2nd March 2022

An Optimization Framework for Elastomer Machine Tools

Master thesis in mechanical engineering with industrial design

Published by
Department of Design Sciences
Faculty of Engineering LTH, Lund University
P.O. Box 118, SE-221 00 Lund, Sweden

Subject: Degree Project in Technical Design (MMKM10).
Division: Division of Product Development
Supervisor: Joze Tavcar
Co-supervisor: Katarina Elner-Haglund
Examiner: Axel Nordin

Abstract

A framework for optimizing the design of elastomer packaging machine tools, so-called plunge tools, has been developed and has reached a proof-of-concept state in this thesis. The framework indicates the capability of decreasing prototype expenses and total development time of new plunge tools by roughly three times compared to the existing iterative design methodology.

A finite element analysis (FEA) model serves as the core of the framework. Physical experiments based on Design of Experiments (DoE) theory have been conducted to validate the model and, with regression analysis, screen system factors influential on plunge tool performance. The experiments were also useful in detecting large differences in plunge tool performance between the regular plunge tools and the additively manufactured plunge tools currently used as prototypes.

Response surface methodology (RSM) has been used together with the FEA model to optimize the design. An optimal space-filling design point scheme used together with a Kriging interpolation response surface was found to be more capable of predicting the FEA model responses than three other configurations. An optimized plunge design was generated with the framework after roughly 24 hours of computation time on an average desktop computer from 2013. The design had large design similarities to a production design developed with iterative design, but performed even better in the simulation.

Keywords: Polyurethane, Elastomer, packaging industry, Design of Experiments, Finite Element Analysis, Response Surface Methodology, multiple linear regression analysis, Additive Manufacturing.

Sammanfattning

Ett ramverk för att optimera designen av elastomera verktyg som används i förpackningsindustrin, så kallade plungeverktyg, har utvecklats och nått ett koncepttestadie (eng. Proof of Concept) i detta arbete. Ramverket tyder på att kunna sänka nuvarande prototypkostnader och utvecklingstider av nya plungeverktyg tre gånger.

Optimeringsramverket består i grunden av en FEM-analysmodell. FEM-analysmodellen har validerats med fysiska experiment som följer försöksplaneringsteori (Design of Experiments, DoE) och som dessutom varit lags till en regressionsanalys för att spåra de systemfaktorer som påverkar tryckbilden mest. Experimenten var även användbara för att hitta stora skillnader i prestanda mellan normala plungeverktyg och 3D-printade plungeverktyg som för tillfället används som prototyper.

Optimering av plungedesignen har utförts med hjälp av en surrogatmodell (eng. Response Surface Methodology, RSM) av FEM-analysen. 4 olika RSM-konfigurationer testades varpå en med optimal space-filling-schema och en Kriging-interpolationsmodell visade sig vara bättre på att uppskatta FEM-analysens respons. En plungedesign som liknar, och som dessutom i FEM-analysen presterar bättre än, en manuellt optimerad plungedesign, kan på detta sätt tas fram efter cirka 24 timmars beräkningstid med en vanlig stationär dator från 2013.

Nyckelord: Polyuretan, Elastomer, förpackningsindustri, Design of Experiments, finita elementmetoden, Response Surface Methodology, regressionsanalys, additiv tillverkning

Acknowledgements

I would like to express my deepest appreciation to my supervisors Joze Tavcar and Katarina Elner Haglund for their encouragement and patience throughout the duration of this project, and for their valuable experiences, advises, and suggestions.

I would also like to extend my deepest gratitude to Simon Holka, Filippa Melin, Per Hagelqvist, Rikard Kärrbrant, Maria Sioland, Kristoffer Schultz, Marie Mårtensson, and all the other people at AR Packaging Systems for their relentless support, guidance, helpful advises, and contributions to travel expenses and hospitality.

I'm extremely grateful to Roger Nilsson at CA Mätsystem for the experienced contributions to experiments and for offering me a drive from Lund to Stockholm.

I would like to thank Rudolf Abelin and the DDG team at LTH for their great amount of assistance and troubleshooting in IT and software.

I would also like to extend my sincere thanks to Axel Nordin for his stellar experience and assistance in troubleshooting FEA.

Stockholm, December 2021

Love Montan Larsson

Contents

List of Acronyms and Abbreviations

AM - Additive Manufacturing
ANOVA - Analysis of Variance
ARPS - AR Packaging Systems AB
CAD - Computer-Aided Design
DoE - Design of Experiments
FDM - Fused Deposition Modeling
FEA - Finite Element Analysis
FEM - Finite Element Method
MLR - Multiple Linear Regression
PU - Polyurethane
RSM - Response Surface Methodology
QC - Quality control

List of Variables

M_{xx} - Mean value of variable xx
D_{xx} - Maximum deviation value of variable xx
bpd - Bottom plate design
el - Expansion length
$mmax$ - Force reaction measured at 7.0 mm compression in the quality control with a Mecmesin uniaxial test machine
$mslo$ - Slope of measured force reaction at 7.0 mm compression in the quality control with a Mecmesin uniaxial test machine
pd - Plunge design
pla - Plunge lip angle
plw - Plunge lip width
pt - Plunge type
sf - Sensor frame number

sha - Hardness (shore A)
tcc - Transverse carton component
$th1$ - Height 1 deviation
$th2$ - Height 2 deviation
tl - Plunge length deviation
tw - Plunge width deviation
$v1$ - Plunge design 1
$v2$ - Plunge design 2
$v3$ - Plunge design 3

1 Introduction

The press plunge tool, or simply ”plunge”, is central in AR Packaging Systems AB’s (ARPS) packaging production systems for the food industry. It was first invented by Åkerlund & Rausing AB (Dahlin, 1987) and has since been subject to many design progresses and modifications implemented by the spin-out ARPS.

The plunge tool is a radially expandable cup-formed polymer body that holds carton components together in a welding process to create package seals. The welding process utilizes induction heat to melt the components’ plastic laminate layers together. One central and resource-demanding activity in maintaining the function of the plunge tool is to redesign and adapt it to new package formats (commonly referred to as optimization). This process has historically been based on iterative design methodology in which 3 iterations are common and each iteration often takes between 6 and 10 weeks of development time.

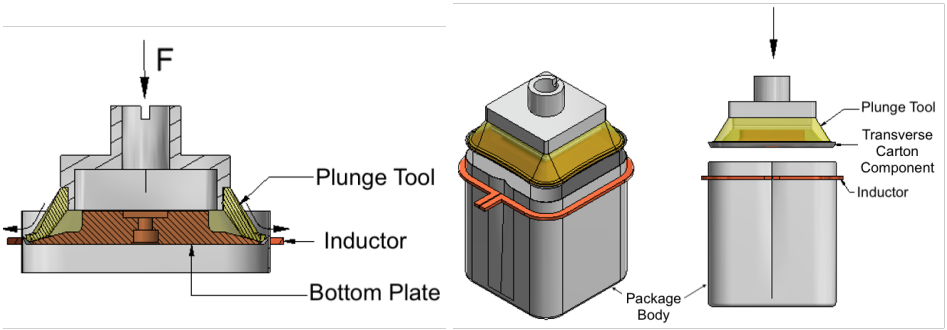

Figure 1.1: Simplified animation of plunge tool, involved package components, and induction coil. (Hagelqvist, 2018)

The aim of this report is to develop an alternative plunge tool adaptation framework with Finite Element Analysis (FEA) and Response Surface Methodology (RSM). The prospect is to enable structural analysis and design exploration at an early stage of the development process while saving time and expenses spent on building physical

prototypes. Physical experiments based on experimental design theory (related to Design of Experiments, DoE), will play a central role in this thesis to validate the FEA and identify influential system factors in the plunge tool operation.

1.1 Purpose

The purpose of developing an alternative plunge tool adaptation framework is to make the process more time and resource-efficient. The development process of the entire packaging solution system can possibly be shortened and enhanced if the framework methods are successful in implementation. The framework will potentially also enable showcasing of finalized package designs earlier in customer relations which potentially can convince more customers to buy products and services from ARPS.

Furthermore, the purpose for me as a student writing this master thesis is to train and test my practical and theoretical engineering experience in a professional setting. This will be the final step of my master of science in engineering degree and the outcome of this project is meant to be shared with readers to spread knowledge.

1.2 Objective

The initial request for the project was stated in a letter as: "To explore if it is possible with tools such as additive manufacturing and FEA, get an understanding of how an initial design of a plunge would function in reality."

As the subject and problem understanding grew and was clarified over the project course, the objectives of the project resulted in:

- Develop an FEA model that adequately can simulate the contact pressure distribution between plunge and package components during the welding mechanism.
- Conduct physical contact pressure distribution experiments with three objectives:
  - Validate the FEA.

  - Screen system factors that influence the plunge tool's performance on the package weld quality.
  - Explore the possibility of using fused deposition modeling (FDM) manufactured plunge tools as prototypes in the development process of polyurethane (PU) plunges.
- Use the FEA model together with response surface methodology (RSM) to develop an initial framework for plunge tool design adaptation (parametric optimization).

1.3 Assumptions

- The contact between plunge lip and carton components can be modeled without carton components and a stiff inductor wall serves as a reaction object instead. The inductor wall is in simulations however protruded the estimated compressed thickness of the equivalent carton components.
- Homogeneous contact pressure distribution between the plunge lip and the inductor wall is optimal in the package welding mechanism. That is, equal pressure magnitude in any area of the contact surface between plunge lip and package.
- Nonexistent vertical shear force between the plunge lip and the inductor wall is optimal.
- The coefficient of friction between the polyurethane plunge and copper bottom plate is 0.4 based on an estimation made by the manufacturer of the polyurethane plunge tools.
- Sliding between carton components in the moment of welding can easily occur due to the surrounding melted PE plastics. Therefore, the coefficient of friction between plunge lip and inductor wall is set low ($\mu = 0.1$) in the FEA.

1.4 Report Structure

This report can be divided into 3 segments:

- Intro Chapters
  - **Introduction**, chapter 1.
  - **Background**, chapter 2. Important information regarding the package solution and plunge expansion mechanism is presented.
- Experimental Chapters
  - **Methodology**, chapter 3. Describes the overall approach and methodologies used in this report.
  - **Contact Pressure Distribution Experiments**, chapter 4. Describes the theories behind and the implementation of the physical experiments.
  - **FEA Model**, chapter 5. Describes how the FEA model was developed.
  - **Indent Optimization**, chapter 6. Contains a summary of used RSM theory and description of an initial implementation of RSM in which three design parameters of a plunge tool are optimized.
  - **Results**, chapter 7. Results from chapters 4, 5, and 6.
- Ending Chapters
  - **Discussion**, chapter 8. Discussion of the methodologies and results. Assessment of meeting the objectives.
  - **Conclusions**, chapter 9. Overall project conclusions.
  - **Further Recommendations**, chapter 10.

2 Background

In this chapter, necessary information regarding the Boardio package, the plunge tool, and the existing plunge tool adaptation process will be described.

2.1 Company Description

ARPS are specialized in developing packaging solutions to the global food industry. Cekacan, Boardio, and Sealio are brands and packaging solutions developed together with their production systems at the headquarters in Lund, Sweden.

The package solution is delivered to customers as flat ready-cut and transportation efficient cartons together with their packaging system. The packages are then assembled in the packaging system on-premise.

2.2 Boardio Package

A focus on plunge tools used in the manufacturing of Boardio packages has been kept in this thesis. The research is however expected to be applicable to other packaging solutions as well. The Boardio packaging solution is ARPS latest addition to their product line. It is designed with lower plastic usage, a low carbon footprint, and a high barrier in mind. The barrier level specifies how well the package can protect its content from external environmental factors. Due to the laminate composition and the tight seals, the Boardio package is designed to ensure a gas-tight barrier if requested by the customer.

2.2.1 Format Parameters

The packaging system has been developed to be adaptable to many different package formats (dimensions). Many customers order a unique format that goes well with their product and brand. Hence, many of the package system components, including the plunge, have to be adapted to the new format.

Only the rectangular Boardio packages will be studied in this report. That is, packages with a cross-section shaped like a rectangle, although they always have rounded corners and might have rounded long and/or short sides. The design and performance of the plunge is heavily dependent on the cross-section package format parameters. They are: package length and width, and the radii of the corners, short, and long sides. All of them can be found in Figure 2.4.

2.2.2 Components

A Boardio package typically consists of five components as shown in Figure 2.1. Depending on what product to be contained in the package and what is desired by the customer, different components can be used for different types of functionalities.

Figure 2.1: The initial components of a Boardio package before assembly and after assembly. The components are: 1. Tape. 2. Body. 3. Assembled package. 4. Toplid. 5. Membrane 6. Base.

The carton components consist of multiple materials that are layered in a laminate structure. Unique properties and functionalities can this way be obtained for each component of the package. The PU plunge tool is designed to assemble three types of transverse carton components. They have specified thicknesses between roughly 450 µm and 600 µm and slightly different amounts of welding plastics (polyethylene, PE) in them.

2.3 Plunge Tool

2.3.1 Plunge Expansion Mechanism

The plunge tool is utilized to create package seals in a mechanism visualized in Figure 2.2. A large portion of the project focus will be kept on this mechanism. From here on it will be called the ”plunge expansion mechanism”. The cycle time for the mechanism is roughly 1 second.

The mechanism is driven mainly by vertical actuators that sequentially displace the involved machine and carton components to different heights. One of the actuations pushes the relatively soft plunge tool into the bottom plate so that it radially expands. The radial expansion of the plunge creates a pushing force on the carton components to be assembled. At the same moment, heat is induced in the aluminium layers of the laminates from a local magnetic field created by an inductor in the inductor wall. The heat melts the plastic layers of the laminates to create a weld. The force has to be sufficiently strong and correctly directed along the entire circumference to create a high-quality seal.

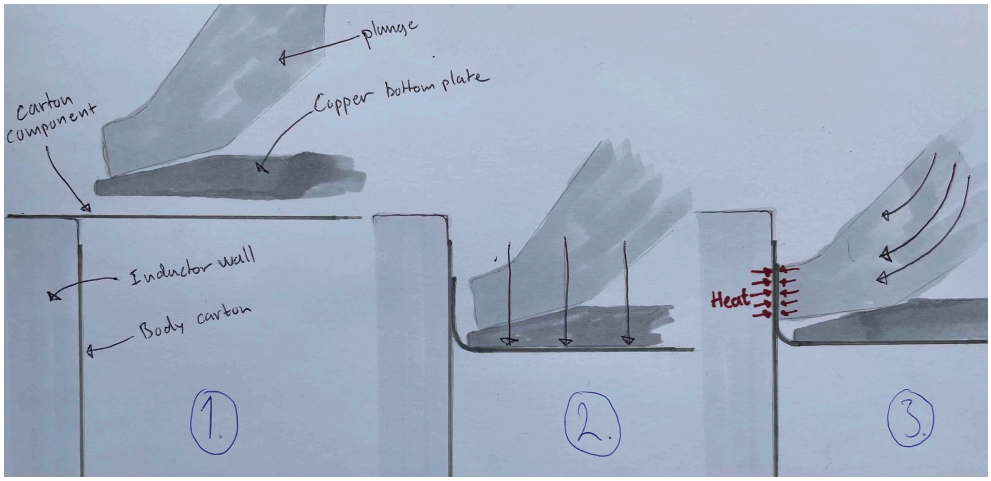

Figure 2.2: Sketched animation of plunge expansion mechanism in a cross-section perspective.

2.3.2 Material Properties

The plunge tools under study in this report are manufactured in a polyether polyurethane material. The plunge tools are heat-compression molded to attain high production quality.

Hardness and Stiffness The material has a specified Shore A hardness of $M_{sha}°$. Shore A hardness denotes the stiffness of a rubber vulcanizate and gives an indirect measure of the elastic properties of the material (Austrell, 1997, p.6). It is measured with an indentation test with a conical tip on the surface of the material.

Experimental Material Data Experimental material data was given for this particular PU material from its manufacturer. The test data was obtained from two ISO-standard tests intended for rubber, vulcanized, and thermoplastic elastomers. The first one is ISO 37, a uniaxial tension test, and the second one is ISO 7743, a uniaxial compression test. The experimental data points are composed in Figure 2.3. Negative elongation corresponds to the data obtained from the compression material test. The data points clearly indicate a nonlinear stress-strain relationship. The most extreme strain levels in a plunge under normal operation are unknown. The FEA model reported equivalent von Mises strains up to 30-50%.

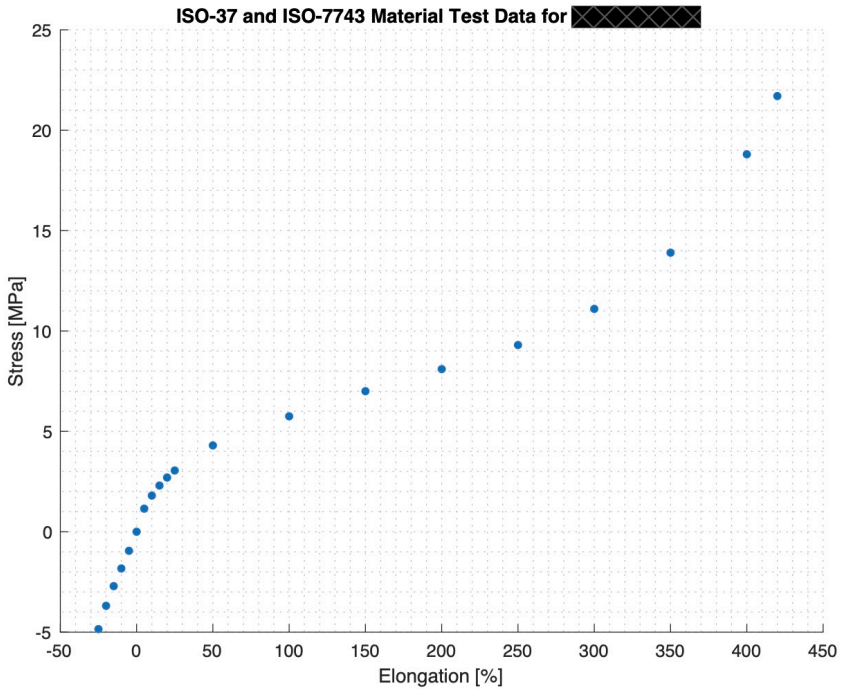

Figure 2.3: Material test data for the PU material. Negative elongation data points are taken from an ISO 7743 test and the positive data points from a ISO 37 test.

The manufacturer describes the mechanical properties of this particular PU material as highly abrasion and fatigue resistant. Plunge units manufactured in this material are expected to withstand several hundred of thousands of cycles. The manufacturer also specified a Poisson's ratio of $\upsilon = 0.499$ which indicates nearly incompressible behavior. Furthermore, the company estimated the coefficient of friction between the material and dry metal surfaces, such as the copper bottom plate in this case, to be between 0.4 and 0.5 at high loads and roughly 0.2 in unloaded cases.

2.3.3 Quality Control

Each plunge batch from the manufacturer undergoes a quality control in which important plunge tool dimensions are controlled, the shore A hardness is measured and a stiffness assessment test is conducted. Stiffness differences between plunge units or between batches have been noticed by ARPS in this test. A Mecmesin uniaxial compression and tension machine is used in this test to compress the plunge unit understudy in a fashion similar to the plunge expansion mechanism in production. The vertical force reaction at a specific expansion length is measured and used as a reference for the overall stiffness of the plunge unit under study. This reference value, from here on denoted as $mmax$, is mainly used to assess plunge units' capability of coping with folds of the transverse carton component appearing in the package welds.

According to quality controls carried out by ARPS with a hardness durometer on plunge units, the measured value can deviate with $\pm D_{sha}°$. However, ARPS points out that this test could be subject to error since it does not fully follow ISO standards due to missing flat surfaces on most plunge tools.

Furthermore, it is believed that the manufacturing method of the plunge tools, especially due to the vulcanization process, can create internal stresses and locally different material properties of the detail.

2.4 Producing a Sufficient Weld

The methodology of adapting plunges to new formats has been developed since the late 1980s within ARPS to its current state. This methodology consists mainly of iterative design with empirical trial-and-error testing until sufficient performance is obtained.

Although the company knowledge and understanding of designing plunge tools have reached a high level (1 design iteration was often enough), the introduction of the new Boardio product raised the requirements on the plunge tool performance. That is partly due to the less amount of PE plastics used for welding in the carton laminates and secondly, due to the more demanding gas-tight barrier of the package that requires exceptional welds and more specific plunge lip pressure distribution. Up to 3 design iterations are often needed for Boardio-related plunge tools which can add up to roughly 30 weeks of development time.

2.4.1 Pressure Distribution

This report is based on an assumption that homogeneous pressure distribution is optimal. Historically, most pressure distribution-related internal research has focused on increasing the corner pressure. The corner pressure has been challenging to attain. Partly because of the plunge design that is bulkier in the corners which causes less deformation as observed in research by Flodberg, Friberg et al. (n.d.[b]). Several methods to increase the plunge lip pressure in corners have been proposed and tested in Flodberg, Eriksson et al. (n.d.[a],[b],[c]) and Flodberg, Friberg et al. (n.d.[a]). Methods such as radially extruding the plunge corners, raising the bottom plate corners, applying anti-friction coating on the bottom plate and the plunge, decreasing the lip height in the corners, and removing material in the corners of the plunge. None of the methods are used today however. Instead, the indenting method as discussed in this report and described in the next section, has been found to be a more successful method in terms of implementation.

2.4.2 Indentation Method

The indentation method can be utilized to increase or decrease the pressure at certain regions. Homogeneous pressure distribution can potentially be obtained by setting suitable indent values. It involves indenting the plunge lip radially at certain regions of the circumference. There are currently three indent design parameters in the CAD design that ARPS adjusts iteratively until consistent satisfactory package welds are obtained. One of them is equivalent to the difference between the format and plunge corner radii. The other two are located on the short and long sides respectively.

The indents of the bottom plate is most often chosen 0.5 mm smaller than the indent values of the plunge.

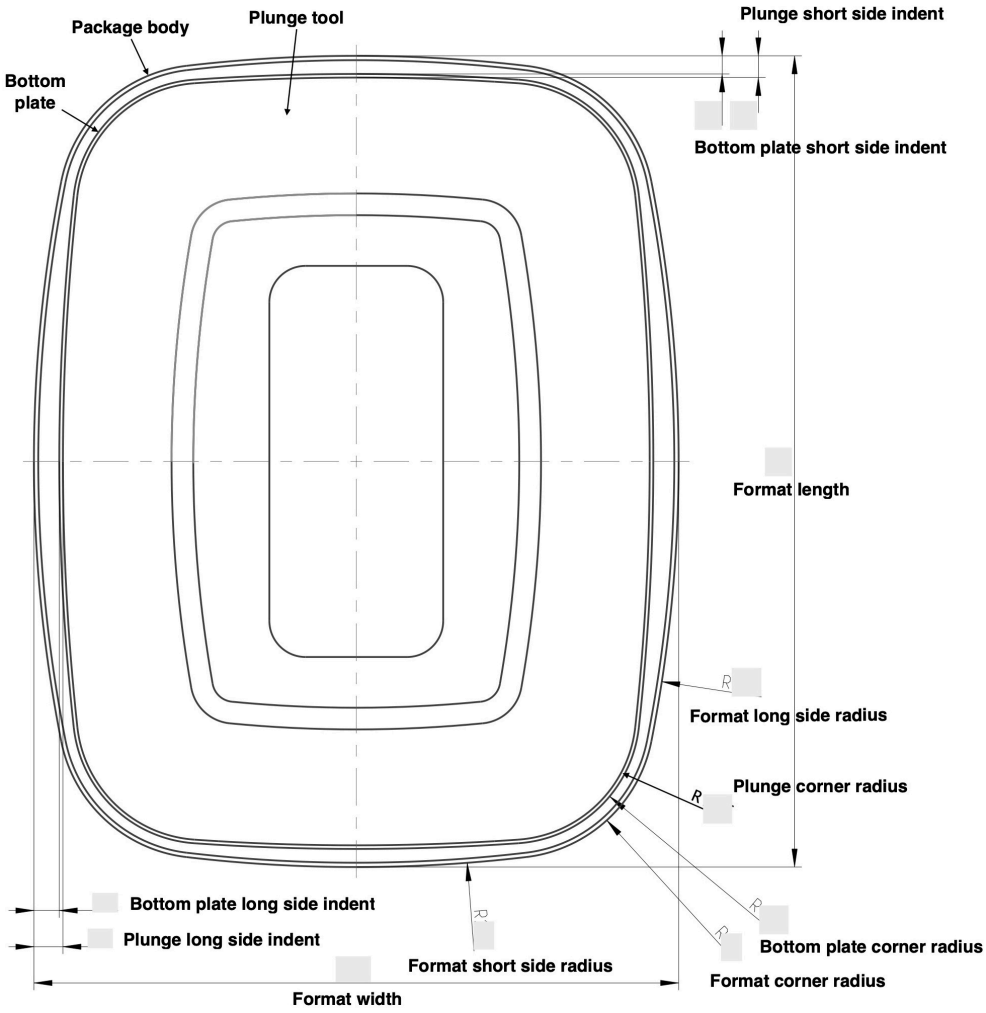

Figure 2.4: View from above of a common Boardio package body carton, bottom plate, and PU plunge with important design parameters.

2.4.3 Package Welding Failure Modes

The indentation method has been observed effective in influencing the quality of Boardio package seals, but it comes with a few complications. The possible failure modes that can occur in the plunge expansion mechanism are described below together with their probable cause. They have been empirically observed by ARPS.

Too Small Indents The gap between the inductor wall and the bottom plate or the plunge tool needs to be no smaller than 2 mm in order to avoid package body impact when the plunge is lowered into the package. This value has been empirically discovered by the company and is used as a design guideline for the plunge. Furthermore, for packages with flat short sides, the body carton occasionally tends to create inward nose tips (see figure 1.1) which demand a further indented plunge and bottom plate in that region.

Low Corner Pressure The transverse carton components develops folds in the package seal when lowered into the package body, especially in the corners of the package. Air channels can easily emerge in these folds. The air channels are unacceptable when creating a gas-tight seal. If the plunge induce sufficiently high pressure onto the weld (especially in the corners), the folds can be flattened or squeezed enough so that the plastic laminate layers are fused together and create a high-quality weld.

Excessive Corner Pressure Due to this relatively pointy pressure peak, protrusions can be visible on the outside of the finished package which is aesthetically unacceptable. It has also been observed that this type of pressure peak can result in internal stresses in the package that cause the final package dimensions to deviate.

Low Pressure on Sides Usually, fewer folds develop along the more gently curved sides than in the corner. It is however equally important to have sufficiently high pressure on the sides to compensate for these folds.

Excessive Pressure on Sides The melted plastic laminate layers of the carton components can be squeezed away if the plunge produce excessive lip pressure. Consequently, the induced current in the aluminum laminate layers of the package components can be shortcircuited. Sparks have been observed in such cases.

Excessive Side Indents The plunge lip tends to bend upward during the end of the expansion mechanism, especially if the indent is large at any point along the circumference. This can cause the plunge lip to hit the transverse carton with vertical misalignment and create a thin weld height. As a result, the weld becomes extra sensitive to internal gas pressure (creep failure) which can occur in certain product cases.

3 Methodology

This chapter broadly presents the methodologies used in this project. The following chapters 4, 5, and 6 contain more thorough explanations of how these methodologies were implemented. The combined methodologies used in this project are visualized in Chart 3.1.

Different research areas, activities, and methodologies, with the common objective to enhance the process of adapting plunge tools to new package formats, were discussed together with APRS and the supervisors at an early stage of the project. Time and resources were considered limiting factors and a prioritization list of activities was developed. This list can be found in the appendices (A.1).

3.1 Creating a Validated FEA

Developing an FEA model was decided as the highest prioritized activity. The majority of the initial project focus was put on developing this model and planning experiments to validate it. The initial aim was to shape the FEA and the experiments as similar to each other as possible so that the expected few remaining uncertainties in the FEA could be detected and calibrated.

The number of considered sources of error grew when the FEA model and the validation experiments began to take shape. These were errors related both to the experiment and the FEA. For instance, the effect of using an inaccurate PU constitutive model or an inaccurate coefficient of friction between the plunge and the bottom plate was unknown. Furthermore, the many types of experimental errors in a physical experiment can be crucial to the usability of the experimental results if not controlled or considered.

The need for an objective experimental methodology to ensure some degree of valid-

ity in the physical experimentation results grew. Thereupon, more research was addressed on experimental design. It is presented in chapter 4.

In addition, sequential testing of different FEA settings was performed to further quantify the uncertainties in the FEA model. They are presented in chapter 5. The computer activities related to developing the FEA are coloured blue in the flowchart 3.1.

3.2 Measuring Other System Factors

Additional use of the experiments was discovered when the sources of error could be quantified. To this point, the indentation method's effect on package welding quality was of the largest interest to be evaluated. The effect of other system factors that are present under production circumstances was not questioned as much. Examples of such factors are dimensional deviations and material-related variances in the plunge tool. Quality control (QC) data on individual plunge units have been used in Analysis of Variance (ANOVA) tests and a regression analysis to quantify the significance of these factors. The activities related to the experiments are orange-colored in the flowchart 3.1and presented in chapter 4.

3.3 Using the FEA

When the FEA had taken its final shape, an RSM framework could be developed and tested. Chapter 6 presents how RSM has been used to optimize the plunge indent design parameters. Activities related to RSM are colored red in the project flowchart 3.1.

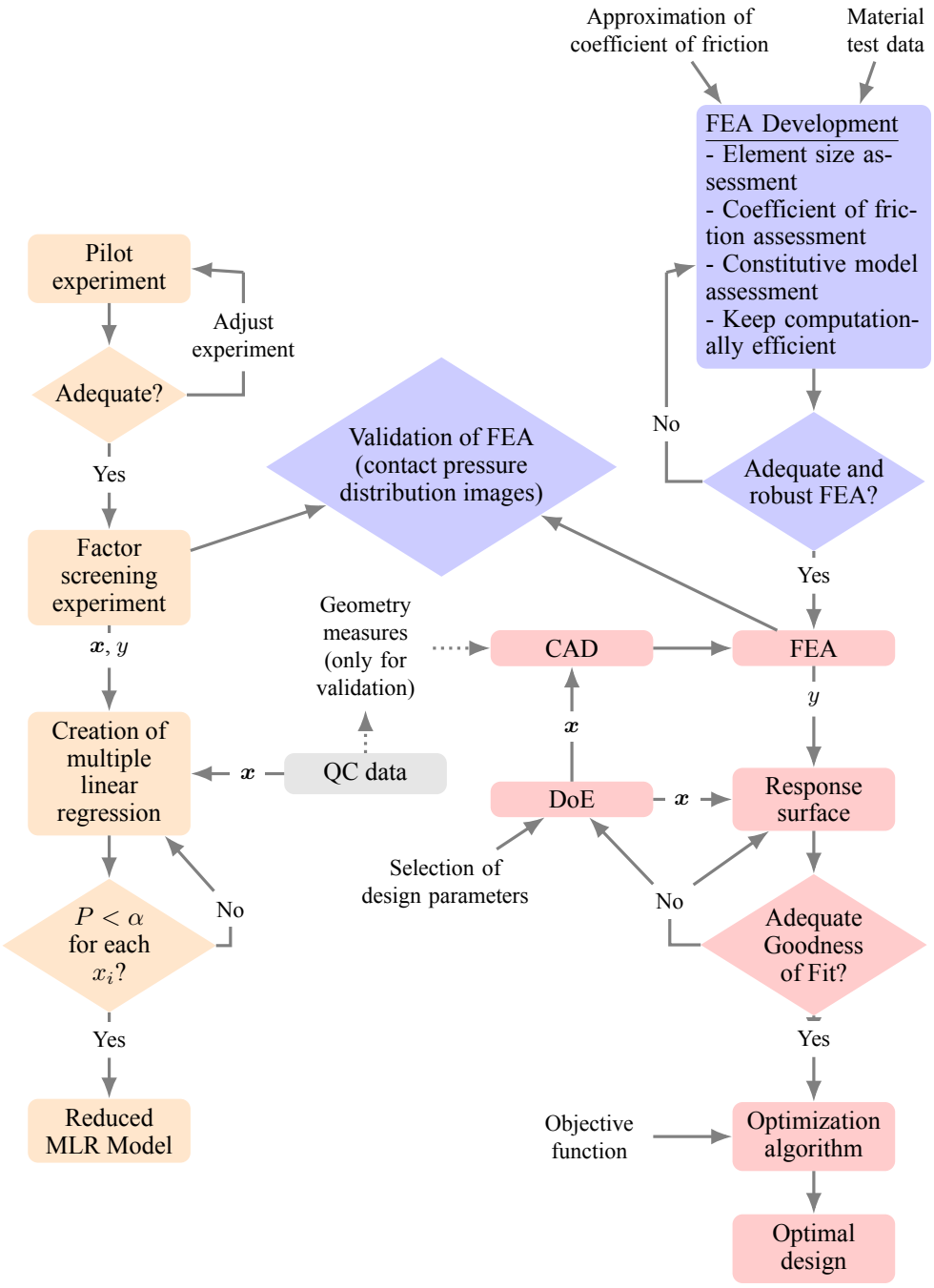

Figure 3.1: Project Flowchart.

4 Contact Pressure Distribution Experiments

In this chapter, the procedure of and the theory behind the contact pressure distribution experiments will be described.

The experiments took place between the 5th and 6th October at the ARPS research lab in Lund together with the company that resells the contact pressure measurement equipment, CA Mätsystem. The theory and implementation of experimental design used in this report is extensively based on the book ”Design and Analysis of Experiments” written by Montgomery (2013) and its preceding article on the same topic Coleman and Montgomery, 1993. The experiments will be described more in detail in sections 4.1 to 4.4.

4.1 Test Rig

The experiments were intended to realistically resemble the plunge expansion mechanism under production circumstances, and to be similarly reproducible in an FEA model. Since a production machine could not be used for the experiments, a similar machine with similar components and mechanisms was used. A tactile sensor, hereafter referred to as a pressure distribution sensor or just sensor, was attached to the test rig to enable measurement of the pressure distribution on the package components caused by the plunge. The test rig components are shown in Figure 4.1.

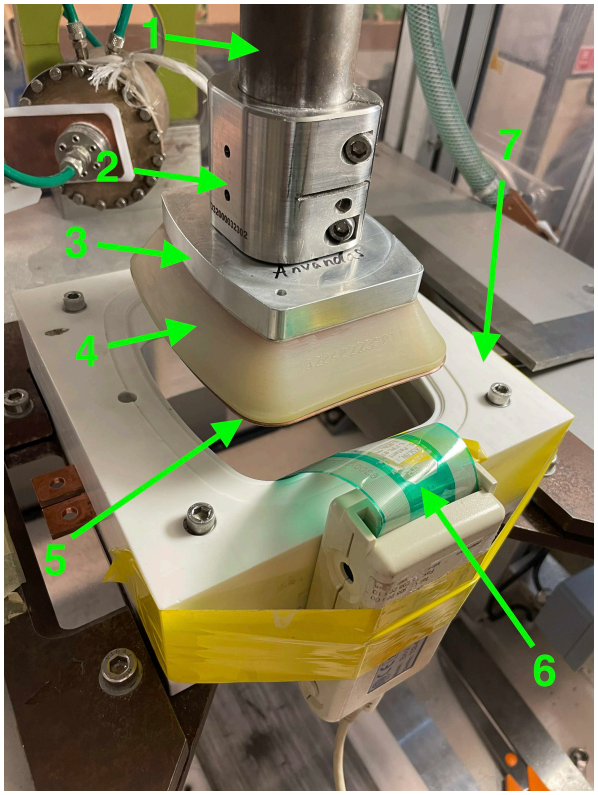

Figure 4.1: The plunge expansion machine with associated components: 1. External servo arm connected to plunge. 2. Adaptor. 3. Aluminum part of plunge. 4. PU part of plunge. 5. Copper bottom plate connected to an internal servo arm. 6. Pressure distribution sensor connector. 7. Inductor wall.

The sensor was attached to the inductor wall as seen in Figure 4.2. The attached layers were, starting from the inductor wall: one layer of 25 mm wide double-sided carpet tape, the sensor film, one additional layer of carpet tape, and then finally a body carton layer. The total thickness added up to roughly 0.9 mm.

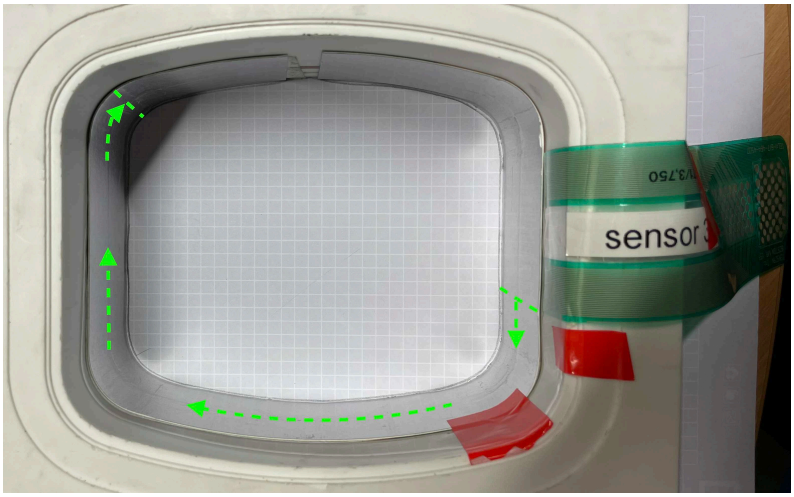

Figure 4.2: Close-up picture of inductor wall and attached sensor and one layer of carton. The green markers and arrows correlate to sensor measurement area and direction of reading columns.

4.1.1 Pressure Distribution Sensor

The I-SCAN 6300 pressure distribution sensor is manufactured by Tekscan. It consists of a semiconducting force-sensing matrix of ”sencells” measuring 33.5 mm (44 sencells) in height and 264.2 mm (52 sencells) in width. The construction of the sensor is shown in Figure 4.3. The normal pressure on a sencell is calculated by the connected computer software by dividing each sencell’s force reading (in the normal direction) with its corresponding area. All sencell’s pressure values were recorded with 100 Hz frame rate and later exported for data analysis. The sensor software was programmed to record 250 frames starting when any sencell’s pressure reading exceeds a threshold value of 0.1 MPa.

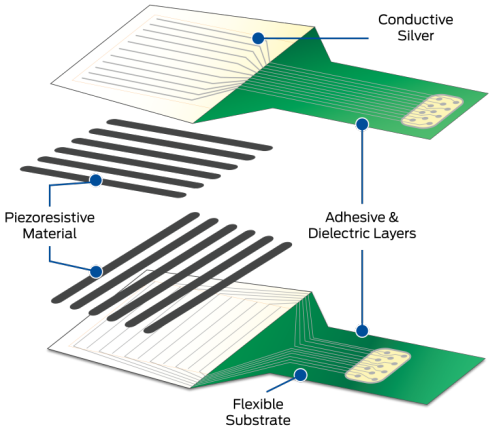

Figure 4.3: Tekscan sensor contruction. (Tekscan, n.d.)

An example of a pressure distribution image from the experiments is given in Figure 4.4. The figure also indicates which segment of the plunge the different segments of the image corresponds to. Due to the size and placement of the sensor, as shown in Figure 4.2, the entire plunge circumference was not recorded.

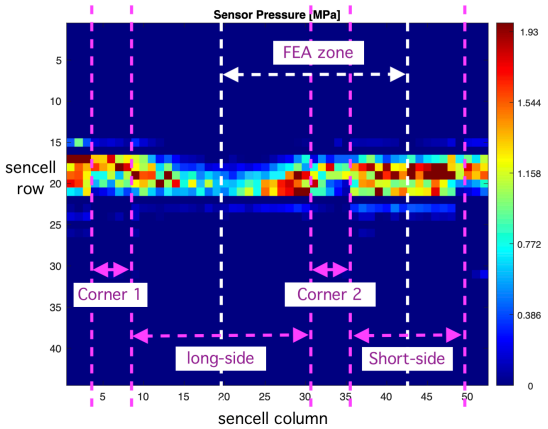

Figure 4.4: Example of pressure distribution image recorded in factor screening experiment in section 4.4. Pink arrows indicate different segments of the plunge lip. White arrow indicates the corresponding zone that the FEA produces results of, but here mirror-inverted.

4.1.2 Test Material

Plunge Units 34 PU plunges of the 140x120 format were available for the experiments. They were of three designs with different design indents. Four with design version 1, four with design version 2, and twenty-six with design version 3. Furthermore, four FDM manufactured plunge units existed, one of each design version and a fourth of an unknown design.

Bottom Plates Four copper bottom plates were accessible for the 140x120 format, one belonging to each of the three plunge designs and one called ”straight”. The bottom plates corresponding to plunge designs are radially extended 0.5 mm along the circumference of the respective plunge design. The straight bottom plate has a constant gap to the inductor wall of 2.0 mm.

Base Carton In production, two layers of carton are pressed between the inductor wall and the radially expanded plunge during welding. That is, one layer of body carton, and one layer of the transverse carton component. The latter one is corrugated in the expansion mechanism which causes randomly located carton folds, especially in the corners (see Figure 4.6b). The folds produce high contact pressure concentrations with little regularity in both placement and magnitude. This was seen as a disturbance when measuring pressure distribution purely contributed by the plunge. Hence, most experiments were conducted without a transverse carton component, except the experiment described in section 4.5.

4.2 Experimental Design

Experimental design is an effective and scientific way of studying and understanding a system or process with statistical methods. It was developed during the 20^{th} century and has today become widely established in science and engineering in a range of industries partly due to the increased availability of computational resources. By conducting systematic experiments and statistical analysis, valid and objective conclusions about how input factors are related to the observed changes in the output response can be drawn. Furthermore, whenever the experimental data is subject to experimental errors, statistical methods are the only objective approach to analysis (Montgomery, 2013, p. 11). The general guidelines for designing an experiment are

1. Recognition of and statement of the problem
2. Selection of the response variable [a]
3. Choice of factors, levels, ranges, and experimental design [a]
4. Performing the experiment
5. Statistical analysis of the data
6. Conclusions and recommendations

[a] In practice, steps 2 and 3 are often done simultaneously or in reverse order.

There are three fundamental principles in experimental design. They will be described in the following paragraphs.

Randomization Statistical methods require the experimental data to be independently distributed random variables. This is achieved by randomly allocating the experiment material and randomizing the order in which the experiment runs are conducted. Randomization also contributes to ”averaging out” extraneous factors that may be present during the experiments.

Replication Replication is the concept of independently repeating runs with the same treatment (input factor combination). For example, if the experimenter wants to assess the differences in response from two different samples (e.g. two different plunge designs) and n copies (plunge units) of each sample are used randomly in the experiment, n replicates are obtained. Firstly, this allows for an estimate of the experimental error, and secondly, the true response y of each sample is more accurately estimated by using the sample mean

$$\bar{y} = \frac{1}{n} \sum_{i=1}^{n} y_i \tag{4.1}$$

Blocking Blocking is used to reduce or eliminate the response variability caused by nuisance factors. Those are factors that may affect the response but are not of interest in the experiment. For example, suppose different batches (blocks) have different mean stiffness and we want to eliminate the effect of varying batch stiffness on the response when comparing stiffness between plunge designs. Then we would design the experiment to include one of each plunge design from every batch in our experiment.

4.2.1 Factors, Levels, and Ranges - Foreword

In sections 4.2.2 to 4.2.4, the different input and output factor categories will be described. Each category's respective factors that have been considered in the following experiments will be listed in each category. Some factors are categorized differently dependent on experiment, these are listed again in corresponding experiment sections 4.3 to 4.5.

There are two different types of factors. *Categorical factors* have a finite amount of levels and are often qualitative, meaning extrapolation between factor levels is meaningless. *Continuous parameters* on the other hand, can take any numerical value, often within a specified range.

Categorizing experiment factors, deciding their levels or ranges, and treating them individually before an experiment, are difficult and uncertain processes. It often requires extensive practical and theoretical process knowledge and understanding.

4.2.2 Response Variables

Measuring the performance of a system can be both quantitative and qualitative. In this case, it is qualitative. The quality of the welding between carton components is seen as the ultimate assessment point but at the same time inappropriate as a response of the system on two levels. One being, welding packages require high temperatures exactly where the sensor is placed. The second reason is on a statistical level, even one failed package welding in a thousand is insufficient in production measures and time-wise out of scope to detect in the following experiments.

To be able to compare the responses of different samples, a quantitative response was needed. Two response variables as functions of the pressure distribution data were developed for comparison.

R1 - Variance of Column Means The response variable was calculated as the population variance of the mean of each pressure distribution image column. A low value of this response variable is seen as good and implies little variance between the mean pressure of each column in the horizontal direction. A value of zero means that the mean pressure detected at all columns along the plunge lip is exactly the same, which could imply a perfectly homogeneous pressure distribution. It is calculated as

$$R1 = \frac{1}{n_{cols}} \sum_{j=1}^{n_{cols}} |\mu_j - \mu|^2 \tag{4.2}$$

where

$$\mu = \frac{1}{n_{cols}} \sum_{j=1}^{n_{cols}} \mu_j \tag{4.3}$$

$$\mu_j = \frac{1}{n_{rows}} \sum_{i=1}^{n_{rows}} p_{i,j} \tag{4.4}$$

and where $p_{i,j}$ is the pressure value of the sencell at row i and column j (sencell rows and columns are visible in Figure 4.4).

R2 - Variance of Segment Means This response function is similar to the first one but with the variance being computed between column group means instead. The groups were selected based on their location on the plunge lip. The plunge lip was in this case segmented into 3 segments (visible in Figure 4.4):

$$\begin{aligned}
\mu_{S1} &= \frac{1}{n_{S1}} \sum_{j \in S1}^{n_{S1}} \mu_j \quad S1 = \{4 \text{ to } 8, 31 \text{ to } 35, 49 \text{ to } 52\} \quad \text{(corners)} \\
\mu_{S2} &= \frac{1}{n_{S2}} \sum_{j \in S2}^{n_{S2}} \mu_j \quad S2 = \{1 \text{ to } 3, 36 \text{ to } 48\} \quad \text{(short sides)} \\
\mu_{S3} &= \frac{1}{n_{S3}} \sum_{j \in S3}^{n_{S3}} \mu_j \quad S3 = \{9 \text{ to } 30\} \quad \text{(long side)}
\end{aligned} \tag{4.5}$$

4.2.3 Potential Design Variables

From all thinkable factors that influence the system response, the experimenter has to select which factors are to be studied in particular and that may be varied in the experiment. These factors can be further divided into 3 groups based on their character and what strategy that should be used with them. They are, design factors, held-at-constant factors, and allowed-to-vary factors. The factors that were chosen to be potential design factors in the experiments are found in Table 4.1.

Table 4.1: Controllable potential design factors.

Factor	ID	Type	Levels/range
Plunge design	pd	Categorical	$v1, v2, v3$
Bottom plate design	bpd	Categorical	$v1, v2, v3, straight$
Plunge type	pt	Categorical	PU, FDM
Transverse carton component	tcc	Categorical	$With, without$
Expansion length	el	Continuous	$5 - 10mm$
Sensor frame number	sf	Categorical	#1, #2, ...#250
Mecmesin max value (only in experiment described in section 4.5)	$mmax$	Categorical	$PU : mmax_{low,PU}$, $mmax_{mid,PU}$, $mmax_{high,PU}$, $FDM : mmax_{mid,FDM}$

Design Factors The design factors are the controllable factors, often of the highest interest. These are factors that the experiment mainly is designed to reveal factor influence on the system response about. A combination of different design factor levels are together often called a treatment.

Held-At-Constant Factors The parameters of less interest in a particular experiment may be held constant to avoid confusion with the factors of high interest. These factors may however be used as design factors in other experiments with other objectives.

Most of the first day's work was spent trying to diminish the measurement system's dependency on several disturbing factors. Listed below are experiment-independent held-at-constant factors and their respective strategy to control their effects. Their effect on the system response after being treated, were assumed to be negligible.

- The bottom plate could be installed in two different directions. The same direction was held in all experiments and runs.
- When exchanging plunge between experiment iterations, slight rotational positioning differences might result in completely different pressure distribution measurements. To reduce the effect of this factor, a special adaptor with a rotational and vertical reference point was used. This facilitated repeatable and almost identical positioning of different plunges.

- Coaxial alignment of extruder and inductor wall was obtained by careful installment of the inductor wall with the help of a half-way extruded plunge as reference and feeler gauges.
- Horizontal pressure drops in the pressure distribution images were visible as pixel rows with close-to-zero pressure values at first. This was assumed to be affected by the copper coil in the inductor wall with different stiffness properties and possible misalignment. The problem was resolved by raising the entire plunge expansion mechanism 3 mm above the copper coil.
- The sensor was aligned horizontally by using the inductor wall edge as a reference.
- Little or no pressure at all was detected in the corners initially. That was resolved by reattaching a new sensor and body carton two times with extra notice to avoid air bubbles in the corners and between the layers of tape. One sensor was attached without carpet tape and instead taped to the wall from the outside using thin single-sided tape on the edges of the body carton strip. This however enabled vertical sensor movement between test iterations and carpet tape was therefore used henceforth.

Allowed-To-Vary Factors Factors with estimated relative low influence on the response or that are difficult to control may be allowed to vary. These factors are often related to the experiment materials, for example, unit-to-unit manufacturing differences. Useful measured data on six geometric features (depicted in Figure 4.5) and stiffness and hardness could be taken from the quality controls that ARPS conducts.

The experimenter may rely on randomization to diminish the effect of uncontrollable allowed-to-vary factors. In the following experiments however, these factors' influence on the response were of interest to be assessed. They are found in Table 4.2.

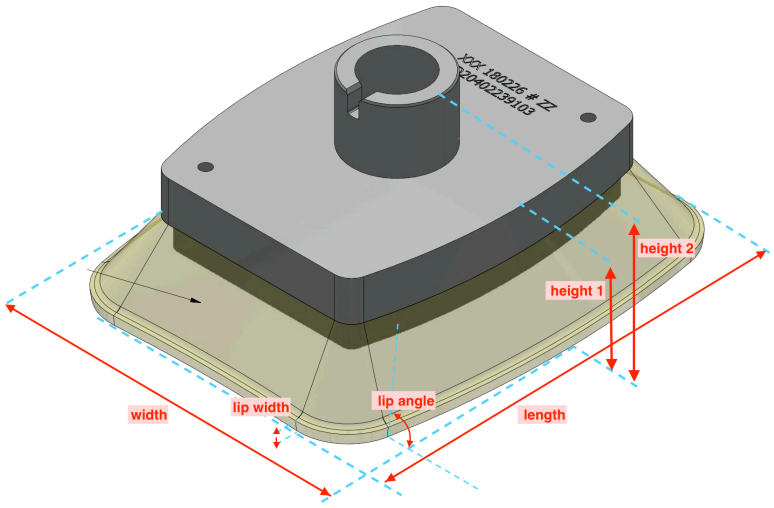

Figure 4.5: Dimensions that are measured in quality control.

Table 4.2: Allowed-To-Vary factors.

Factor	ID	Type	Levels/Range
Height 1 deviation	$th1$	Continuous	$\pm D_{th1} mm$
Height 2 deviation	$th2$	Continuous	$\pm D_{th2} mm$
Width deviation	tw	Continuous	$\pm D_{tw} mm$
Length deviation	tl	Continuous	$\pm D_{tl} mm$
Plunge lip width	plw	Continuous	$M_{plw} \pm D_{plw} mm$
Plunge lip angle	pla	Continuous	$M_{pla} \pm D_{pla}°$
Hardness (shore A)	sha	Continuous	$M_{sha} \pm D_{sha}°$
Mecmesin max value	$mmax$	Continuous	$M_{mmax} \pm D_{mmax} N$
Mecmesin slope value	$mslo$	Continuous	$M_{mslo} \pm D_{mslo} N$

4.2.4 Nuisance Factors

Nuisance factors are unavoidable and are often not of interest. Due to these factors' possible large effect however, they need to be accounted for in ways dependent on their further categorization.

Controllable Factors The controllable nuisance factor levels can be set by the experimenter and their influence on the response is often controlled by using blocking. No such nuisance factors are considered in the following experiments.

Uncontrollable Factors An uncontrollable nuisance factor that can be measured, is often compensated for with a procedure called *analysis of covariance*. The environment temperature is commonly referred to as an uncontrollable but measurable factor and may have a large influence on the response if the system or process is temperature sensitive. No uncontrollable nuisance factors have been considered in the following experiments.

Noise Factors The remaining factors that can not be controlled nor measured are grouped into noise factors. The noise factors that were considered in the following experiments are:

- The sensor is very fragile to shear forces and movements which is why a layer of body carton was kept on the outside of the sensor in all experiments. Persistent damages and thus faulty pressure readings were not detected to a substantial degree. However, accumulated deformations in the body carton layer could have a similar persistent effect.
- The sencells can measure pressure up to 1.93 MPa but are not damaged beyond that. This magnitude was unfortunately recorded at a few senscells in most experiments and hence, eventual exceeding magnitudes were not recorded. ”Cutoff” sencell recordings were detected already at 5.5 mm expansion length. A significant effect on the response was assumed to take place at expansion lengths above 7.0 mm when the pressure distribution images contained a remarkable portion of cutoff sencells.
- The noise level in the sencells pressure readings was ±5% according to CA Mätsystem.
- Possible variances due to the expansion machine and its operation except expansion length were unknown, but also not detected.

4.3 Pilot Experiment

A couple of trial experiment runs and after that, a pilot experiment, were conducted at first. The intention was to increase the chance of sampling useful data in the main experiments, so that the statistical evidence would be more apparent, and so that meaningful insights could be obtained. The yields from the trials and the pilot experiment were:

- The sensors ability to read pressure distributions could be confirmed.
- The usability of the response function applied on the raw data could be evaluated.
- The distributions and variances of design and error factors could be analyzed.
- Unwanted variance in the test rig before the main experiments could be detected and eventually diminished.
- Valuable insights on how the proceeding experiments would be designed could be given.

Most of the strategies to diminish unwanted variance mentioned in section 4.2.3 and 4.2.4 were determined after the trial runs and some of them after the pilot experiment. The experiment conditions could in that way be improved before the main experiments.

This experiment was conducted with two different treatments, two levels of the plunge design factor, v1, and v3. All other potential design factors were held constant, see Table 4.3.

Furthermore, only one plunge unit for each treatment was used. Since all allowed-to-vary factors are dependent solely on the plunge unit, the only factors that remain accountable for the measured variance in response can be assumed to be the plunge design and nuisance factors (the random error).

Table 4.3: Design and held-at-constant factors of the pilot test.

Factor	ID	Type	Used levels/range
Plunge design	pd	Categorical	$v1, v3$
Bottom plate design	bpd	Categorical	$v1$
Plunge type	pt	Categorical	PU
Transverse carton component	tcc	Categorical	$Without$
Expansion length	el	Continuous	$7mm$
Sensor frame number	sf	Categorical	Average of frames #60 - #99

4.3.1 One-Way ANOVA Theory

Suppose that $y_1, y_2, ..., y_n$ represents a sample of response observations. An objective way to test the test rig's ability to detect treatment differences, would be to find conjecture of difference in mean response between the two treatments, $\bar{y}_1$ for the $v1$ plunge design population and $\bar{y}_3$ for the $v3$ plunge design population. A clear difference in-between the treatment means indicates that the experiment is useful in detecting the effect of different treatments. Small variances within treatments indicate relatively low experimental error caused by nuisance factors.

A widely adopted method of comparing the different level responses of a single factor is the one-way ANOVA (analysis of variance). Useful statistical plots and indicators can be obtained from the test results in this method to help the user in deciding whether to reject or failing to reject the null hypothesis H_0 against the alternate hypothesis H_1, denoted as

$$\begin{aligned} H_0 &: \mu_1 = \mu_2 \\ H_1 &: \mu_1 \neq \mu_2 \end{aligned} \tag{4.6}$$

There are two possible errors that may appear when testing these hypotheses. The first one is rejecting the null hypothesis when it is true and the second is failing to reject the null hypothesis when it is false. The probability of these errors are often denoted as

$$\begin{aligned} \alpha &= P(\text{type I error}) = P(\text{reject } H_0 | H_0 \text{ is true}) \\ \beta &= P(\text{type II error}) = P(\text{fail to reject } H_0 | H_0 \text{ is false}) \end{aligned}$$

Usually, a maximum allowable value is set on α before the experiment, a common

limit value is 0.05 and will be used throughout this project. After a level has been selected, most statistical software packages calculate the probability that the test statistic will take on a value more extreme than the observed value of the statistic when the null hypothesis is true. This probability is often called P-value and its exact formulation will not be written here, see Montgomery (2013) for a more thorough explanation. The P-value is then compared to the chosen α-level and if $P < \alpha$, then it is statistically likely that the null hypothesis can be rejected. An alternative interpretation of the P-value is; the smallest level of α at which the data are significant.

The one-way ANOVA test assumes that the observations are obtained independently and completely random, that the data of each factor level have a normal distribution, and that the variances of the treatments are equal.

The response values of the treatments in a randomized experiment can often be assumed to have a normal distribution. The treatment normal distribution $N(\mu, \sigma^2)$ can be estimated with the statistics; sample mean given in equation 4.1 and the sample variance

$$\sigma^2 \approx S^2 = \frac{1}{n-1} \sum_{i=1}^{n} (y_i - \bar{y})^2 \tag{4.7}$$

To verify that the assumptions are met, the normality and equal variance assumptions can be checked with a normal probability plot of the two treatment responses. The normality assumption is verified if the responses resemble two straight lines on the plot. The assumption of equal variances can be expected to be true if the two lines have similar slopes.

The usual statistical indicators calculated in a one-way ANOVA are found in Table 4.4. It is based on analyzing the components of the total variability, which is split into variability in-between treatments and variability within treatments. Variability is here computed as the sum of squares and the total variability can hence be written as $SS_T = SS_{treatments} + SS_E$. The ratio F_0 computed as in equation 4.8 can be compared to a tabular value $F_{\alpha,a-1,N-a}$ that is dependent on the chosen significance level and the number of degrees of freedom. If $F_0 > F_{\alpha,a-1,N-a}$, then it is statistically likely that the treatment means differ and the null hypothesis can be rejected. This is an alternative to using P-values when testing for significance.

Table 4.4: The one-way analysis of variance table.

Source of Variation	Sum of squares	degrees of freedom	Mean square
Between treatments	$SS_{treatments} = n\sum_{i=1}^{a}(\bar{y}_{i.} - \bar{y}_{..})^2$	$a-1$	$MS_{treatments}$
Error (within treatments)	$SS_E = SS_T - SS_{treatments}$	$N-a$	MS_E
Total	$SS_T = \sum_{i=1}^{a}\sum_{j=1}^{n}(\bar{y}_{ij} - \bar{y}_{..})^2$	$N-1$	

where

$$
\begin{aligned}
a &= \text{number of treatments} \\
n &= \text{number of replicates} \\
N &= a * n \\
y_{i.} &= \sum_{j=1}^{n} y_{i,j} \quad \bar{y}_{i.} = y_{i.}/n \quad i = 1,2,\ldots,a \\
y_{..} &= \sum_{i=1}^{a}\sum_{j=1}^{n} y_{ij} \quad \bar{y}_{..} = y_{..}/N
\end{aligned}
$$

$$
F_0 = \frac{MS_{treatments}}{MS_E} \tag{4.8}
$$

4.4 Factor Screening Experiment

Full factorial or fractional factorial experimental designs are common DoE designs and very effective for screening influential factors. They require all factors of high interest to be controllable and were hence not considered convenient in this case. The low amount of plunge units with v1- and v2-designs, and plunge units being FDM-manufactured, was also considered a preventing cause.

An experiment with randomized runs with all available plunges, as mentioned in section 4.1.2, was instead conducted. Multiple linear regression (MLR) was chosen to be modeled on the obtained experimental data to create an empirical model of the

relation between the factors and the response. Low-order regression models are commonly used for creating such empirical models and Montgomery (2013) mentions its frequent use to analyze data from unplanned experiments such as those including multiple uncontrollable factors.

This experiment was conducted with the design and held-at-constant levels in Table 4.5, resulting in 6 different treatments. To compensate for the few FDM manufactured plunges and the v1- and v2-design PU plunges, these were observed with two replications each, unlike the v3-design PU plunges observed only once each. A total of 50 runs were conducted in this experiment, of which 2 runs with the FDM plunge with the unknown design were chosen to be excluded from the modeling. The regression model was modeled with both response variables for comparison.

Table 4.5: Design and held-at-constant factors in factor screening test.

Factor	ID	Type	Used levels/range
Plunge design	pd	Categorical	$v1, v2, v3$
Bottom plate design	bpd	Categorical	$v1$
Plunge type	pt	Categorical	PU, FDM
Transverse carton component	tcc	Categorical	$Without$
Expansion length	el	Continuous	$7mm$
Sensor frame number	sf	Categorical	Average of frames #60 - #99

4.4.1 Multiple Linear Regression Theory

In general, the relationship between a response variable y and a couple of independent so-called *predictors* or *regressor variables* $x_1, x_2, \ldots, x_k$ can be approximated with the mathematical model

$$y = \beta_0 + \beta_1 x_1 + \beta_2 x_2 + \cdots + \beta_k x_k + \epsilon. \tag{4.9}$$

where ϵ is the error. This is called a multiple linear regression (MLR) model due to its linear relation between the response variable y and the unknown regression coefficients β_j, $j = 0, 1, \ldots, k$.

It is also possible to use the MLR technique with more complex models, for example, the equation

$$y = \beta_0 + \beta_1 x_1 + \beta_2 x_2 + \beta_{11} x_1^2 + \beta_{12} x_1 x_2 + \epsilon. \tag{4.10}$$

with the second-order term x_1^2 and *interaction* term x_1x_2. By introducing the linear terms $\beta_3x_3 = \beta_{11}x_1^2$ and $\beta_4x_4 = \beta_{12}x_1x_2$, equation 4.10 can be linearized and usable in a MLR-model with the new form

$$y = \beta_0 + \beta_1x_1 + \beta_2x_2 + \beta_3x_3 + \beta_4x_4 + \epsilon. \tag{4.11}$$

The regression coefficients are often estimated using the least-squares method. Suppose an experiment with $n > k$ observations on the response variable, then the equation 4.9 can be rewritten in matrix form as

$$\mathbf{y} = \mathbf{X}\boldsymbol{\beta} + \boldsymbol{\epsilon} \tag{4.12}$$

where

$$\mathbf{y} = \begin{bmatrix} y_1 \\ y_2 \\ \vdots \\ y_n \end{bmatrix}, \mathbf{X} = \begin{bmatrix} 1 & x_{11} & x_{12} & \dots & x_{1k} \\ 1 & x_{21} & x_{22} & \dots & x_{2k} \\ \vdots & \vdots & \vdots & & \vdots \\ 1 & x_{n1} & x_{n2} & \dots & x_{nk} \end{bmatrix}, \boldsymbol{\beta} = \begin{bmatrix} \beta_0 \\ \beta_1 \\ \vdots \\ \beta_k \end{bmatrix}, \text{and } \boldsymbol{\epsilon} = \begin{bmatrix} \epsilon_0 \\ \epsilon_1 \\ \vdots \\ \epsilon_k \end{bmatrix}. \tag{4.13}$$

The least-squares method chooses estimated regression coefficients $\hat{\boldsymbol{\beta}}$ so that the sum of the squares of the errors ϵ_i, is minimized. It can be shown, as by Montgomery (2013, p.452), that this is satisfied when

$$\hat{\boldsymbol{\beta}} = (\mathbf{X}'\mathbf{X})^{-1}\mathbf{X}'\mathbf{y} \tag{4.14}$$

The equation for the fitted multiple regression model becomes

$$\hat{\mathbf{y}} = \mathbf{X}\hat{\boldsymbol{\beta}}. \tag{4.15}$$

The difference between observed response and corresponding fitted response is called residual and denoted as $e_i = y_i - \hat{y}_1$. The residual sum of square, or often just called *error* of the MLR model becomes $SS_E = \sum_{i=1}^{n} e_i^2 = \mathbf{e}'\mathbf{e}$. The total sum of squares for the model is computed with $SS_T = \sum_{i=1}^{n} e_i^2$ and can be split into the error sum of squares and the model (regression) sum of squares SS_R which is computed with

$$SS_R = \hat{\boldsymbol{\beta}}'\mathbf{X}'\mathbf{y} - \frac{(\sum_{i=1}^{n} y_i)^2}{n} \tag{4.16}$$

The variance σ^2 can be estimated with $\hat{\sigma}^2 = SS_E/(n-k-1)$.

4.4.2 Hypothesis Testing with Multiple Linear Regression

The hypothesis-testing procedure that will be used in this case is called the *extra sum of squares* method. It is used to find out the contribution of an individual or a subset of regression parameters to the model. This is very useful when determining which predictors should be included to create a well-founded model. In contrast to the often used *sequential sum of squares* method, this method produces results independent on occurrence order of predictors in the model and therefore gives more reliable insights. The test requires that the errors in the model have the independent normal distribution $\boldsymbol{\epsilon} \sim NID(0, \sigma^2)$. This can be checked using a normal probability plot of the residuals. If the residuals are scattered unstructured and close to the regression line of this plot, the normality of the experiment data can be assumed. The experimenter should focus on observing the center of the plot. The two other plots, *residuals versus fits*, and *residuals versus order* plots should also be observed, in which unstructured and randomly distributed residuals should be existent.

The hypothesis-testing procedure goes as follows. Consider the regression coefficients being partitioned into two sets:

$$\boldsymbol{\beta} = \begin{bmatrix} \boldsymbol{\beta_1} \\ \boldsymbol{\beta_2} \end{bmatrix} \tag{4.17}$$

where $\boldsymbol{\beta_1}$ is the subset of r coefficients being tested and $\boldsymbol{\beta_2}$ is the rest $k + 1 - r$ regression coefficients. Then a hypothesis-test can be set up as

$$\begin{aligned} H_0 &: \boldsymbol{\beta_1} = \mathbf{0} \\ H_1 &: \boldsymbol{\beta_1} \neq \mathbf{0} \end{aligned} \tag{4.18}$$

in which F_0 can be computed as

$$F_0 = \frac{(SS_R(\boldsymbol{\beta}_1|\boldsymbol{\beta}_2)/r}{SS_E/(n-k-1)} = \frac{(SS_R(\boldsymbol{\beta}) - SS_R(\boldsymbol{\beta_2}))/r}{SS_E/(n-k-1)} \tag{4.19}$$

The numerator can be interpreted as the regression sum of squares of $\boldsymbol{\beta_1}$ given the model

$$\mathbf{y} = \mathbf{X_1}\boldsymbol{\beta_1} + \mathbf{X_2}\boldsymbol{\beta_2} + \boldsymbol{\epsilon}. \tag{4.20}$$

Then F_0 can be compared to a tabular value the same way as in section 4.3.1. If $F_0 > F_{\alpha,r,n-k-1}$, then H_0 can be rejected which implies that it is statistically significant that at least one of the parameters in $\boldsymbol{\beta_1}$ is not zero. Consequently, this means that at least one of the predictors $x_1, x_2, \ldots, x_r$ is contributing significantly to the MLR-model. An ANOVA table with F-value testing for the entire model and each predictor in the model will be presented in 7.2.

4.4.3 Model Adequacy Checking

A common statistical indicator is the R-squared (R^2) value of the model. It can be interpreted as the proportion of the total variability of y derived from the MLR-model and is computed as follows:

$$R^2 = \frac{SS_R}{SS_T} \tag{4.21}$$

Adding more predictors to the model will always result in a higher R^2-value (fit of the data). Hence, the *adjusted* R-squared defined as

$$R^2_{adj} = \frac{SS_R(n-k-1)}{SS_T(n-1)} \tag{4.22}$$

which takes the number of predictors into consideration, is less biased by the amount of predictors. A R^2_{adj} that greatly differs from R^2, probably implies that many insignificant predictors have been added to the model.

Fitting the model to noise instead of the true response (often called signal) is called overfitting and Harrell (2015, p.72) gives a general thumb rule to not exceed the ratio of 1:15 between predictors and the number of observations. Hence, given 48 observations, a model of not more than 3 predictors would be legitimate in this case.

A third useful R-squared is the R^2_{pred} which indicates the predictive capability of the MLR-model. It is defined as

$$R^2_{adj} = 1 - \frac{PRESS}{SS_T} \tag{4.23}$$

where $PRESS$ is the prediction error sum of squares and is calculated by square-summing the $PRESS$ residuals. The ith PRESS residual $e_{(i)}$ is calculated by removing the ith observation from the model, fitting the model to the rest $n-1$ observations to predict the withheld observation $y_{(i)}$, and then taking the difference between these two responses $e_{(i)} = y_i - \hat{y}_{(i)}$. $PRESS$ can then be computed as

$$PRESS = \sum_{i=1}^{n} e^2_{(i)} \tag{4.24}$$

Occasionally, a subset of the data has a disproportionate influence on the model, and in such case, it is important to understand why. For instance, these data points might have been subject to excessive measurement error and the model might resemble the true response better if these ”bad” data points are excluded. Such outliers can be

spotted in the normal probability plot of *standardized residuals* which are computed as

$$d_{ij} = \frac{e_{ij}}{sqrtMS_E} \tag{4.25}$$

If the standardized residuals are normally distributed, 95% of them should fall in-between the ±2 theoretical quantiles. A threshold level for standardized residuals of ±3 is often used to detect outliers.

Outliers can also be detected by computing the hat diagonals h_{ii} found in the hat matrix

$$\mathbf{H} = \mathbf{X}(\mathbf{X}'\mathbf{X})^{-1}\mathbf{X}' \tag{4.26}$$

The hat diagonals h_{ii} may be interpreted as the amount of leverage y_i exerts on $\hat{y}_i$. A useful guideline to identify outliers is to look for $h_{ii} > 3(k+1)/n$ and $h_{ii} > 0.99$ (Minitab, n.d.).

An objective approach that can be useful to test the model's ability to predict response on new data, to detect problems like overfitting or selection bias is the *k-fold cross-validation*. Its algorithm will not be described here but many statistical software packages have functions for it.

Lastly, good process knowledge is valuable in order to evaluate the model approximation of the true response. For instance, the legitimacy of different predictors' influence on the model can in many cases be reasoned out.

4.4.4 Evolution of Regression Model

A first regression model was constructed with the treatment and allowed-to-vary factors mentioned to this point. After analyzing the model adequacy with tools mentioned in the previous section, many alternative models with different sets of predictors and observations could be tested. Both response variables were tested in each model. The most adequate models found will be presented in chapter 7.

4.5 Experiment With Transverse Carton Components

The last experiment that will be addressed is one conducted with transverse carton components included in the plunge expansion mechanism as seen in Figure 4.6. A

new transverse carton component was put in place just as in production, before every expansion. The experiment consisted of 4 different treatments listed in Table 4.6. Three PU plunge units of the v3-design were selected dependent on plunge stiffness. One with a very high $mmax$ value, one average, and one with a very low $mmax$ value. In addition, one v3 FDM plunge with an average stiffness value was included. Thus, the stiffness factor can be considered categorical in this experiment.

The experiment objective was to explore the correlation between plunge stiffness and observed difference in response when including transverse carton components. This could potentially indicate whether stiffness has an impact on treating carton fold-related issues and consequently package seal quality.

(a) Before Expansion.

(b) After Expansion.

Figure 4.6: Experiment conducted with a transverse carton component.

Table 4.6: Design and held-at-constant factors in plunge stiffness assessment experiment.

Factor	ID	Type	Used levels/range
Plunge design	pd	Categorical	$v3$
Bottom plate design	bpd	Categorical	$v1$
Plunge type	pt	Categorical	PU, FDM
Transverse carton component	tcc	Categorical	$With$
Expansion length	el	Continuous	$7mm$
Sensor frame number	sf	Categorical	Average of frames #60 - #99
Mecmesin max value	$mmax$	Categorical	$PU : mmax_{low,PU}, mmax_{mid,PU}, mmax_{high,PU}$, $FDM : mmax_{mid,FDM}$

This experiment is subject to some critical errors related to the experimental design and violations related to the experiment implementation. Hence, the validity and usability of this experiment can be questioned. The results from the experiment will however be presented in chapter 7. The errors are:

- Observations with transverse carton components were noticed to introduce a lot of noise caused by the transverse carton component's random location of folds.
- Only 4 plunge units were used, one for each treatment. Hence, the variability between treatments can be related to any factor, not necessarily plunge stiffness.
- The experiment was conducted without randomization. After conducting the previous experiments, no time-dependent extraneous factor had directly been noticed. To speed up the experiment, each treatment was run sequentially. First the $mmax_{mid,PU}$-plunge, second the $mmax_{high,PU}$-plunge, third the $mmax_{low,PU}$-plunge and finally the $mmax_{mid,FDM}$.
- The transverse carton component folds created pressure peaks well above the sensor pressure limit of 1.93 MPa. This could be concluded after inspecting the early data frames of the sensor recordings. Limit pressure of 1.93 MPa was observed after only a few frames, corresponding to a few millimeters of expansion. Hence, the actual peak pressures could not be recorded at 7 mm and the R1 response is expected to be biased as a result of this.
- One observation was lost in data management.

5 FEA Model

The aim of this section is to present how the FEA was developed and why so. The purpose of the FEA is to adequately represent the real pressure distribution between the package wall and the plunge lip in a plunge expansion mechanism. By fulfilling that, the FEA is intended to be able to predict how prospective plunge designs function in reality. In addition, the FEA is to be used in RSM to optimize the plunge design. Therefore, other factors that are expected to have a large influence on the plunge lip pressure distribution, such as mesh resolution, coefficients of friction, and choice of constitutive (material) model are to be assessed.

Optimally, the FEA model should also be robust, computationally efficient, and reproducible in other commercial FEA software packages in extent to what has been used in this project, ANSYS Workbench 2020 R1.

The software settings used in the following analyses have been chosen based on recommendations from the ANSYS Mechanical documentation (ANSYS Inc., 2017), ANSYS lecture material, ANSYS tutorial videos, ANSYS help forum, other FE community fora and websites, and the writer's subject knowledge retrieved from FE courses taken on the university. Mathematical theories and concepts concerning the finite element method and its modeling technologies, will in general not be elaborated on in this report. Instead, more software-related and procedural terms and descriptions will be used.

5.1 Geometry

The CAD-geometries were developed in ANSYS DesignModeler for its robust and easily managed parametric support with ANSYS Workbench. Different instances of the CAD design, so called design points in ANSYS, can automatically be reproduced by altering design parameter values this way. This is particularly beneficial when

conducting structural RSM optimization where many different geometries have to be simulated.

The plunge expansion mechanism was modeled as a simplified assembly consisting of three components: The PU part of the plunge, the copper bottom plate, and the inductor wall as seen in Figure 5.1. Symmetry was used to scale down the assembly to a quarter for computational efficiency. All results from the FEA in this report correspond only to a quarter of an entire plunge. Vertical force reaction results are however always multiplied with 4 in this report to be easily compared with the practical equivalent $mmax$ obtained from the quality control data conducted by ARPS.

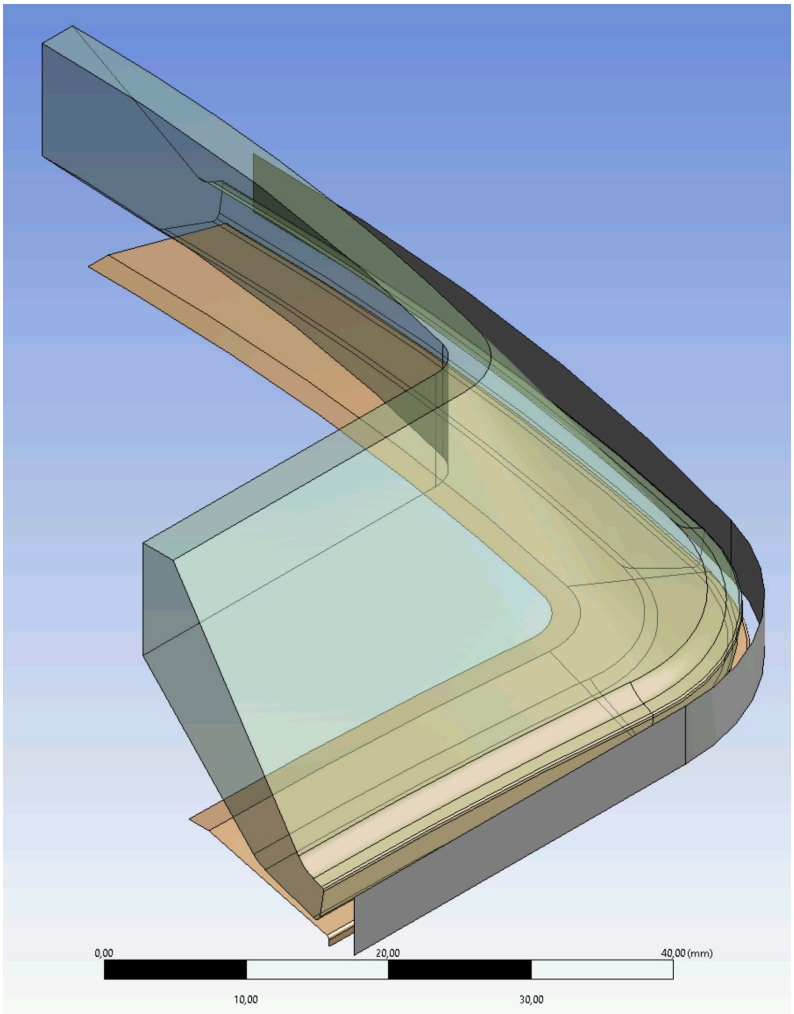

Figure 5.1: FEA geometry from ANSYS DesignModeler.

In reality, the package body blank and the concerned carton component to be welded, are squeezed in-between the inductor wall and the plunge lip as seen in Figure 2.2. To simplify the model and to avoid the complexity of modeling the carton as well, the two layers of carton were assumed to be a 1mm thick part of the inductor wall. Therefore the inductor walls were protruded 1mm.

An initial gap of roughly 0.5mm between plunge and the bottom plate was found useful to avoid overlapping geometries. This was especially occurring when the bottom plate indents were substantially different from the plunge indents, causing a varied gap distance along the plunge circumference.

Further geometrical dimensions are directly taken from drawings provided by ARPS except for three additional corner fillets visible in Figure 5.2. These were added to avoid sharp corners and stress singularities and were assumed to have negligible influence on the accuracy of the results. In fact, similar roundings have been observed in reality due to manufacturing factors and the abrasion taking place in regular operation.

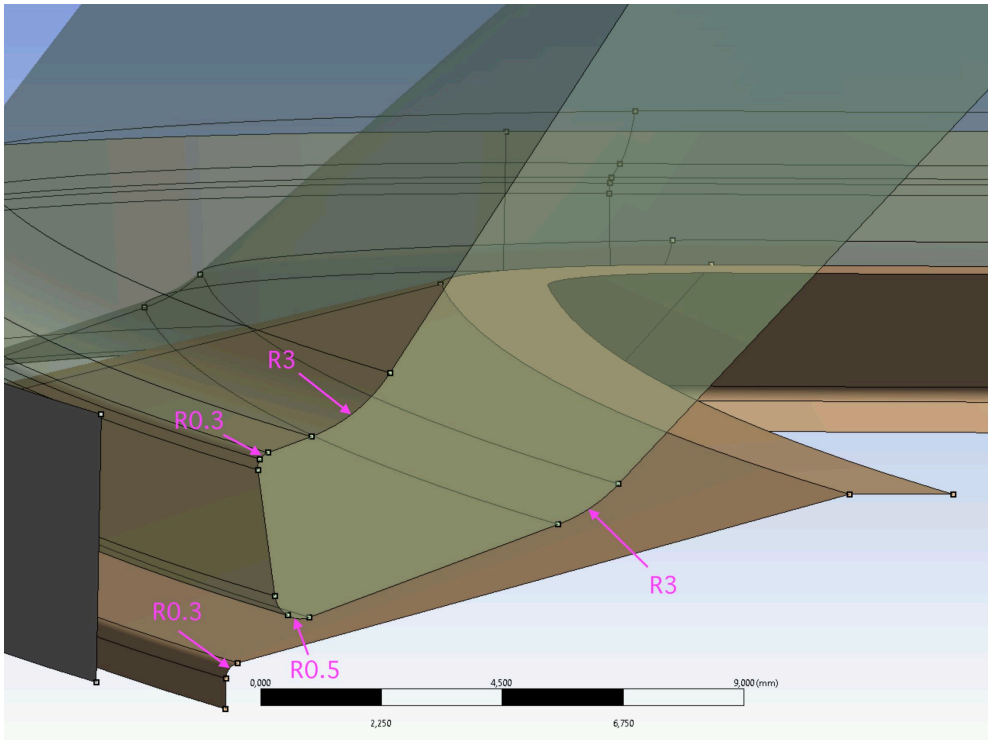

Figure 5.2: Close up of the FEA cross section geometry from ANSYS DesignModeler showing different roundings used in the geometry.

CAD Topology faces and edges were merged where possible and without causing too much geometry distortion. The meshing algorithms used could create smoother meshes with fewer vertices and edge constraints this way. Extra edges were added on the middle of some of the earlier mentioned fillets as seen in Figure 5.2. It was found to help the meshing algorithm create consistent meshes on those fillets.

Deformations in the inductor wall and the copper bottom plate were assumed to be negligible considering the purpose of the FEA and were therefore modeled as thin fixed surfaces for computational efficiency.

5.2 Loads and Boundary Conditions

The inductor wall and the copper bottom plate were assumed to have no displacement and therefore modeled with displacement boundary conditions (see figure 5.3a) set to zero in all degrees of freedom. That practically results in boundary conditions similar to fixed supports. Fixed supports could not be applied to rigid surface bodies in ANSYS.

All faces and edges in contact with the symmetry planes were constrained with frictionless supports (see figure 5.3b), meaning no displacement in the normal degree of freedom.

A displacement in negative y-direction was applied to the upper and inner faces of the plunge to resemble the plunge expansion mechanism. A real expansion length of $7mm$ was modeled as $7.5mm$ displacement distance, taking the initial $0.5mm$ gap between plunge and bottom plate into consideration. A frictionless support was also applied to the inner plunge face as seen in Figure 5.3b to restrict movement in normal direction. The intention was to simulate the contact to the inner aluminum part of the plunge as fully bonded.

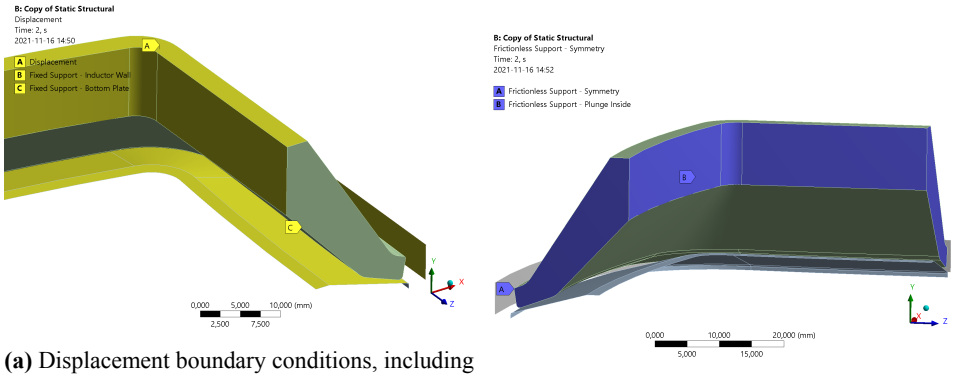

(a) Displacement boundary conditions, including simulated fixed supports.

(b) Frictionless support boundary conditions.

Figure 5.3: Boundary conditions.

5.3 Mesh

The assembly was globally meshed using the default automatic meshing algorithm in ANSYS Workbench but with a few adjustments and additional local settings:

- Linear elements were used and found more stable than quadratic elements. The large deformations in the plunge occasionally caused overlapping edges and high distortion errors when higher-order (quadratic) elements were used.
- The node density, i.e. mesh resolution, was increased in curved areas of the assembly for geometry preservation. That was obtained by turning on the *capture curvature*-setting with a *curvature normal angle* of 35° which forces the meshing algorithm to create nodes along geometry curves every 35° change in the normal direction. A local curvature normal angle of 2° was set on the inductor wall due to its more gentle geometric curvature.
- The *growth rate* setting was set globally to 1.5 which kept the refined mesh regions more concentrated and the element count low.
- The plunge was modeled using solid tetrahedral elements (SOLID285 in ANSYS). Compared to *current technology* solid tetra- or hexahedral elements, this element type was found more stable in facilitating solution convergence in the FEA related to incompressible material behavior. SOLID285-elements have an extra degree of freedom for hydrostatic pressure and hence, good capability

of modeling near or fully incompressible materials. The use of tetrahedral elements was found to increase the computation time for the simulation due to the substantially larger amount of elements in the model in comparison to when using hexahedral elements. Hexahedral elements with a hydrostatic pressure degree of freedom are however not available in ANSYS. As a result, a computationally more effective structured mesh using hexahedral elements together with a meshing method such as the sweep method, could not be used.

- The face meshing tool was applied to the fillet on the bottom plate to create even mesh surfaces on these surfaces.
- The plunge lip, which was seen as the region of interest in the model, was also meshed with the face meshing tool to create a structured mesh over these surfaces. A close-up image of The plunge lip mesh can be seen in Figure 5.4b.
- The element size was set to 2mm after assessing (see section 5.3.1) the element size effect on results of interest and the computation time.

The entire mesh is visible in Figure 5.4a.

The use of rigid surface modeling on the inductor wall and the copper bottom plate implies that no particular element was used to mesh these parts. Contact elements can however be meshed onto rigid surfaces which allow pressure to be computed on these surfaces. The contact element types used were CONTA174 and TARGE170 in ANSYS.

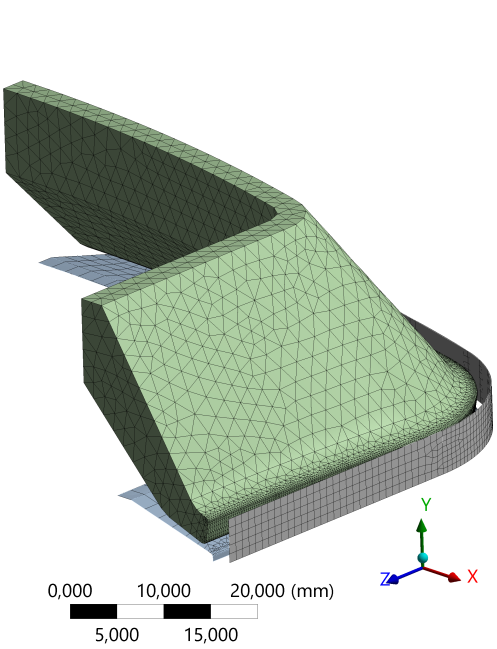

(a) Overview image of the mesh for the entire assembly.

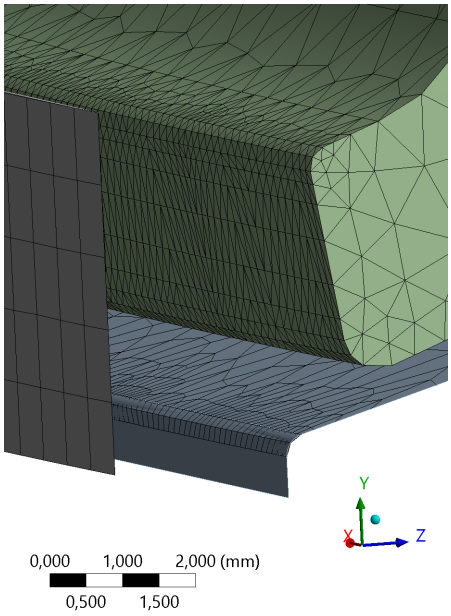

(b) Close-up image of mesh in plunge lip region.

Figure 5.4: Mesh used in FEA.

5.3.1 Element Size Assessment

The procedure of choosing element size for the plunge geometry has required consideration of many factors. Smaller elements produce more detailed results and in general stresses and strains closer to reality. On the other hand, larger elements result in fewer elements and hence, less computation time. The goal with the element size assessment is to find a sweet spot in element size. So that the computation time is reasonable and the results are accurate. I.e, the accuracy of the results are not considerably increased when the element size is further lowered.

Accuracy in results in this case is almost entirely limited to the accuracy of the pressure distribution on the plunge lip surface. The exact accuracy of point stresses was wished-for but not as important. Results in the rest of the FE model was seen as insignificant as long as the plunge lip pressure distribution was not heavily affected.

Another aspect to consider when choosing element size is model robustness. Elements exposed to the large strains in the model were needed to be of high quality to avoid high distortion errors and to obtain solution convergence. Element quality

can be measured in many metrics. One is the aspect ratio (ratio between the longest and shortest side of an element) that should be close to 1. Smaller element sizes have been recommended in FE communities for convergence issues related to large deformations and contacts. Decreasing the element size on the protruded plunge lip however resulted in worse element qualities in the most demanding regions of the model. From experience developing this FEA, a coarser mesh functioned equally well or even better for the purpose of this FEA in some scenarios.

The element size assessment was carried out by altering the global element size in 4 different FEA simulations to assess the impact on plunge lip pressure distribution. The resolution of the face mesh on the plunge lip surface was unchanged in all runs. The friction coefficient between the plunge and the bottom plate was set to 0.1, and between the plunge and the inductor wall to 0.4. The 3-parameter Mooney-Rivlin nearly incompressible constitutive model with the parameters described in 7.4.3 was used. All other settings in the FEA model were identical to other simulations in this report. 4 Intel i7-3770 processor cores with a clock speed of 3.4 GHz were used for all FEA computations in this report, including this experiment. The computation time for the FEAs with different element sizes will also be presented in the results chapter.

5.4 Contacts

There are two contact regions in the FEA model, one between plunge and bottom plate and one between plunge and inductor wall. ANSYS uses two different element types for *rigid-flexible* contacts. One contact element side that usually is selected for the softer more curved side that will undergo more deformation. The other side becomes the target element side and is usually harder and flatter. The plunge was selected as the contact side in both contact regions. All contact surfaces used in the model are visible in Figure 5.5.

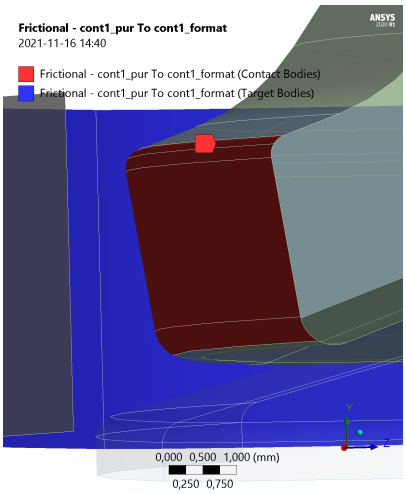

(a) Contact (red) and target (blue) surfaces in plunge-inductor wall contact region.

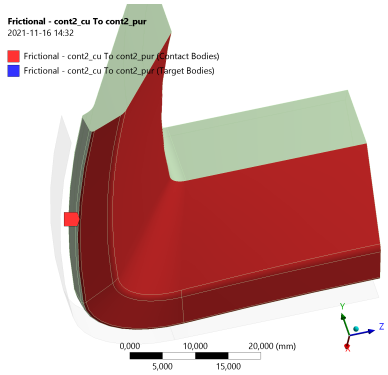

(b) Contact surfaces in the plunge-bottom plate contact region

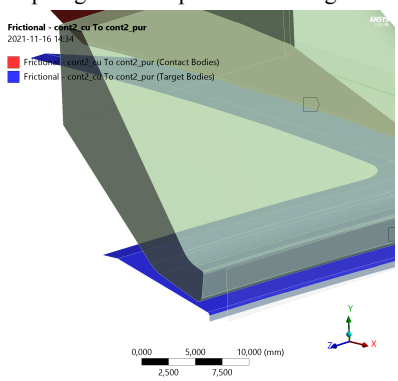

(c) Target surfaces in the plunge-bottom plate contact region

Figure 5.5: Contact and target surfaces used in FEA.

The contact elements have contact detection points that ”search” for nearby target surfaces within the *pinball radius* defined by the user. In a friction contact, the contact pairs can have 4 different types of statuses in ANSYS; open far-field, open near-field, sliding, and sticking. Far-field status requires the least amount of computation and near-field status is more complex and has higher computational demands. The most complex calculations occur when the contact and target elements are in contact, that is sliding or sticking status. The contact status, normal pressure, and frictional stress are calculated dependent on chosen contact algorithm.

Both contacts were modeled with friction coefficients, denoted as μ. The contact between plunge and the bottom plate was modeled with $\mu = 0.4$ based on the approximation from the plunge manufacturer and after the experiment described in section 5.4.1. The friction coefficient for the plunge-inductor wall contact region was set to $\mu = 0.1$ based on the assumption of low friction as a result of melted PE plastics as

mentioned in 1.3. Higher friction coefficient values and the rough contacts settings in ANSYS, were found to cause convergence difficulties in some simulations due to *contact chattering*.

Using contacts in FE models entails complex non-linear mathematical equations and uncertainties that are difficult for FE solvers to solve. There are many different algorithms and techniques used by commercial FE codes to work around these difficulties which in many cases also comes with the cost of less accuracy in results.

Determining appropriate FE model settings that operates well together, independently on simulation factors such as geometry and constitutive model, has been a challenging and time consuming process but of highest prioritization. Consequently, alternative settings that yield more accurate results were at times disregarded. The following listed combination of ANSYS contact settings were able to accomplish converging solutions for the considered CAD geometries, constitutive models, and other simulation settings. They have been used in this entire project. The methodology of finding these particular settings have mostly been based on trial and error and by reading the ANSYS documentation.

- Gauss points were used as contact detection points in both contacts. It is a computational effective option and convergence issues were recognized with the use of alternative settings.
- Asymmetric contact behaviour was used in both contact regions, meaning that the contact element nodes are unable to penetrate the target elements but the target nodes can penetrate the contact elements.
- The Augmented Lagrange contact algorithm was found more stable than other algorithms and used in both contacts. The algorithm is penalty-based, meaning that penetration between contact pairs is penalized with a contact normal stiffness factor K_n. The contact pressure is computed by iteratively updating the penalty until the Lagrangian multipliers (contact tractions) are found. The method is less sensitive to the magnitude of K_n and is better at overcoming ill-conditioning of the stiffness matrix $\boldsymbol{K}$ than the *pure-penalty* algorithm. However, this method usually requires more computation.
- The normal stiffness factor was set to 0.5 in the plunge-inductor contact and 0.6 in the plunge-bottom plate contact. In general, high values lead to convergence difficulties and low values decrease the accuracy of the results.
- The *update stiffness*-option was set to *each iteration, aggressive* and was found to remedy chattering problems causing convergence issues. Chattering problems occur when the contact status for multiple elements is close to the limit

between far- and near-field, or sliding and sticking status. This algorithm automatically updates the normal stiffness factor throughout the analysis to convenient values.

- The option *small sliding* was turned off. This setting connects contact and target elements only once at the beginning of the analysis and hence, improves performance and robustness but is not suitable for large deformation analysis.
- The stabilization damping factor was set to 0.0 in the final model but was found useful in earlier models with a factor value of 0.2 to remedy convergence issues when present.
- The pinball radius was automatically calculated by the software dependent on element size in each contact region. In the case of $2mm$ global element size, the values were calculated to roughly $0.5mm$ for the plunge-inductor wall contact and $1.5mm$ for the plunge-bottom plate contact.
- The *trim contact*-option was turned off. This option excludes eventual far-field contact and target elements before the simulation begins.
- The interface treatment option was set to *add offset, ramped effect* with an offset value of $0.05mm$ for both contacts. This setting adjustment appeared to remedy some contact initialization difficulties for some analyses. The alternative *adjust to touch*-setting was not useful due to the large initial gaps in both contacts. Contact pairs were connected using the relatively large pinball radii, ramped displacement, and a relatively large number of solver substeps instead.

An APDL post-processor script was written with the purpose of computing the contact pressure variance on the plunge lip surfaces. The script exports the element contact pressure results on the plunge lip surface at the end of simulation and then calculates the population variance among these. Every individual element contact pressure is calculated as the average of contact element node normal pressures. The contact surfaces used to compute pressure results in this script are fewer than the surfaces of the entire plunge lip contact seen in 5.5a. The uppermost row of surfaces visible in this image was skipped in the APDL script since they most often contained noisy or close to zero pressure values. The individual contact element pressure values and coordinates are in this script saved to a file. The script also computes the contact pressure variance between all elements among other statistics, and returns it to ANSYS workbench to be used as a response variable in the optimization described in chapter 6.

5.4.1 Friction Coefficient Assessment

The coefficient of friction μ between plunge and the bottom plate was unknown but estimated by the plunge manufacturer between $0.4 < \mu < 0.5$ in loaded condition and on dry metal surfaces such as the bottom plate. It was also considered difficult and excessive to conduct physical tests to measure it since the actual value might change over time and between different packaging machines, plunge units, and bottom plates.

It was however of interest to examine what effect different values on μ had on the plunge lip pressure distributions in the FEA. Thereupon, four simulations were run with the coefficient of friction values 0.2, 0.4, 0.6, and 0.8 respectively. Besides that, the experiment was conducted with the same conditions as in the element size assessment experiment except from a global element size of 3mm.

It was not confirmed whether the contact between plunge and inductor wall (in reality between plunge and the two layers of carton), is sliding or sticking. That is, whether the plunge lip can move vertically upon contact with the carton and hence move the contact weld with it, or if the plunge lip sticks to the same height as contact is initialized. A low friction coefficient that implies sliding conditions was in the end assumed in this contact as mentioned in the thesis assumptions.

5.5 Constitutive Model

The stress-strain relation in a material is in an FEA specified with a constitutive model, a mathematical expression usually consisting of strain variables and material-dependent constants. The constants are chosen so that the difference between model and experimental stress-strain data is minimized. This minimization operation will hereafter be called fitting.

The plunge body is manufactured in a PU material classified under elastomers. Elastomers can be modeled with linear elastic theory, i.e. Hooke's law, but only as a rough approximation and for very small strains. Instead, modelers often deploy hyperelastic constitutive models based on strain energy density functions, also known as stored energy functions. Uniaxial, biaxial, and shear test data is optimal for fitting such models to cover the different modes of strains in an elastomer. Only uniaxial test data have been used in this project.

Elastomers consist of long and flexible chain molecules called polymers that can with-

stand large strains, often up to several hundreds of percent, without causing permanent deformation. Nonlinear elasticity, viscoelasticity, and stress softening after initial loading cycles known as the Mullins effect, are mechanical phenomena that characterise elastomers. The material modeling in this FEA will be limited to static elastic behavior and consideration of dynamic effects and Mullins effect will be neglected.

There are many static-elastic constitutive models to choose between. Subject research and a comparison experiment with different models (see section 5.5.2), was used to decide model. In particular, the review of models for rubber-like materials given by Ali et al. (2010) has been adopted. More detailed mathematical explanations of the central concepts of constitutive models for elastomers are taken from Austrell (1997).

5.5.1 Strain Energy Density Function

The strain energy density function $W(\lambda)$, that is strain energy per undeformed volume, can be derived in the one-dimensional case by considering a nonlinear elastic bar with the undeformed length L being elongated the distance u or stretched the length ratio $\lambda = l/L$ due to a force P as in Figure 5.6.

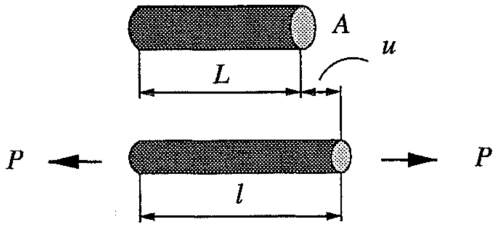

Figure 5.6: Nonlinear elastic bar loaded by force P (Austrell, 1997, p.17).

Total strain energy U in the bar is calculated by multiplying the undeformed volume with W

$$U = ALW(\lambda) \tag{5.1}$$

where A is the cross-sectional area. By assuming energy balance between incremental work done on the bar by the force P and increment in total strain energy, one gets

$$Pdu = ALdW = AL\frac{dW}{d\lambda}d\lambda \tag{5.2}$$

By inserting $du = Ld\lambda$ in equation 5.2, the energy balance equation can be further

simplified and rearranged to create the relation

$$\frac{P}{A} = \frac{dW}{d\lambda} \tag{5.3}$$

where P/A equals the nominal stress, i.e. force per undeformed cross-section area derived directly from the strain energy density function $W(\lambda)$. Stresses are computed similarly in the three-dimensional case in finite element codes when a hyperelastic constitutive model is used. Although, different models have different mathematical expressions. Different models have also been found useful in different types of applications based on what type of elastomer is to be modeled, what experimental data is available, and what stretch interval is to be accurately modeled.

Without immersing in the research field of hyperelastic constitutive models, a couple of them were examined, fit to the available experimental data, and then tested as described in the following section.

5.5.2 Comparison of Constitutive Models

Constitutive models will in this project be compared by conducting multiple identical FEA simulations of the plunge expansion mechanism but with different constitutive models. More exactly, the plunge lip pressure results and vertical plunge force reactions corresponding to the different models will be compared.

Many commercial FE codes have functions for fitting constitutive models to experimental data. The hyperelastic constitutive models in this project have been fit with the non-linear least square fitting method in ANSYS Workbench 2020 R1.

It is important to check for instability when a model has been fit to experimental data, especially models of higher-order. This can be checked by plotting the strain energy function $W(\lambda_1, \lambda_2)$ as a function of the two principal stresses λ_1 and λ_2 for an incompressible isotropic hyperelastic material. A physically realistic behavior of the model is obtained when the function is bowl-shaped with one extreme point in $W = 0$. The model is unrealistic if the plot has more than one extreme point and in such a case, the finite element equation $\boldsymbol{F} = \boldsymbol{K}\boldsymbol{u}$ will be to solve. Another thumb rule that can be used to detect unsatisfying material behavior is to look for negative slopes in any of the uniaxial, shear, or biaxial stress-strain curves of the model.

The constitutive models in the following paragraphs have been fit to test data and proven stable in terms of the thumb rule criteria mentioned above. Some of the models were fit with a portion of the available experimental data to obtain this stability.

Equivalent strains up to roughly 50% were computed in initial FEA runs of the plunge expansion mechanism. Consequently, model accuracy for strains exceeding 50% was not prioritized.

Aruda-Boyce The Aruda-Boyce models are based on statistical mechanical representations of the molecular chains in elastomers. The strain energy function is derived from assuming that the total strain is equivalent to the strain in all randomly oriented polymer chains in the material. The model is fit using only uniaxial test data and material behavior in other strain modes such as simple shear and equibiaxial tension may not be captured as accurately as in multi-parameter models. A 1^{st} order Arruda-Boyce model fit to strain data up to 100% was found stable and used in the forthcoming experiment.

Linear A linear model with a Young modulus fit to strain data up to 450%, i.e. E =4.48 MPa, and a Poisson's ratio of $\upsilon = 0.499$ was also created and tested.

Ogden The Ogden constitutive model is an empirical model based on continuum mechanics in contrast to being based on experimental or physical concepts (Marckmann and Verron, 2005). It can be very accurate when material data is available from multiple different tests. The model has material constants as exponents which can make it difficult to fit to experimental data. The strain energy function can be expressed as a function dependent on the three stretches or the three stress invariants. The order N of the model can be increased to fit S-shaped curves in large strains. In the case of incompressibility, the third stretch can be derived from the other two. The strain energy function is generally written as

$$W(\lambda_1, \lambda_2, \lambda_3) = \sum_{i=1}^{N} \frac{2\mu_i}{\alpha_i^2} \left(\lambda_1^{\alpha_i} + \lambda_2^{\alpha_i} + \lambda_3^{\alpha_i} - 3\right) + \frac{1}{D_1}(J-1)^2 \tag{5.4}$$

where

$$\begin{aligned} \lambda_k &= \text{The principal stretches} \quad k = 1, 2, 3 \\ N &= \text{order of the model} \\ \alpha_i, \mu_i &= \text{material constants where, for a stable model, } \alpha_i \mu_i > 0 \\ J &= \text{Elastic volume ratio. } J = 1 \text{ for incompressible materials.} \end{aligned} \tag{5.5}$$

Mooney-Rivlin The Mooney and Rivlin Constitutive model is another model that, similar to the Ogden model, is based on mathematical concepts and hence has material

parameters that can be difficult to identify. The strain energy function in its general form is

$$W(\bar{I}_1, \bar{I}_2) = \sum_{i=1,j=0}^{N} C_{ij}(\bar{I}_1 - 3)(\bar{I}_2 - 3)^j + \frac{1}{D_1}(J-1)^2 \tag{5.6}$$

where

$$\begin{aligned} \bar{I}_k &= \text{The strain tensor invariants} \quad k = 1, 2, 3 \\ C_{ij} &= \text{material constants where } C_{00} = 0, \text{and for a stable model, } C_{01} + C_{10} > 0 \end{aligned} \tag{5.7}$$

By putting $N = 2$, $\alpha_1 = 2$, and $\alpha_2 = -2$ in equation 5.4, the 2-parameter Mooney-Rivlin model is obtained where $C_{10} = \mu_1/2$ and $C_{01} = \mu_2/2$. The 3-parameter Mooney-Rivlin has a third material parameter C_{11}.

Yeoh The Yeoh model is a reduction of the *polynomial* constitutive model. It is better suited for filled rubbers and is often mentioned as effective at predicting the stress-strain behavior in all deformation modes even though only a uniaxial tension test has been conducted.

5.6 Solver and Analysis Settings

The FEA was solved in two load steps with different solver settings. The displacement was ramped-up from 0 mm to 1 mm over the first load step with the intention to initialize contact between contact elements, and from 1 mm to 7.5 mm during the second load step. The high non-linearity in the FEA required many incremental load substeps for the solution to converge. Especially for the second load step with larger strains. Substeps are intermediate solution points of a load step in which the finite element equation $\boldsymbol{F} = \boldsymbol{K}\boldsymbol{u}$ is solved.

The ANSYS setting *automatic time stepping* was used for the second load step. The algorithm optimizes the time length of each substep and consequently the displacement size as well. Smaller displacement increments can be applied to sequences of the simulation with convergence difficulties and otherwise, larger load increments are used to speed up the simulation. The initial and minimal amount of substeps was set to 200 and the maximum allowed substeps to 1500. The first load step was not as difficult to solve and hence, the program-controlled settings could be used with good convergence stability.

ANSYS has several different solvers to compute the stiffness matrix $\boldsymbol{K}$ in the finite element equation. An iterative, in contrast to a direct, solver was used due to computer resource limitations. A direct solver might however be more robust and more efficient if applicable, especially for solving Lagrangian multipliers.

5.7 Validating the FEA Model

The FEA with the software settings chosen in previous sections and experiments of this chapter, could be validated by comparing its plunge lip pressure distribution results with the experimental results.

The FEA was slightly modified for the validation experiments to resemble the pressure distribution experiments as closely as possible. The coefficient of friction between plunge and inductor wall was increased to $\mu = 1.0$ to eliminate sliding in this contact. It was assumed to be higher in the experiments than in production considering the lack of melted weld plastics functioning as a lubricant. Six real PU plunges (two of each design) with the geometric deviations $th1$, $th2$, tw, tl, plw, and pla were CAD-modeled and then analyzed in the FEA.

The vertical force reactions computed in the FEAs and measured in the quality control stiffness assessment test described in section 2.3.3, could also be used for validation.

6 Indent Optimization

In this chapter, parts of the theory behind Response Surface Methodology (RSM) will be summarized. Concurrently, an implementation of it using the final FEA model described in the previous chapter will be developed. This way, design parameter values that optimize the contact pressure distribution between plunge and inductor wall can be found.

RSM will in this case be implemented in ANSYS DesignXplorer. Alternative software tools with the same capabilities however exist. Such as writing a script in the open source language R and using it in combination with data gathered from an FEA software.

The theory in this chapter is mainly based on the chapter about RSM in Montgomery (2013, Chapter 11), the literature review on RSM by Myers et al. (2004), and the reviews on response surface designs for computer experiments by Jones and Johnson (2009) and Joseph (2016). The optimization algorithm theory is based on the two chapters about genetic algorithms in Arora (2017) and the ANSYS *DesignXplorer User's Guide* (2020).

6.1 Response Surface Methodology

RSM is a methodology covering many statistical and mathematical tools to model and analyze a process or system. In many cases with the intent to optimize it. For instance, DoE can be used to effectively generate response data of the system under study. RSM has been a research field for the past 70 years and has been used extensively in a wide range of industries. It can be used together with both physical and numerical experimentation, of which an example of the latter is structural FEA.

In RSM employed for structural FEA, DoE is conducted on an FEA model where

input design parameters are systematically changed to generate data about the relation between input design factors $\boldsymbol{x}$ and the output responses $\boldsymbol{y}$. A mathematical response surface model, also known as a metamodel or surrogate model, can then be fit onto the data of each response variable to specify the relation between $\boldsymbol{x}$ and $\boldsymbol{y}$. This allows for predicting the response at any input design parameter combination within the feasible design space. Which can be used to optimize the system.

If the structural FEA model has been verified, validated, and calibrated so that it can make accurate predictions of the true system, the optimal design parameter combination of the response surface can be assumed to represent the optimal conditions for the real system as well. Since the mathematical response surface computationally is relatively cheap to find extreme points for, the number of FEA simulation can be reduced and the total time it takes to find an optimal solution lowered.

RSM employed together with FEA can speed up product development processes while saving expenses spent on building prototypes. On the other hand, conducting designed experiments with FEA can be costly and time-consuming (the same thing applies to the development of the simulation model that may never reach an adequate level of representing the true system). The FEA run time is largely dependent on the speed and amount of processors used. It is therefore of great interest to choose an experimental design with a minimal amount of simulations needed, but that at the same time produces meaningful data for the response surface.

It applies to all experimental designs that the required number of runs grows quickly with the number of design factors. It is therefore common practice to reduce the number of design factors if there are many, perhaps in a DoE factor screening, and then conduct RSM on the most influencing design factors.

The optimization in this chapter is conducted on the FEA model developed in chapter 5, i.e. the 140x120 format plunge, and with a coefficient of friction between plunge lip and format wall of 0.1. As an initial test, only three design parameters will be optimized, the three indentation design parameters. Their considered ranges will be described in the next section.

6.2 Design Parameters

The cross-section Figure 2.4 can be used to locate the design parameters. The corner indent is derived by subtracting format corner radius with plunge corner radius and the total carton thickness that was estimated to be 1 mm. The plunge lip angle, depicted

in Figure 4.5, is set to a constant value close to the manufactured mean taken from quality control data.

The design parameter ranges are listed in Table 6.1 and were limited by two design constraints. Firstly, pci has a lower constrain of 2.5 mm (assuming that the bottom plate has a 0.5 mm smaller indentation) to avoid edge impact with the body carton component in the plunge expansion mechanism. Secondly, due to the CAD model configuration, psi could not be set lower or equal to pci.

Process knowledge was used to decide further parameter boundaries, i.e. the optima were estimated to be within these ranges. The design parameter ranges were set relatively narrow to increase the concentration of design points and hence increase response surface accuracy.

Table 6.1: Selected design parameters.

Description	ID	Allowable range in optimization
Plunge long-side indent	pli	$3.01 - 4.5$mm
Plunge short-side indent	psi	$3.01 - 4.5$mm
Plunge corner indent	pci	$2.5 - 3$mm

6.3 Experimental Designs Used With RSM

The process of choosing a suitable experimental design and mathematical response surface is largely dependent on the nature of the system under study. The mathematical complexity of the plunge FEA responses as a function of the considered input factor ranges is unknown. Therefore, a few different experimental designs and response surfaces will be examined and tested in the following two sections.

RSM was initially developed for chemical and process industries and based on the philosophy of sequential experimentation. I.e. experiments are added to the experimental design sequentially. Central Composite Designs (CCD) are very efficient in such applications. Furthermore, CCDs often include replicated runs, especially in their central design point, which is beneficial in the case of physical experimentation where every observation is subject to random error.

FEA is however a deterministic type of simulation, meaning that there are no errors between replicated runs. Hence, the need for replication, randomization, and blocking

is eliminated (Wu, 2015). The absence of random error also allows for spreading out the design points over larger experimental regions. Furthermore, factor levels are easy to change in computer simulations. As a result, experimental designs with a large number of factor levels are easier to implement than in physical experimentation. In conclusion, RSM for computer simulations often has a different approach compared to RSM for physical experimentation.

6.3.1 Central Composite Design

CCDs generally consist of a 2^k factorial design with n_f factorial runs, n_c center runs, and $2k$ axial runs where k is the number of design factors. Figure 6.1 demonstrates CCDs in the cases of 2 and 3 design factors respectively, assuming factor ranges between -1 and 1. There are many variants of CCD-designs such as the rotatable, the face-centered (figure 6.2), and the spherical design. CCD-variants have different number of center runs n_c (always 1 for deterministic experimentation), and different α-values, the distance from the design center to the axial runs. The experimenter may choose a suitable variant based on what is known about the true system response curvature. In short, different design variants are good at finding curvature and extreme points in different regions and directions of the design space.

In the following optimization implementation, the ANSYS default VIF-optimal CCD will be used. It computes α by minimizing the Variance Inflation Factor (VIF), the degree of non-orthogonality in the model.

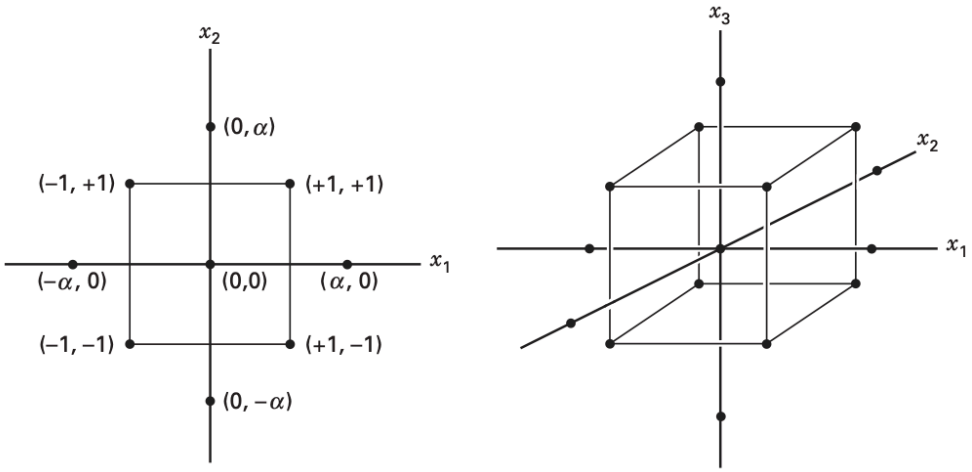

Figure 6.1: Central composite designs for 2 and 3 design variables (Montgomery, 2013).

6.3.2 Box-Behnken

The Box-Behnken Design (BBD) is an alternative design to the face-centered CCD (both seen in the Figure 6.2). The design can be very efficient although it generally requires fewer runs than CCDs. Similar to the spherical CCD, all design points are located equally far away from the design center. Box-Behnken designs are often used when any extreme (corner) point of the design space is unfeasible to conduct experiments at.

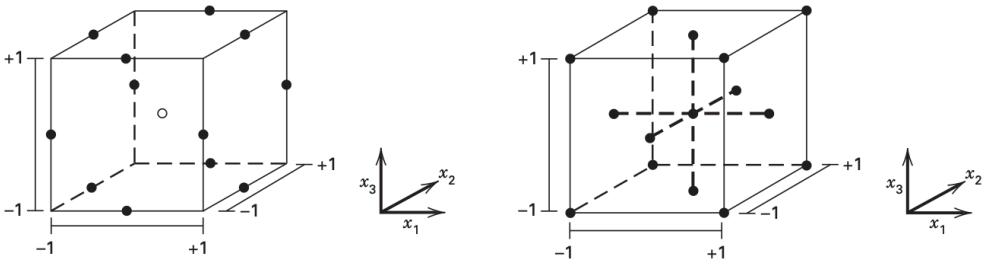

Figure 6.2: Box-Behnken design to the left and face-centered CCD to the right. Both for 3 design variables. (Montgomery, 2013)

6.3.3 Space-filling Designs

The face-centered CCDs and the BBDs only require three levels of each design parameter which often is favorable in physical experimentation where the levels may not be easily controllable. Space-filling designs have an almost opposed strategy, the design points are more evenly distributed throughout the design space to increase the chance of an arbitrary point in the experimental region being close to a design point. This feature also allows for response curvature more likely to be detected at all places in the design space. Two types of space-filling design will be tested in this project, the Optimal Space-Filling (OSF) design and the Latin Hypercube Design (LHD).

Since deterministic simulations have no random error, two design points close to each other will produce similar results. The objective in an OSF design (also called maximin distance design and sphere packing designs) is to maximize the minimum distances among design points in the experimental region (see Figure 6.3). One disadvantage with this design is that design points, by occurrence, might have the same or similar design parameter levels. If that design parameter has little effect on the system response, some design points might be wasted in describing this parameter's influence on the response. The LHD is a solution to this problem. An LHD of n runs

is generated by dividing each design parameter range into n equal spaced intervals. The design points are then placed so that no design parameter interval is observed multiple times. I.e. design points are placed so that no other design point occurs at the same level in any dimension (see Figure 6.3).

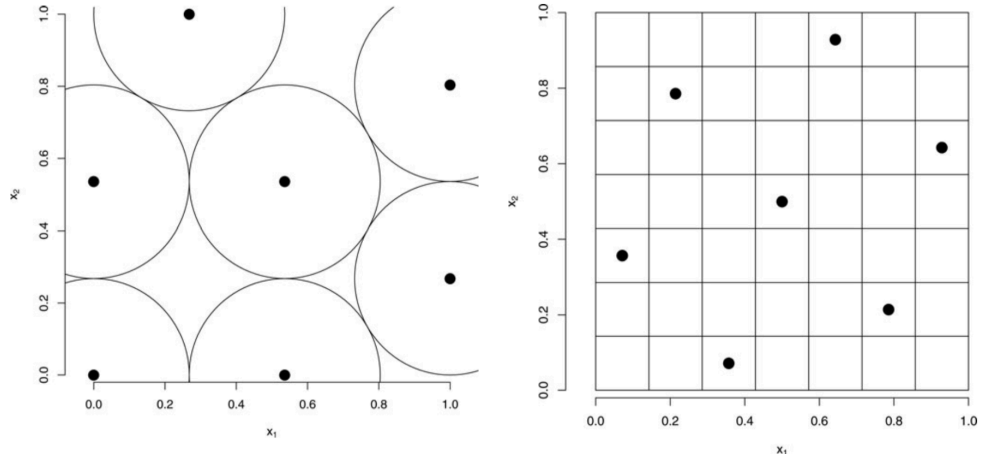

Figure 6.3: An OSF design to the left and an LHD to the right. Both for 2 design variables and 7 runs. (Joseph, 2016)

6.4 Response Surfaces

6.4.1 Second-Order Polynomial Model

CCDs and BBDs are perfect for fitting 2^{nd}-order polynomial surface models. Equation 4.10 is an example of such a model and in general, polynomial models are straightforward to fit using the least-squares method. 2^{nd}-order polynomial surface models are often enough to represent a system in smaller design regions and is sometimes preferred if the FEA is inaccurate and has large numerical uncertainty.

6.4.2 Interpolation Models

Joseph (2016) mentions a couple of challenges with modeling deterministic simulations with polynomial regression-based methods. Firstly, the residuals do not exist in reality and are thus uninterpretable. Secondly, eventually large design spaces are usually not well modeled with low-order polynomial models.

Interpolating methods such as *Kriging*, which can model highly nonlinear surfaces are often preferred in computer simulations (Jones and Johnson, 2009). A Kriging surface consists of a polynomial model, suitable for describing global curvatures of the response, and a Gaussian stochastic process that enables local curvature deviations. However, interpolation models often entail higher requirements on simulation response accuracy since the models tangent each experimental design point.

6.5 Indentation Optimization Problem

A complete surrogate model is established when the designed experiments have been conducted and the response surface has been fit. The model can then be used to optimize the system dependent on the chosen objective function. In the following implementation, four different RSM configurations will be tested. They are:

Table 6.2: 4 different RSM configurations.

ID	Experimental Design	Response Surface	Number of Design Points
$RS1$	Latin Hypercube Design (LHD)	Kriging	15
$RS2$	Optimal Spac-Filling (OSF)	Kriging	15
$RS3$	VIF-Optimal Central Compostite Design (CCD)	2^{nd}-order polynomial	15
$RS4$	Box-Behnken Design (BBD)	2^{nd}-order polynomial	13

The main objective in this design optimization is to homogenize the contact pressure distribution between the plunge lip and the inductor wall in the FEA. However, using this objective function solely might cause certain problems. For instance, large friction stresses induced by the plunge tool on the package components are unwanted.

This might occur for larger indents on the plunge lip where the plunge lip tends to displace vertically in the end of the expansion mechanism. This phenomenon might also counteract contact in regions of the plunge lip causing the APDL script to avoid extracting contact pressures for non-contacting elements. Hence, fewer contact elements will be considered in the variance computation and the results get biased. This problem was accounted for by introducing a second objective, to minimize the average friction stress in the contact so that normal directed contact is promoted.

The mathematical formulation of the optimization problem becomes:

$$\begin{aligned} \text{minimize} \quad & \text{Var}_\sigma(pci, pli, psi) \\ \text{minimize} \quad & \text{Avg}_f(pci, pli, psi) \\ \text{subject to} \quad & 2.5 \leq pci \leq 3.0 \\ & 3.01 \leq pli \leq 4.5 \\ & 3.01 \leq psi \leq 4.5 \end{aligned} \tag{6.1}$$

where

$$\begin{aligned} \text{Var}_\sigma &= \text{Variance of contact element pressures from the FEA.} \\ \text{Avg}_f &= \text{Average of contact element friction stresses from the FEA.} \end{aligned} \tag{6.2}$$

To increase the likelihood of stable APDL script results, the number of plunge lip surfaces used in the APDL script computation were decreased compared to as described in section 5.4. The lower row of surfaces was discarded so that no fillet surfaces were used (as seen in Figure 6.4)

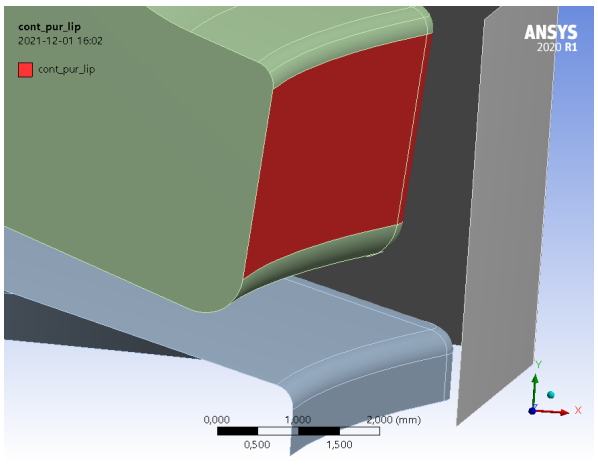

Figure 6.4: Included surfaces in the computation of contact pressure variance and contact friction stress.

6.6 Optimization Using Multi-Objective Genetic Algorithm

Genetic Algorithms (GAs) are popular in response surface optimization since they do not require a continuous or differentiable response surface, in contrast to other *direct search methods*. Evaluation of points within the design space is the only requirement and GAs can hence be effective on a wide range of functions including complex response surfaces. The downsides of GAs are the large number of function evaluations required and that there is no guarantee that the global optima in the design space is obtained.

In GAs, the optima of a function are searched for with nature-inspired methods. GAs generally consist of first initializing a random population of designs and then iteratively ”breeding” new populations with inherited characteristics from the best performing designs in the foregoing population. The algorithm is stopped when no further improvement in terms of the objective function is attainable. GAs consist of three operators that are used in each iteration:

1. *Reproduction*. A new equally sized population of designs is randomly selected from the foregoing population. Better performing designs are given a higher probability of being selected and hence, duplicates of the best performing designs are likely.
2. *Crossover*. The characteristics of the designs in the new population are exchanged in-between designs to introduce new variations to the population.
3. *Mutation*. A safeguard operation that preserves the highest performing characteristics from foregoing populations to the new population. This prevents valuable genetic information from being prematurely discarded.

Multi-Objective Genetic Algorithms (MOGA) are extended versions of single-objective GAs where the definition of fit (previously written as performance) of a design point is redefined. It is often not possible to find a unique solution to a multi-objective optimization problem that optimizes all objective functions simultaneously. In fact, infinitely many possible solutions may exist, called the Pareto optimal set, or Pareto front. A design point is called Pareto optimal if there exists no other design point in the design space that optimizes at least one objective function without regressing another one.

The MOGA stops when a specified percentage of the population design points are Pareto optimal or when the algorithm has reached a stable state, meaning that no further substantial change between the populations takes place. The designer then has

to choose the design point on the Pareto front that is preferred. ANSYS DesignXplorer gives an option to define the importance of each objective and based on the user input, the objective functions get weighted into a single objective function. This enables a single candidate optimal design point to be chosen by the software. In the following implementation, the importance of the two objectives was set equal.

6.7 Adequacy Checking

After all N FEA design points have been solved in the experimental design, the response surface needs to be verified after being fitted to the response data. This process can be performed by introducing further verification design points (conducting further arbitrary experiments) in the design space and then comparing these responses $\boldsymbol{y}$ to the equivalent predicted responses $\hat{\boldsymbol{y}}$ on the response surface. The residuals, i.e. the difference in predicted and observed verification response values, can then be used to assess the goodness of fit for the response surface. An identical set of 20 verification points was used to verify the goodness of fit for all 4 RSM configurations.

One measure that is frequently used to quantify this quality is the *root mean square error* (RMSE) also known as *root mean square deviation*. RMSE is the square root of population variance in residuals and can hence be interpreted as the standard deviation of residuals.

$$RMSE = \sqrt{\frac{\sum_{i=1}^{N}(\hat{y}_i - y_i)^2}{T}} \tag{6.3}$$

Lastly, to assess the overall usability of an RSM configuration and its optimization objective, the performance of its predicted optimal design will be verified by evaluation in the FEA. The computed results at these points can then be compared to the equivalent FEA results of the v1, v2, and v3 designs. I.e. comparing contact pressure distribution plots for instance.

The RSM configuration and its objective will be considered useful if its optimal design is observed to be better than the v1, v2, and v3 designs. A perfect RSM would accurately predict the true global optimal design in that systems design space.

7 Results

This chapter contains results from the pressure distribution experiments, the FEA model experiments, and the FEA optimizations.

7.1 Pilot Experiment - ANOVA

The trial runs and the pilot experiment allowed for many test rig adjustments and new strategies to diminish or eliminate disturbing factors as mentioned in section 4.2.3. Examples of pressure distribution images recorded in the pilot experiment with the two different treatments are given in Figure 7.1. A clear difference between the pressure distributions in corners 1 and 2 (where pixel column 6 and 33 is located) is noticeable in both figures. To decrease this effect, coaxial realignment between the plunge assembly and the inductor wall was implemented after this experiment. In addition, a new sensor was installed after this experiment to diminish any possible effect caused by air bubbles in-between the layers of tape.

Furthermore, 7.1a indicates a higher pressure on the long side of the plunge which potentially can be described by the different indent values between the designs. All pressure distribution images from the experiment are found in the appendices

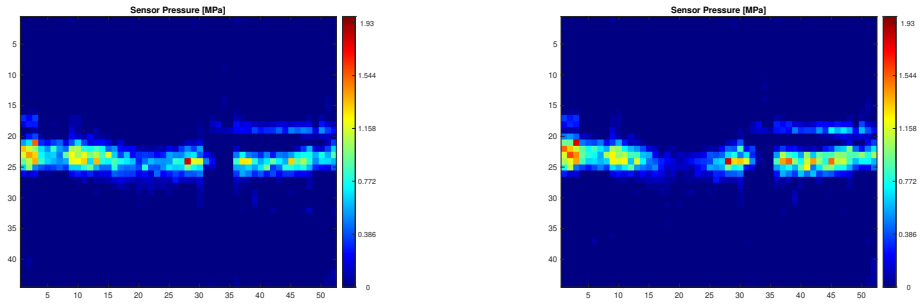

(a) $pd = v3$ (test run #19).

(b) $pd = v1$ (test run #20).

Figure 7.1: Pressure distribution images of two different plunge designs.

The first response function R1 was used throughout this experiment. The ANOVA-related statistics are found in Table 7.1 and Equation 7.1.

Table 7.1: ANOVA results from the pilot experiment.

Source of Variation	Sum of squares	DoF	Mean square
Between treatments	$SS_{design} = 1.77e + 18$	1	$MS_{design} = 1.77e + 18$
Error (within treatments)	$SS_E = 9.94E + 16$	18	$MS_E = 5.52e + 15$
Total	$SS_T = 1.86e + 18$	19	

$$F_0 = \frac{MS_{treatments}}{MS_E} = 319.51 \tag{7.1}$$

The tabular F-value is $F_{\alpha,a-1,N-a} = F_{0.05,1,18} = 4.41 < 319.51$ from which we can deduce significant difference between the two treatments means.

Figure 7.2 contains results obtained from R (7.2a and 7.2b) and Minitab (7.2c and 7.2d). The normality and equal variance assumptions required in ANOVA, can be assumed fulfilled looking at Figure 7.2a. The two theoretical normal distributions have similar slopes and the observations are approximately located at the lines except for 3 outliers. No observations are located outside the ±2 quantiles which are unlikely for normal distributions.

The box plot contains boxes for each treatment with edges representing the lower and upper quartile, a median line in-between, blue dots representing the treatment means,

and the rest of the scattered dots representing observations. The box plot clearly indicates a difference in response between the two treatments.

The 3 previously mentioned outliers are further visible in figures 7.2c and 7.2d. In the latter plot, the outliers can be correlated to observations 1, 2, and 6. Aside from these observations, the residuals seem to have a random and unstructured distribution which signifies independence among the residuals.

The cause of the outliers is suggested to be related mainly to the rotational misalignment in the plunge fixture that was more present in this experiment. The special adaptor with a rotational reference point that improved the alignments, was implemented after this experiment. Hence, the outlier dispersion was expected to decrease in forthcoming experiments.

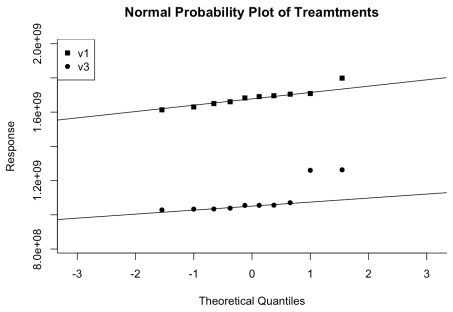

(a) Normal probability plot of treatments.

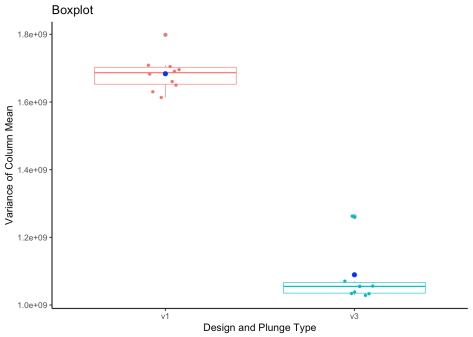

(b) Box plot with scatter of observations. Blue markers are treatment mean.

S

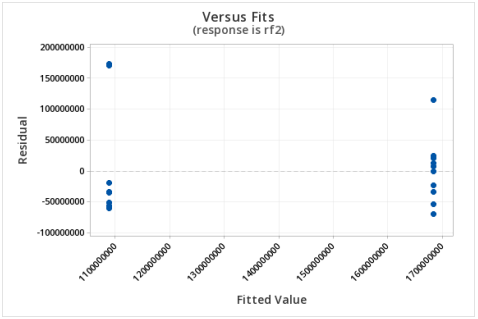

(c) Residuals over fitted value.

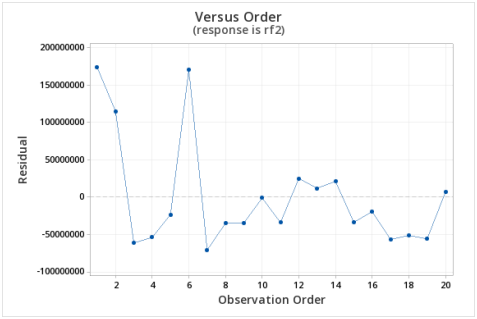

(d) Residuals over observation order

Figure 7.2: Result plots for the pilot experiment.

7.2 Factor Screening Experiment

Arbitrary examples of pressure distribution images recorded with the six different treatments are given in Figure 7.3. The left column depicts the PU plunge units and the right column FDM plunge units. Each row represents a *pd* (plunge design) level which pressure distributions are visible to differ slightly. It is also noticeable how the FDM plunge units reached or exceeded the pressure sensing limit of 1.93 MPa more than the PU plunge units.

The plunge expansion mechanism was before this test raised 5 mm above the copper coil, and then lowered 2 mm due to the assumed broken pixel row (#16). As a result, the less sensitive pixel row #22 was reintroduced, which was assumed to be on the edge of the copper coil in the inductor wall. This was believed to be the best possible position between two improperly functioning pixel rows even though the pressure distribution readings were affected. More than that, the implemented adjustments in advance of this experiment seemed to have a positive effect. Few or no outliers at all were noticed in this experiment and the pressure distribution images showed more symmetric loading in the corners of the inductor wall.

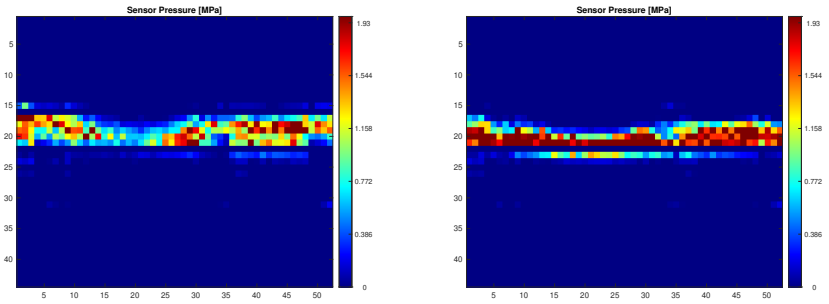

(a) $pd = v1$, $pt = PU$ (test run #19) **(b)** $pd = v1$, $pt = FDM$ (test run #48)

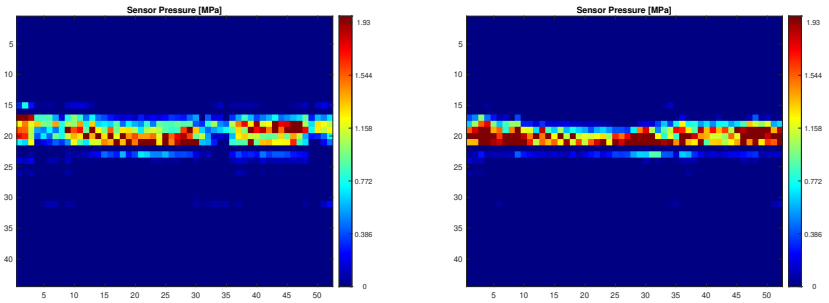

(c) $pd = v2$, $pt = PU$ (test run #23) **(d)** $pd = v2$, $pt = FDM$ (test run #50)

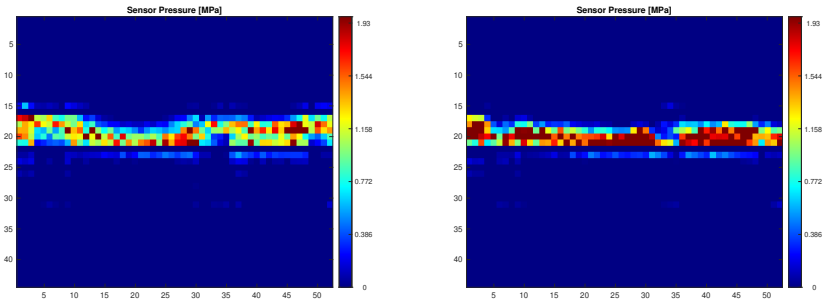

(e) $pd = v3$, $pt = PU$ (test run #26) **(f)** $pd = v3$, $pt = FDM$ (test run #49)

Figure 7.3: Sample of pressure distribution images observed with different plunge designs and types.

A boxplot of the 48 observations grouped into the 6 different treatments is given in Figure 7.4. The plot indicates that there are significant differences between plunge designs for PU plunge units but not as much for FDM plunge units. Differences in treatment variances are also apparent, meaning a possible violation of the ANOVA assumption of equal variances.

Figure 7.4: Box plot with scatter of observations.

In the following 4 sections, 4 different MLR models fitted to the factor screening experiment data is to be described. Following that, comes a section with a summary of the 4 models containing tables and different types of result plots. All models presented here have been fit using the first response variable R1. Equivalent models using the R2 response variable had a substantially poorer fit.

7.2.1 Model A - Initial MLR model

An initial MLR model was developed with factors pd and pt being separated as suggested in chapter 4. 48 observations where used for this model of which 42 with $pt = PU$ and 6 with $pt = FDM$.

The ANOVA-related statistics are listed in Table 7.2. The results are obtained from Minitab and R using the methods described in chapter 4. The amount of predictors used in the model is questionable given only 48 observations. Hence, overfitting might occur. The most significant predictors are pd, sha, pt, plw, tl, and $th1$.

Table 7.2: ANOVA results.

Term	DoF	$SS_R(\boldsymbol{\beta}_1\|\boldsymbol{\beta}_2)$	F_0	$P-Value$
Regression	12	$6.55e+10$	25.48	0.000
sha	1	$1.92e+9$	8.96	0.005
pla	1	$5.31e+2$	0.00	0.999
plw	1	$1.35e+9$	6.30	0.017
tw	1	$5.56e+7$	0.26	0.613
tl	1	$1.31e+9$	6.10	0.018
$th2$	1	$1.28e+8$	0.60	0.445
$th1$	1	$8.67e+8$	4.05	0.052
$mmax$	1	$8.94e+5$	0.00	0.949
$mslo$	1	$4.31e+7$	0.20	0.656
pd	2	$2.13e+10$	49.79	0.000
pt	1	$1.76e+9$	8.2	0.007
Error	33	$7.50e+9$		
Total	47			

7.2.2 Model B - Alternative MLR model

The MLR model in this section was developed with the factor pt being integrated with factor pd to form 6 levels of pd instead. The same 48 observations as in model B were used for this model. The most significant predictors in the model are pd, plw, and $th1$.

The ANOVA-related statistics are listed in Table 7.1.

Table 7.3: ANOVA results.

Term	DoF	$SS_R(\boldsymbol{\beta}_1\|\boldsymbol{\beta}_2)$	F_0	$P-Value$
Regression	14	$7.01e+10$	58.00	0.000
sha	1	$2.16e+8$	2.50	0.123
pla	1	$1.15e+8$	1.33	0.258
plw	1	$4.01e+8$	4.65	0.038
tw	1	$4.42e+4$	0.00	0.982
tl	1	$2.20e+7$	0.25	0.617
$th2$	1	$4.54e+7$	0.53	0.474
$th1$	1	$3.12e+8$	3.61	0.066
$mmax$	1	$1.02e+7$	0.12	0.733
$mslo$	1	$1.56e+7$	0.18	0.674
pd	5	$3.15e+10$	72.88	0.000
Error	33	$2.85e+9$		
Total	47			

7.2.3 Model C - Reduced MLR Model

In this section, a reduced model containing only 3 predictors, is presented. The choice of predictors is based on the significance level of predictors in the foregoing model. The FDM plunge unit observations were removed from this model, resulting in a total of 42 observations. It is possible that leaving out the FDM-related observations leads to a more homogeneous data set that is simpler fitting an MLR model to. The P-levels for the remaining predictors have improved in this model compared to the foregoing.

Table 7.4: ANOVA results.

Term	DoF	$SS_R(\boldsymbol{\beta}_1\|\boldsymbol{\beta}_2)$	F_0	$P-Value$
Regression	4	$6.06e+10$	173.67	0.000
plw	1	$4.95e+8$	5.67	0.022
$th1$	1	$5.11e+8$	5.86	0.021
pd	2	$5.07e+10$	290.84	0.000
Error	37	$3.23e+9$		
Total	41			

7.2.4 Model D - Reduced MLR Model with Interaction

In this section, a reduced model containing three predictors, of which one is an interaction term, is presented. The choice of predictors was found using *stepwise* MLR with 10-fold cross-validation in Minitab. The fit of the model was increased using all 48 observations in the model compared to 42 observations. The interaction term can be interpreted as plunge design pd being dependent on shore A hardness sha.

Table 7.5: ANOVA results for reduced MLR model with interaction.

Term	DoF	$SS_R(\boldsymbol{\beta}_1\|\boldsymbol{\beta}_2)$	F_0	$P-Value$
Regression	7	$6.99e+10$	128.00	0.000
plw	1	$5.20e+8$	6.67	0.014
$th1$	1	$5.48e+8$	7.02	0.011
$pd*sha$	5	$6.12e+10$	156.87	0.000
Error	40	$3.12e+9$		
Total	47			

7.2.5 Model Comparison

Table 7.6 contains a summary of R-squared statistics for each model. Model A has a considerably worse fit in all four R-squared measures than the other models. Model B has the highest R^2-value with the same set of predictors, aside from pt being integrated in pd. This signifies that the difference in response related to pd and pt, is better modeled with 6 individual regression terms as in model B, than with $2+3=5$ regression terms as in model A.

The reduced models C and D also have high R^2-values and as mentioned before, are less likely overfitted. This is further indicated with their slightly higher R^2_{pred} and 10-fold R^2 values. That is, these models are likely better at fitting and predicting "new" data sets or observations if such would be available.

Table 7.6: Model Summary.

Model	R^2	R^2_{adj}	R^2_{pred}	10-fold R^2
A	89.73	86.21	76.90	0.00
B	96.09	94.44	91.25	90.62
C	94.94	94.40	93.11	92.12
D	95.73	94.98	93.90	93.76

Figure 7.5 contains normal probability plots of the standardized residuals in contrast to the observed responses of the separate treatments as in Figure 7.2a. The straight lines represent theoretical normal distributions. All models can be assumed to follow the normal distribution assumption of regression modeling judging by the standardized residuals proximate location to these lines. Furthermore, there are very few residuals with more extreme values than ±3.

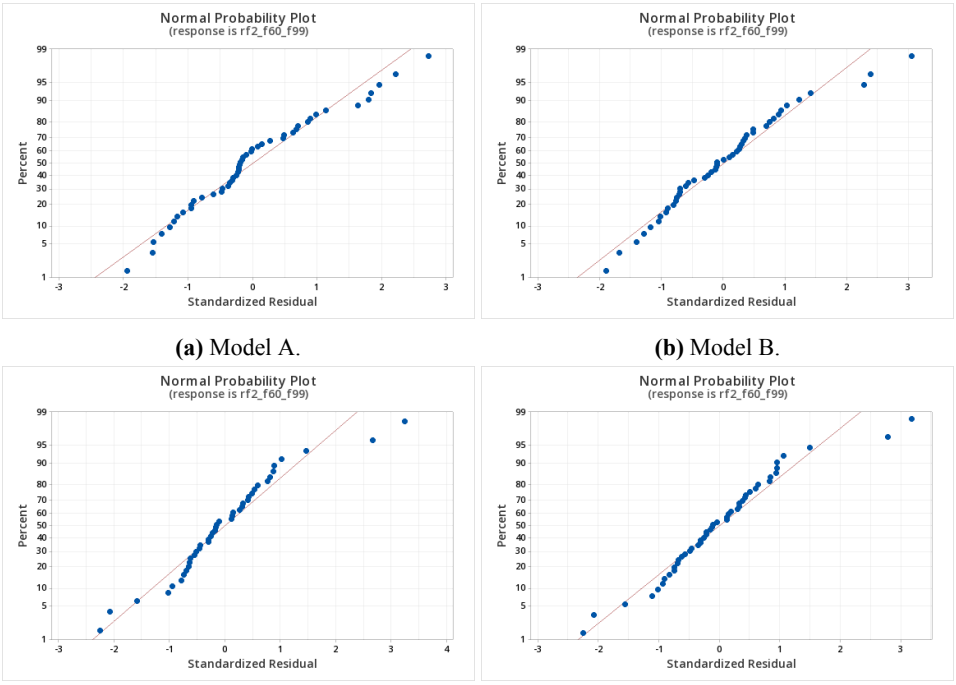

(a) Model A. **(b)** Model B.

(c) Model C. **(d)** Model D.

Figure 7.5: Normal probability plot of standardized residuals.

The Pareto charts in Figure 7.6 contain the *standardized effects* of the model which is an alternative way of presenting significant predictors in the model based on t-testing.

The red dashed line corresponds to the chosen significance level α. Significant predictors have longer staples. The plunge design factor pd or the interaction term it belongs to in model D, is clearly the most influential factor. Followed by that, $th1$ and plw have a relatively high significance in all models.

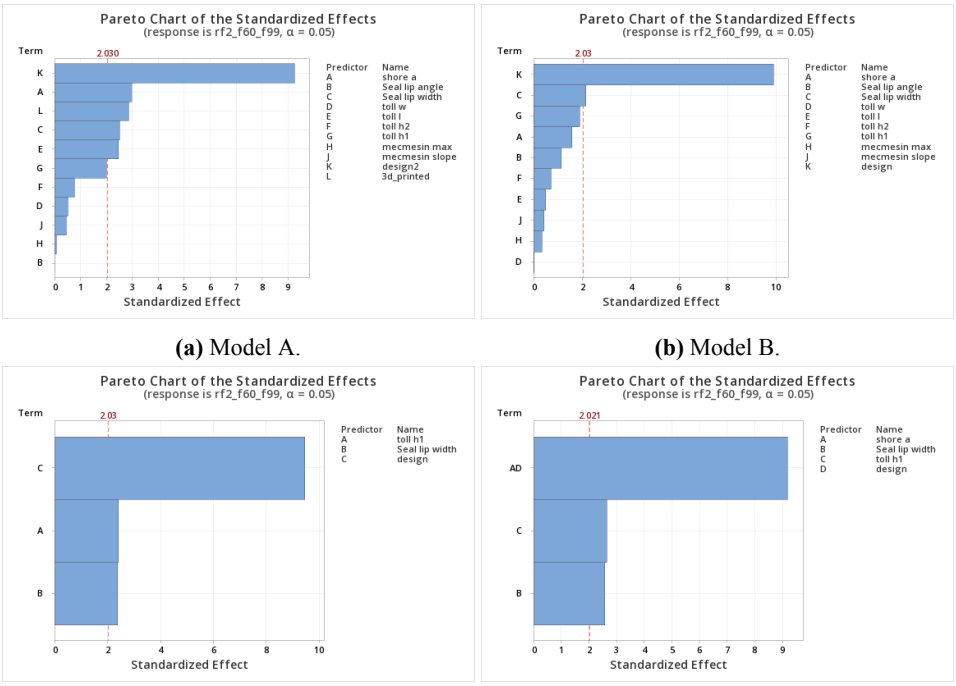

(a) Model A. **(b)** Model B.

(c) Model C. **(d)** Model D.

Figure 7.6: Pareto chart of standardized effects.

Figure 7.7 depicts the standardized residuals over fitted values. It can be used to assess the model fit to certain groups of data. In general, the models can be seen to have more difficulty to model the behavior of observations with high response values. That is plunge units with less homogeneous pressure distribution. Looking at Figure 7.4 again, these observations are likely the $v1$-plunge units.

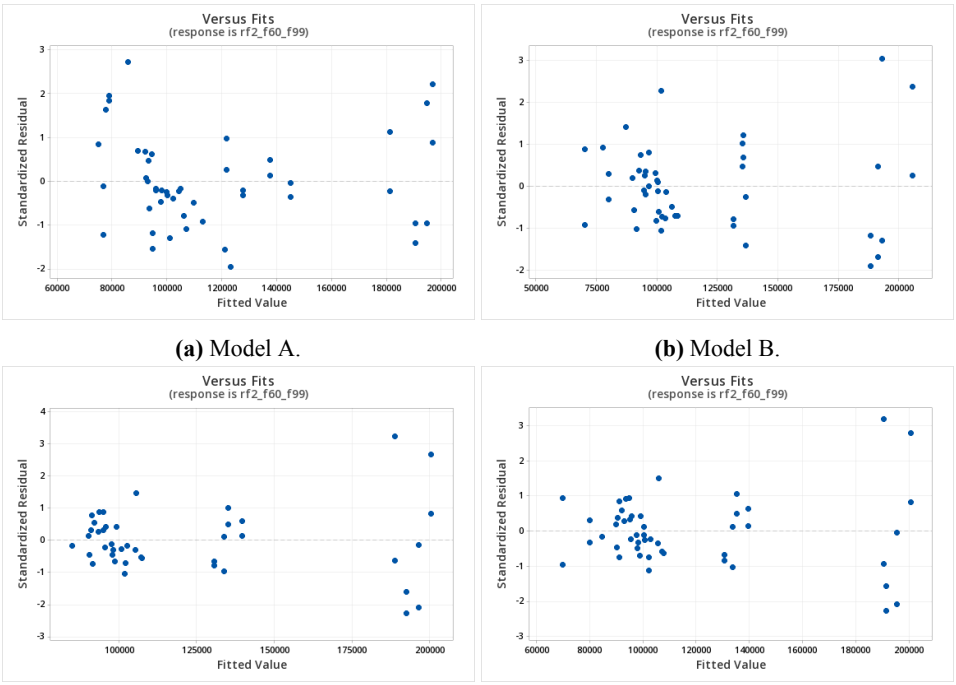

(a) Model A. **(b)** Model B.

(c) Model C. **(d)** Model D.

Figure 7.7: Standardized residuals over fitted value.

The standardized residuals plotted for each model over observation order are depicted in Figure 7.8. It is useful to assess if a model is biased to any observation order-dependent factors that might affect the response during the experiment. The plots show no signs of such behavior which is positive. These plots are also useful to recognize which observations are more difficult to fit the MLR models to, such as observations #10, #18, #28, and #44. It is possible that for some reason, more experimental errors were present in these runs.

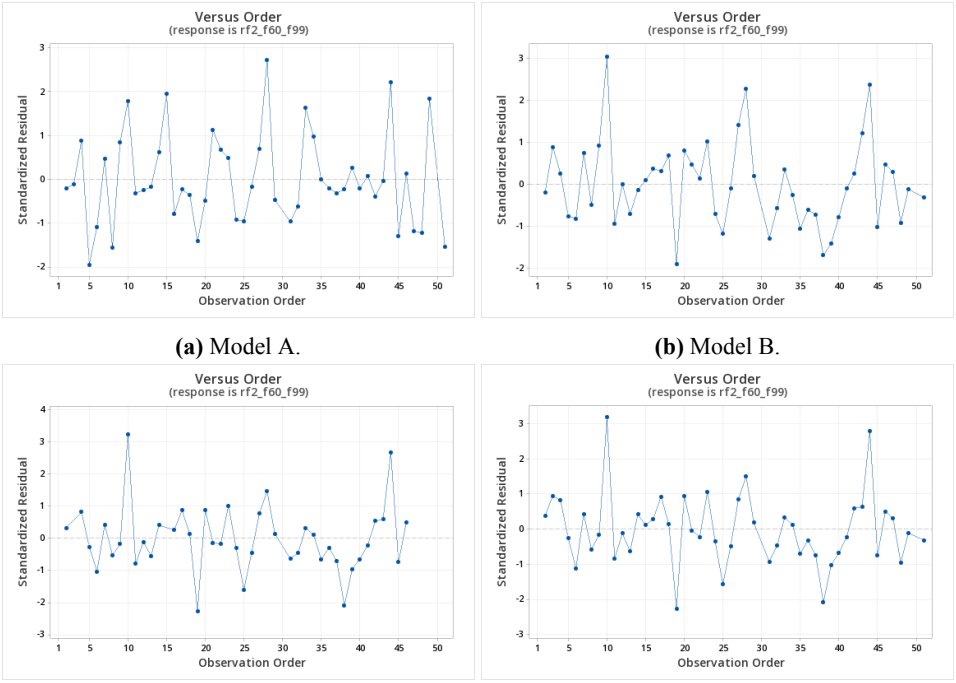

(a) Model A. **(b)** Model B.

(c) Model C. **(d)** Model D.

Figure 7.8: Standardized residuals over observation order.

By taking the regression coefficients β_j, $j = 0, 1, \ldots, k$ from Minitab or R, the MLR relation between response and predictors for model C becomes

$$\begin{aligned} RF = &-118078 + \ 26335th1 + \ 83743plw \\ &+ 52190pd_{v1} - \ 6605pd_{v2} - 45585pd_{v3} \end{aligned} \qquad (\text{Pa}^2) \qquad (7.2)$$

and for model D

$$\begin{aligned} RF = &-161736 + 85824plw + 27324th1 + sha(1053.6pd_{v1,PU} \\ &- 473.7pd_{v1,FDM} + 362.4pd_{v2,PU} \\ &- 639.3pd_{v2,FDM} - 98.9pd_{v3,PU} - 204.1pd_{v2,FDM}) \end{aligned} \qquad (\text{Pa}^2) \qquad (7.3)$$

The categorical factors are binary and only one can be set to 1 simultaneously.

7.3 Experiment With Transverse Carton Components

Arbitrary pressure distribution images from every treatment are visible in Figure 7.9. The folds from the transverse carton components are clearly visible, especially at the long side as randomly located pressure peaks. All 39 images are available in the appendices B.3.

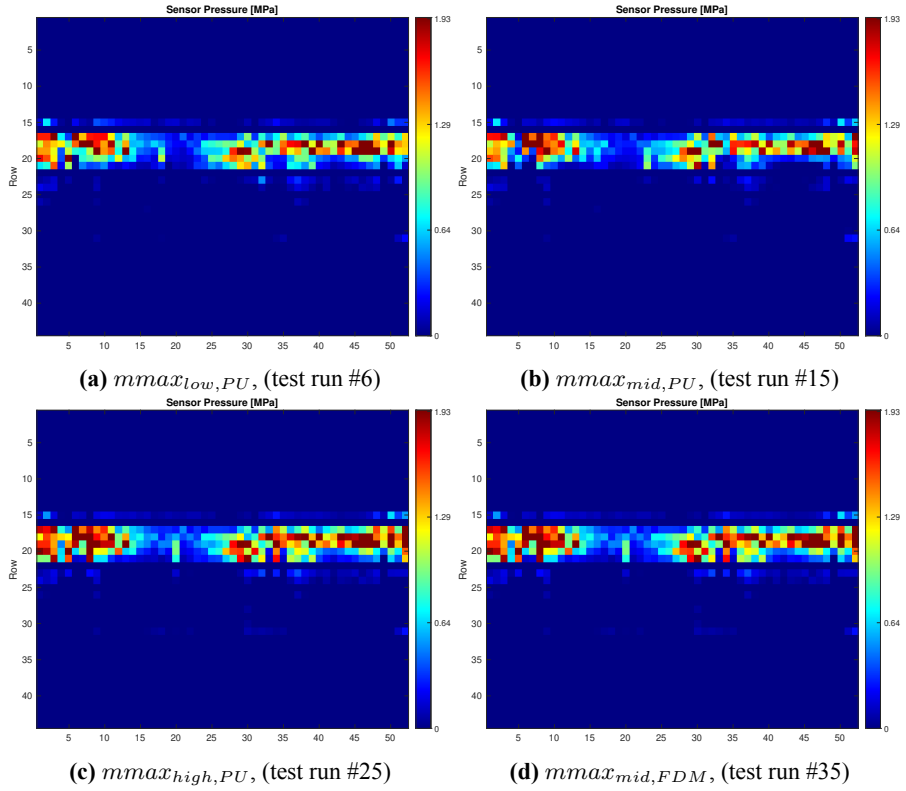

(a) $mmax_{low,PU}$, (test run #6)

(b) $mmax_{mid,PU}$, (test run #15)

(c) $mmax_{high,PU}$, (test run #25)

(d) $mmax_{mid,FDM}$, (test run #35)

Figure 7.9: Sample of pressure distribution images observed with different plunge designs and types.

The boxplot in Figure 7.10 contains R1 response values for the 4 treatments. A clear difference between treatments is noticeable. The FDM plunge produced the most homogeneous pressure distribution, followed by the soft plunge, the medium plunge, and at last the stiffest plunge.

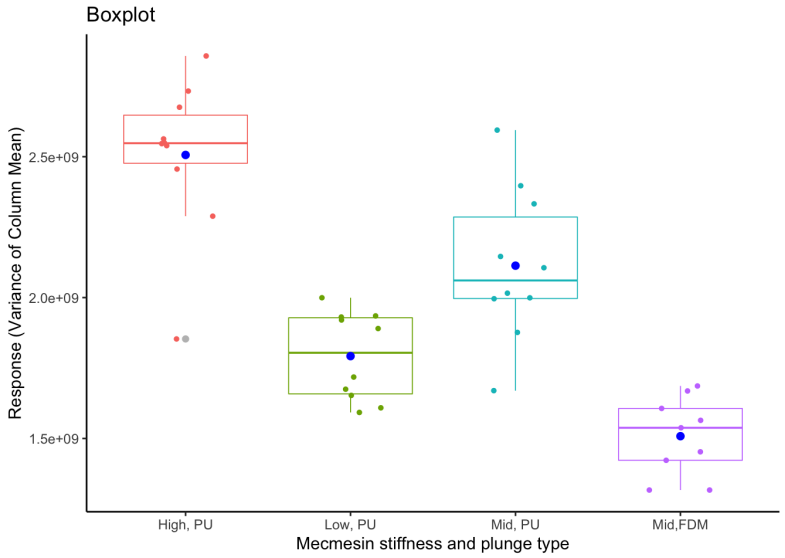

Figure 7.10: Box plot with scatter of observations.

A regression model with the Mecmesin max stiffness $mmax$ as a categorical factor with 4 levels was developed. Only 3 degrees of freedom for predictors could be included in the model as a result of only using 4 plunges in the experiment (thus 4 degrees of freedom in all predictors). The ANOVA Table 7.7 of the regression model (in practice a one-way ANOVA model) also indicates a clear significance in $mmax$. Large errors were also present in the experiment as seen in Figure 7.10 and Table 7.7. A larger portion of error than in succeeding experiments.

Table 7.7: ANOVA results for the regression model.

Term	DoF	$SS_R(\boldsymbol{\beta}_1\|\boldsymbol{\beta}_2)$	F_0	$P-Value$
$mmax$	3	$5.30e+18$	36.07	0.000
Error	35	$1.71e+18$		
Total	38			

The regression model fit in terms of R-squared statistics is listed in Table 7.8.

Table 7.8: Model Summary.

R^2	R^2_{adj}	R^2_{pred}	10-fold R^2
75.56	73.47	69.76	68.62

The regression model becomes:

$$\begin{aligned} R1 = {} & 1979971951 + 526226042 mmax_{High,PU} \\ & - 187676508 mmax_{Low,PU} + 133298281 \qquad (\text{Pa}^2) \\ & mmax_{Mid,PU} - 471847815 mmax_{Mid,FDM} \end{aligned} \tag{7.4}$$

Figure 7.11 visualizes the response values in terms of R1 and R2 over test run (time). Clear order-dependent behavior is noticeable in the R2-response in 7.11b.

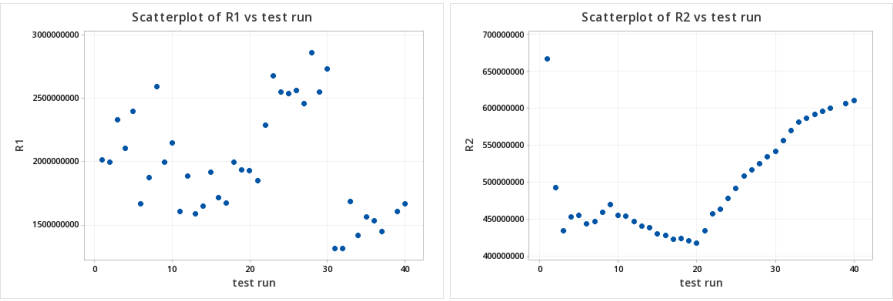

(a) R1 response versus test run. **(b)** R2 response versus test run.

Figure 7.11: R1 and R2 responses versus test run.

7.4 FEA Model

An arbitrary plunge design was used in the following three experiments in this section. It has no correlation to the v1, v2, or v3 designs mentioned in this project.

7.4.1 Element Size Experiment

The results from the element size experiment are shown in Table 7.9. Attention has been held on the results of highest interest in this FEA, the plunge lip contact pressure results.

All assembly parts are included in the reported number of elements in the second column of the table. Notice that most elements are located in the plunge lip region of the plunge mesh and were left unchanged throughout this experiment. The total number of elements does therefore stay above 60 000 elements even for coarser meshes. The computation time in the third column time is noticed to have a strong correlation with the number of elements.

Max R_y in the fourth column of the table, are the maximum vertical force reactions computed in the FEAs. That is, at full 7.5 mm FEA displacement (end of simulation), corresponding to 7 mm real expansion due to the initial gap in the model. The computed value is multiplied 4 times to compensate for symmetry and to easier be compared with $mmax$ from the quality control stiffness assessment test described in section 2.3.3.

The three columns with pressure values have been computed from the pressure result files generated by the APDL script. The pressure variance is calculated as in the sample variance equation 4.7 where y_i corresponds to contact element pressures on the plunge lip surface.

Table 7.9: FEA statistics and plunge lip pressure distribution results for analyses with different element sizes.

Element Size [mm]	N. of Elements	Computation Time	Max $4 * R_y$ [N]	Pres. Max [MPa]	Pres. Mean [MPa]	Pres. Variance [MPa]
4	62433	1h 32m	3001	4.885	2.596	0.705
3	64883	1h 41m	3281	5.010	2.601	0.727
2	74831	1h 54m	3398	4.874	2.574	0.728
1	186848	3h 56m	3402	4.846	2.612	0.738

7.4.2 Coefficient of Friction Experiment

Table 7.10 contains plunge lip pressure results computed the same way as in the previous section but here instead, dependent on the coefficient of friction between plunge unit and bottom plate.

Table 7.10: Plunge lip pressure distribution results from FEAs with different friction coefficients between plunge and copper bottom plate.

μ	Max $4 * R_y$ [N]	Pres. Max [MPa]	Pres. Mean [MPa]	Pres. Variance [MPa]
0.2	2999	5.208	2.817	0.747
0.4	2965	4.930	2.595	0.723
0.6	3043	4.785	2.378	0.699
0.8	3082	4.662	2.156	0.731

The figures in 7.12 visualize the computed contact pressure results in the FEAs at full 7.5 mm displacement. Each point in the scatter plots represents a contact element pressure value on the plunge lip surfaces. The left edge of the plot area is equivalent to the symmetry line of the short side. The x-axis represents the distance in millimeters along the undeformed plunge circumference and ends at the symmetry line of the long side.

Both the max and mean pressure values in the table, and the pressure distribution plots indicate that the pressure results increase when the coefficient of friction μ is decreased.

It is furthermore worth pointing out that *Max* $4 * R_y$ is not substantially affected by the change in μ.

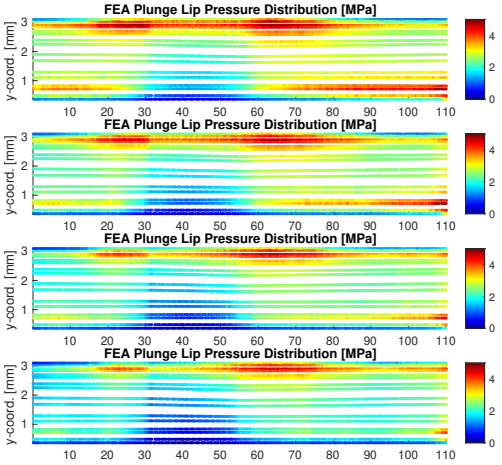

(a) $\mu = 0.2$

(b) $\mu = 0.4$

(c) $\mu = 0.6$

(d) $\mu = 0.8$

Figure 7.12: Plunge lip pressure distribution from FEAs with different friction coefficients μ between plunge and copper bottom plate. Plots have inaccurate aspect ratios.

7.4.3 Constitutive Model Assessment

The results from the simulations with the seven different constitutive models are presented in Table 7.11, Figure 7.13, and Figure7.14. The results indicate that all the constitutive models produce similar results except the linear model. One hyperelastic model was modeled nearly incompressible and no substantial difference could be found in its results in comparison with the other incompressible hyperelastic models.

Table 7.11: Plunge lip pressure distribution statistics dependent on different constitutive models.

Constitutive Model	Upper Limit ε	Incompressible	Mathematical Parameters [MPa]	Pres. Max [MPa]	Pres. Mean [MPa]	Pres. Variance [MPa]
Arruda-Boyce	100%	yes	$\mu = 4.8605, \lambda = 7.3603e+7, D_1 = 0$	4.751	2.201	0.573
Linear	420%	nearly	$E = 4.48, \upsilon = 0.499$	4.124	0.871	0.295
Mooney-Rivlin	150%	yes	$C_{10} = 1.1643, C_{01} = 1.3553, D_1 = 0$	5.097	2.317	0.641
Mooney-Rivlin	420%	yes	$C_{10} = 0.90913, C_{01} = 1.577, C_{11} = 0.030822, D_1 = 0$	4.934	2.252	0.619
Mooney-Rivlin	420%	nearly	$C_{10} = 0.90913, C_{01} = 1.577, C_{11} = 0.030822, D_1 = 0.0080446$ (Poisson's ratio=0.49)	4.996	2.318	0.622
Ogden	150%	yes	$\mu_1 = 14.977, \alpha_1 = 0.70576, D_1 = 0$	5.134	2.403	0.671
Yeoh	100%	yes	$C_{10} = 2.4303, D_1 = 0$	4.746	2.180	0.562

The force reaction plot further indicates that the hyperelastic models deform similarly throughout the simulation. Contact with the inductor wall can be seen as initialized at roughly 4 mm displacement. The linear model has a different deformation character.

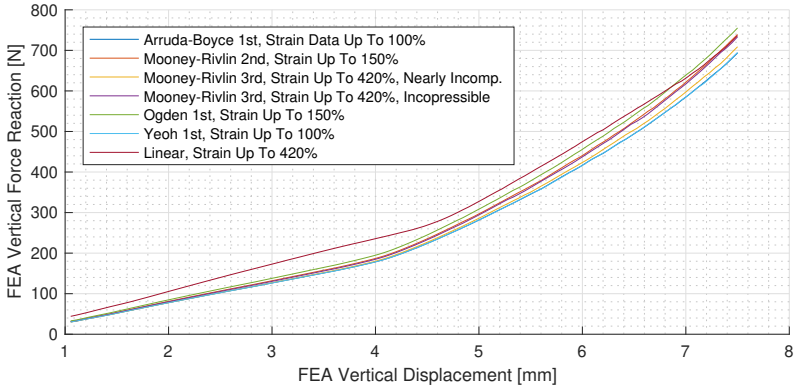

Figure 7.13: Force reaction in the y-direction as a function of FEA displacement and constitutive model.

Figure 7.14 signifies that no substantial difference in pressure distribution is noticeable between the hyperelastic constitutive models.

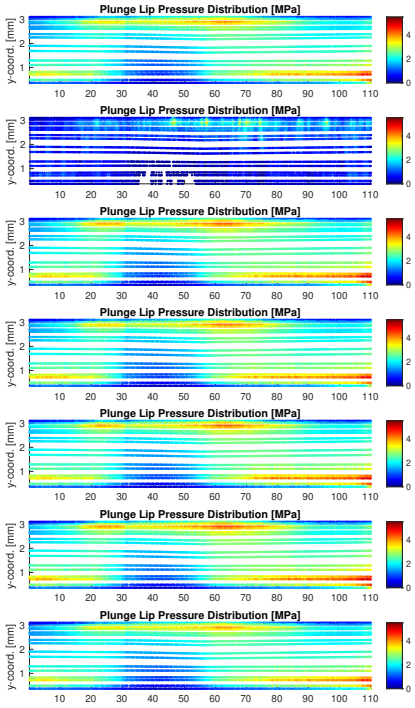

(a) Arruda-Boyce 1st order with strain data up to 100%. Incompressible.

(b) Linear with strain data up to 420%. Nearly incompressible.

(c) 2-parameter Mooney-Rivlin with strain data up to 150%. Incompressible.

(d) 3-parameter Mooney-Rivlin with strain data up to 420%. Nearly incompressible.

(e) 3-parameter Mooney-Rivlin with strain data up to 420%. Incompressible.

(f) Ogden 1st-order with strain data up to 150%. Incompressible.

(g) Yeoh 1st-order with strain data up to 100%. Incompressible.

Figure 7.14: Plunge lip pressure distribution from FEAs with different constitutive models. Plots have inaccurate aspect ratios.

The 2-parameter Mooney-Rivlin model was decided to be used in all forthcoming FEAs. Its fit to test data between -25% and 150% strain is visualized in Figure 7.15

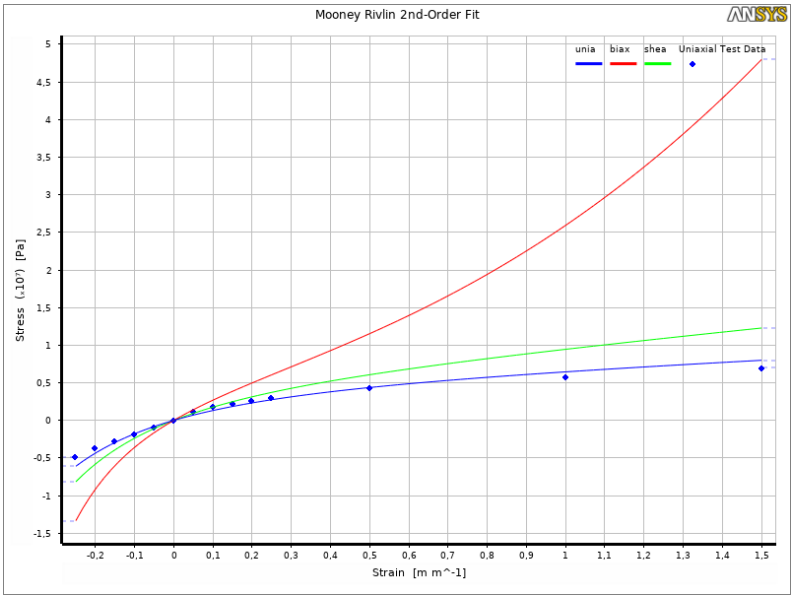

Figure 7.15: Uniaxial, biaxial, and shear stress-strain curves for 2-parameter Mooney-Rivlin model. Blue markers are uniaxial compression and tension test data.

7.4.4 FEA Validation

Table 7.12 contains FEA pressure distribution statistics for each of the 6 plunge units. The pressure statistics indicate much higher contact pressures in the FEA than in experiments. The table also contains both measured and computed vertical force reactions that show little correlation.

Table 7.12: Results from FEA validation experiments with 2 arbitrary plunge units from every plunge design.

Plunge Details		Mecmesin Results	FEA Results			
Serial Number	pd	$mmax$ (Measured) [N]	$4*$ Vertical Force Reaction @7.5 mm Expansion (FEA) [N]	Pres. Max [MPa]	Pres. Mean [MPa]	Pres. Variance [MPa]
40	$v1$	2320	3023	13.244	3.128	2.586
07	$v1$	2286	2598	15.224	2.677	2.705
35	$v2$	2177	2821	12.136	2.686	2.561
25	$v2$	2548	2789	14.737	2.682	2.846
110	$v3$	2242	3003	16.558	3.055	3.296
012	$v3$	2705	2943	14.772	2.948	2.850

The pressure distribution results in Figure 7.16 from the FEA validation experiments are noticeably different from previous simulations. The visibly more concentrated pressure peaks are assumed to be a result of using a coefficient of friction high enough to prevent sliding in the contact.

There are mainly 5 similarities between the FEA and experimental results that indicate a relatively realistic FEA model. They are:

- The mid-long side pressures in the v1- and v3-designs are significantly lower than other designs and have no or little contact at all in higher y-coordinates.
- The corner pressures in v2-designs are lower.
- The mid-long side pressures in v2-designs are vertically more spread-out.
- All results have higher pressures at the bottom of long sides.
- The beginning of the long side is often the region with the highest pressures.

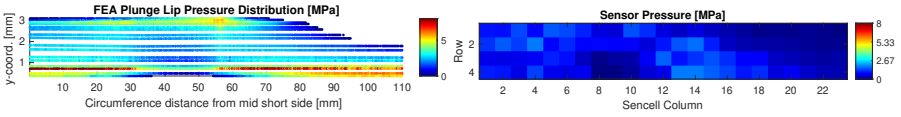

(a) From FEA, $pd = v1$, serial#40. pci=2.5 mm, pli=5 mm, psi=3.5 mm

(b) From experiment, $pd = v1$, serial#40. pci=2.5 mm, pli=5 mm, psi=3.5 mm

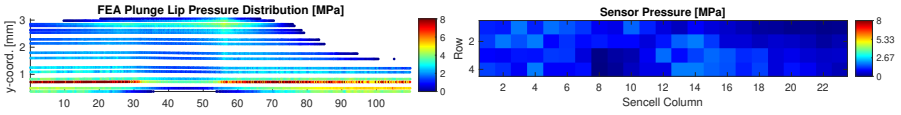

(c) From FEA, $pd = v1$, serial#07. pci=2.5 mm, pli=5 mm, psi=3.5 mm

(d) From experiment, $pd = v1$, serial#07. pci=2.5 mm, pli=5 mm, psi=3.5 mm

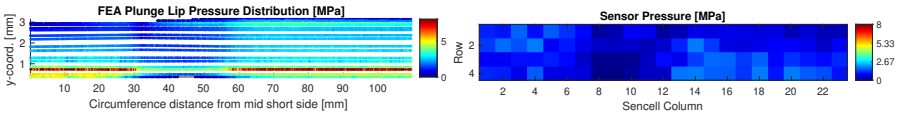

(e) From FEA, $pd = v2$, serial#35. pci=3 mm, pli=3.5 mm, psi=3.5 mm

(f) From experiment, $pd = v2$, serial#35. pci=3 mm, pli=3.5 mm, psi=3.5 mm

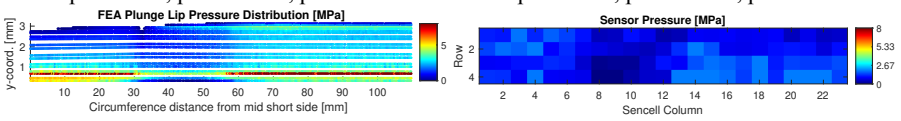

(g) From FEA, $pd = v2$, serial#25. pci=3 mm, pli=3.5 mm, psi=3.5 mm

(h) From experiment, $pd = v2$, serial#25. pci=3 mm, pli=3.5 mm, psi=3.5 mm

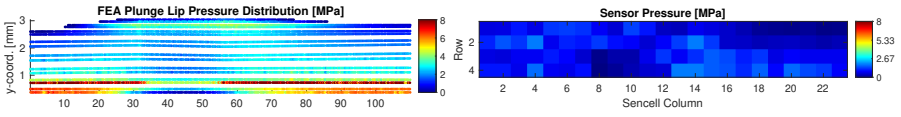

(i) From FEA, $pd = v3$, serial#110. pci=2.5 mm, pli=4 mm, psi=4 mm

(j) From experiment, $pd = v3$, serial#110. pci=2.5 mm, pli=4 mm, psi=4 mm

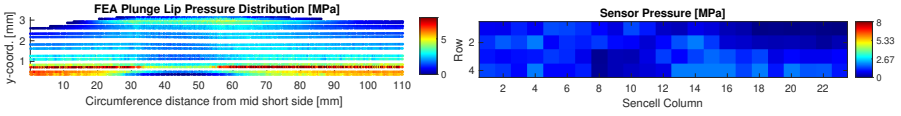

(k) From FEA, $pd = v3$, serial#012. pci=2.5 mm, pli=4 mm, psi=4 mm

(l) From experiment, $pd = v3$, serial#012. pci=2.5 mm, pli=4 mm, psi=4 mm

Figure 7.16: Plunge lip pressure distributions.

7.5 Indent Optimization

In this section, the four different RSM configurations will be compared by looking at their RMSE in relevant responses and the pressure distribution of their suggested optimal designs.

The 4 different RSM configurations are visible in Figure 7.17. The grey markers are some of the FEA experiments pressure variance responses as a function of psi, pli, and pci. The pressure variance response surfaces are also visible in the plots as functions of pli and psi and with the corner indent parameter pci having a constant value of 2.75 mm. Slight differences between response surfaces are visible and all of them have relatively flat minima near the center of the design space.

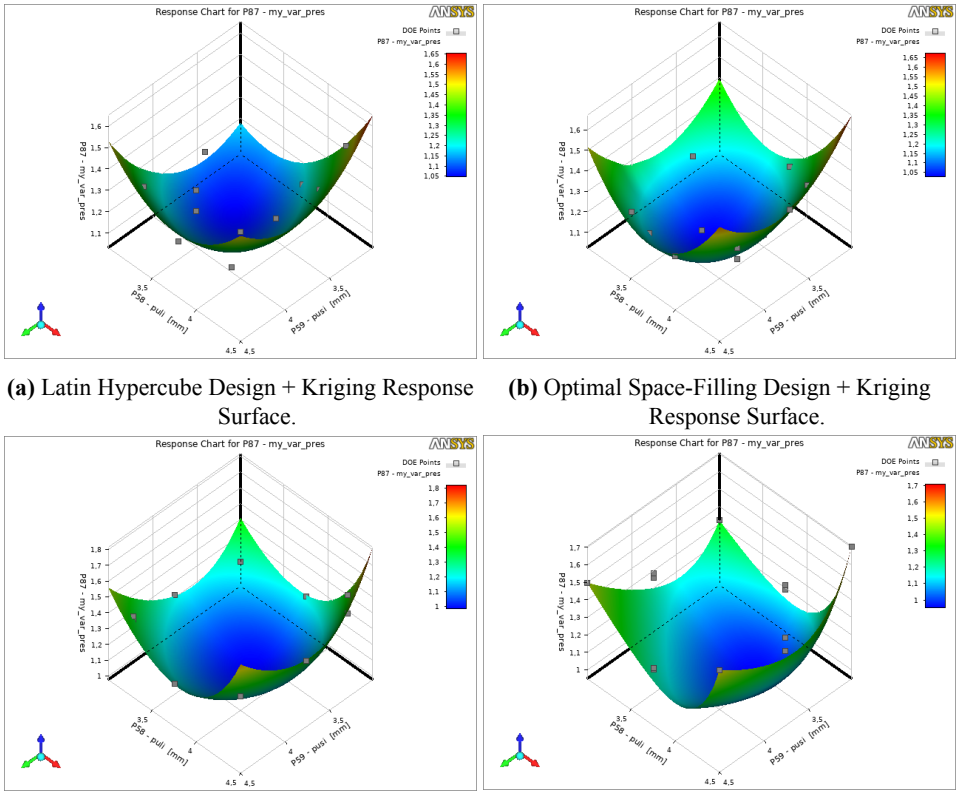

(a) Latin Hypercube Design + Kriging Response Surface.

(b) Optimal Space-Filling Design + Kriging Response Surface.

(c) VIF-Optimal Central Composite Design + 2^{nd}-order polynomial Response Surface.

(d) Box-Behnken Design + 2^{nd}-order polynomial Response Surface.

Figure 7.17: Pressure variance response surface as a function of plunge long side and short side indents. pci = 2.75 mm. Grey markers are DoE design points,

Table 7.13 contains a summary of the RSM configurations and their respective goodness of fit in terms of contact pressure variance RMSE and average friction stress RMSE. RS2 has the response surface with the best fit to pressure variance data and RS3 has the response surface with the best fit to average friction stress data.

Table 7.13: Goodness of fit data for the 4 different RSM configurations.

RSM Information				Root Mean Square Error (20 Verification Points)	
ID	Experimental Design	Response Surface	Number of Design Points	Pressure Variance [MPa^2]	Average Friction Stress [MPa]
RS1	LHD	Kriging	15	0.115	0.0042
RS2	Optimal SF	Kriging	15	0.043	0.0039
RS3	CCD VIF-Optimal	2^{nd}-order polynomial	15	0.075	0.0024
RS4	BBD	2^{nd}-order polynomial	13	0.056	0.0182

Figure 7.18 visualizes the goodness of fit of the 4 RSM configurations in predicted vs. observed charts. All response values have been normalized. The yellow markers represent the pressure variance response data and the blue markers, average friction stress data. Square markers are design points from the DoE that the response surfaces are fitted to. Round markers are verification design points. The Kriging interpolation response surfaces (7.18a and 7.18b) are visible having a perfect fit to the DoE data. The optimal space-filling RSM configuration seems to predict the verification points better than others. It has the best fit for higher response values as well.

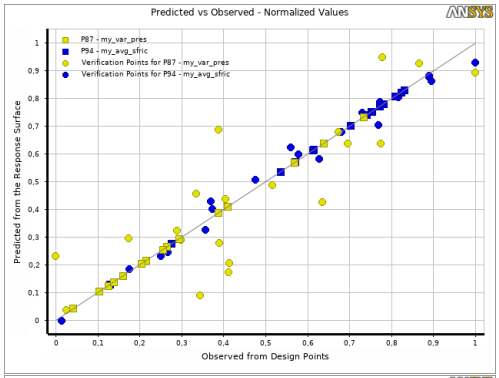

(a) Latin Hypercube Design + Kriging Response Surface.

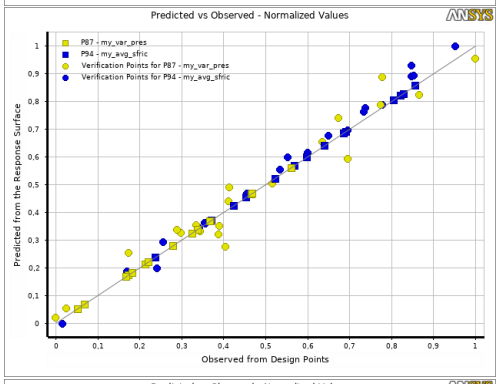

(b) Optimal Space-Filling Design + Kriging Response Surface.

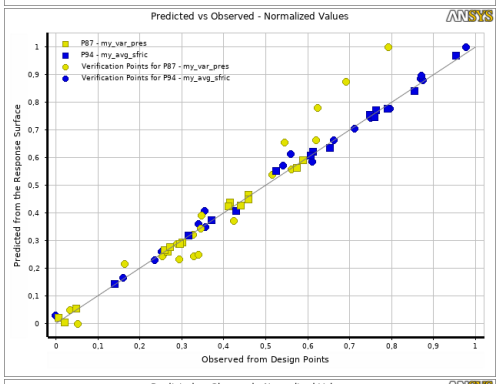

(c) VIF-Optimal Central Composite Design + 2^{nd}-order polynomial Response Surface.

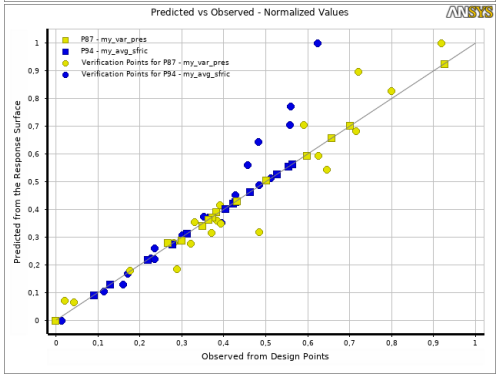

(d) Box-Behnken Design + 2^{nd}-order polynomial Response Surface.

Figure 7.18: Observed vs. predicted design point values.

Table 7.14 contains the response (output) and design parameter (input) values for optimal designs, 1 for each RSM configuration. In addition, three equivalent FEAs are listed for the v1, v2, and v3 140x120 plunges. The results are verified, meaning that they have been computed with the FEA with that design.

It is noticeable how the pressure distribution is least homogeneous with the v1 design, followed by v2 and then by the optimized designs and the v3 design. The RS2 optimal design received the lowest pressure variance (most homogeneous) even though the differences to the next designs are negligible. There is a smaller observed difference in average friction stress between the designs.

The optimal designs are similar to the v3 design but however with larger corner indents (pci).

Table 7.14: Design parameter values and verified results for optimal designs obtained from the 4 different RSM configurations and three old 140x120 designs.

	Contact Results (Verified)		Design Parameter Values [mm]		
ID	Pressure Variance [MPa^2]	Average Friction Stress [MPa]	psi	pli	pci
RS1	1.031	0.240	3.94	3.89	2.68
RS2	1.027	0.222	3.95	3.84	3.00
RS3	1.048	0.228	3.79	3.94	2.91
RS4	1.095	0.220	3.85	4.08	2.89
v1	1.820	0.210	3.50	5.00	2.50
v2	1.116	0.249	3.50	3.50	3.00
v3	1.090	0.247	4.00	4.00	2.50

The contact pressure distribution plots for the 7 designs, v1, v2, v3, and the 4 optimal designs from different RSM configurations, are visible in Figure 7.19. High pressures are apparent on the lower areas on the sides for all designs. The designs that have larger corner indents generally have lower corner pressures and smaller pressure peaks in the upper areas of the corners.

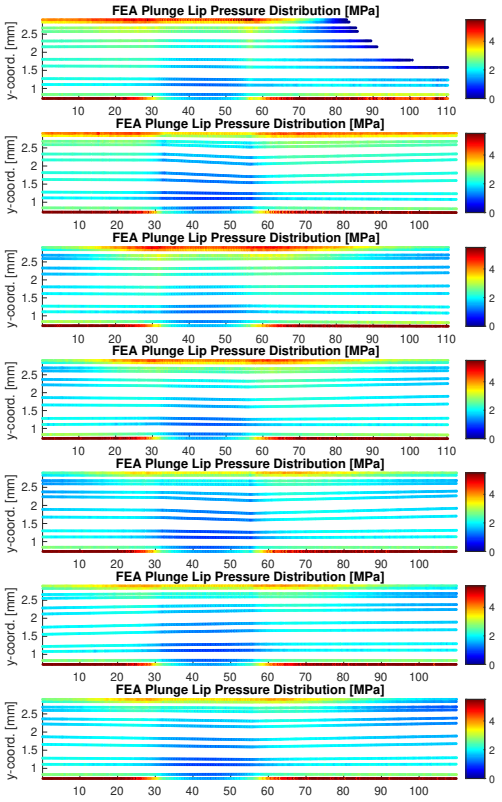

(a) v1 plunge design.

(b) v2 plunge design.

(c) v3 plunge design.

(d) Latin Hypercube Design + Kriging Response Surface.

(e) Optimal Space-Filling + Kriging Response Surface

(f) VIF-Optimal Central Composite Design + 2^{nd}-order polynomial Response Surface.

(g) Box-Behnken Design + 2^{nd}-order polynomial Response Surface.

Figure 7.19: FEA plunge lip pressure distribution for the four RSM optimizations and the v1, v2, and v3 designs for reference.

8 Discussion

This chapter begins with a list of accumulated limitations of this project. The results from the pressure distribution experiments, the FEA experiments, and the indent optimization will then be discussed. How the thesis methodologies and results were capable of achieving the objectives, will be assessed simultaneously as subjects are addressed.

8.1 Limitations of Study

Several limitations have been chosen to avoid pitfalls and to constrain the scope of the project to a level in accordance with the time frame. They are:

- The effects on the package seal quality caused by carton folds were not considered in the FEA nor the physical experiments except from the experiment with transverse carton components. A few conclusions can be drawn from this experiment and are further discussed in section 8.4.
- Dynamic and softening behaviour of the plunge material were neglected in the FEA modeling. So were changes in material properties due to environmental factors such as humidity and temperature as well.
- The mechanical behavior and effects of carton components were not considered in the FEA. The model was limited to analysis of the pressure distribution between the plunge and the inductor wall. However, the inductor wall was protruded with the thickness of the package components to more accurately resemble the actual distance between plunge lip and reaction components.
- Only three assessment experiments have been taken into consideration when developing the FEA in this project. The contact stiffness factors in both contacts are other settings whose levels potentially has a large influence on the

contact pressure levels. This can be tested in a fourth assessment, although the convergence stability might be endangered for higher contact stiffness factor levels.

The outcome of these simplifications are partially unknown and would, if considered, enhance the certainty of the research to develop a well-grounded framework for plunge tool optimization. Especially consideration taken to the carton folds as they have been a recurrent issue for ARPS. It was not found out how an effective and not too complicated consideration of carton folds would have been practically executed in the scope of this research.

The other two simplifications were however chosen in accordance with personnel at ARPS with deep subject knowledge and assumed to have relatively little effect on research accuracy.

8.2 Pilot Experiment - ANOVA

The pilot experiment indicated normality, observation independence, and similar treatment variances aside from 3 outlier observations. These are suggested to be caused by rotational misalignment of the plunge installment in these runs and could be remedied. The ANOVA F-value results using response function R1, indicating a significant difference in treatment means, can therefore be approved. The equivalent results using the R2 response function were less significant.

The experiment can be concluded to be successful considering its objective, to ensure significant treatment variances, to detect and treat test rig variance before the main experiments, and to test the response function.

8.3 Factor Screening Experiment

Looking at the box plot in 7.4, the differences in treatment variances are remarkable which might indicate violations of ANOVA assumptions. It is on the other hand not definitive for the overall experiment validity. The treatment means are still clearly separate for instance.

The difference in treatment variances as seen in 7.4 for PU plunge units, is believed to be caused by several factors. One is the different treatment population sizes, the v1 and v2 PU plunge units have fewer observations and thus less determined distributions. There is a possibility that this causes larger variances by occurrence. On the contrary, the smaller populations include replicate runs which should imply less variance. This applies to the FDM plunge units especially.

The smaller variances among treatments with lower response values could also be caused by the pressure reading limit of the sensor. This cut-off effect of pressure peaks results in less recorded variance than in reality. As mentioned, this is especially noticeable for FDM-plunge units. The box plot 7.4 indicates a much lower response variance for FDM populations.

8.3.1 Possible Use of FDM in Prototyping

Unfortunately, no correlation between PU and FDM plunge units with the same design have been noticed except for design v3. That is, the FDM plunges produced pressure distributions vastly different from the PU-plunge as seen in boxplot 7.4. This is believed to be caused by:

- In contrast to PU plunge units, they are not bonded to their aluminum adaptor, enabling more radial deformation.
- They are manufactured with an inner lattice structure (infill) that gives them different deformation properties compared to solid materials. As an effect, the measured shore A hardness values does not portray the entire plunge unit.
- They had pointier and thinner plunge lips that possibly caused pressure amplitudes exceeding the sensor reading limit and thus, resulting in low variance between column means.

Other possible causes with less known influence are:

- They have non-isotropic material properties caused by their filament structure.
- The geometries between PU and FDM plunge units differ not only in the measured dimensions but possibly also in other regions (surfaces, edges, etc) due to different manufacturing methods.

8.3.2 Screening Significant Factors

The 4 different MLR models had adequate fit and showed signs of meeting regression assumptions. Hence, the significant factors in these models are likely to be significant in reality as well. The most trustworthy models are the reduced models C and D judging from the four different R-squared measures and the plots of the standardized residuals. However, validation of the MLR models can be enhanced in several ways and Harrell (2015, p.110) points out that testing the model on a new data set is an especially effective one.

All of the 4 different MLR models distinguished the pd factor as the most significant. This is an important finding since it confirms that the indentation method is effective in changing the plunge lip pressure distribution. It is also promising that the other factors considered showed much less contribution to variance in pressure distribution, which is an important finding in robustness terms.

After assessing the different MLR models and their respective adequacy, the second most significant factors after pd are: $th1$ (height 1 deviation) and plw (plunge lip width). $th1$ is believed to be directly related to the effective expansion length of the mechanism and hence, might realistically also affect the pressure distribution variance. A physical explanation of relating plw to the pressure distribution variance could be that a wider plunge lip results in more plunge lip volume which causes more deformation resistance in radial expansion. Especially in corners where the plunge is protruded further, and as a result, the plunge is deformed unevenly when the plunge lip width is deviating.

The more insignificant factors are: tw (width deviation), tl (length deviation), $mmax$ (Mecmesin stiffness max value), $mslo$ (Mecmesin stiffness slope), and pla (plunge lip angle). The insignificance of the pla factor can possibly be explained with the use of the $R1$ response function since it only calculates the mean values for each pixel column and hence ignore vertical pressure differences.

It is important to understand that the chosen response variable in this experiment does not have to be correlated to package welding quality. Hence, the significant factors pointed out here may not be significant when producing a good package weld. The objective of this experiment has been to identify the most significant factors contributing to homogeneous pressure distribution.

8.4 Experiment With Transverse Carton Components

A correlation was found between Mecmesin stiffness and homogeneous pressure distribution (response function R1) for the PU plunge units as seen in the boxplot in Figure 7.10. The softest PU plunge unit produced the most homogeneous pressure distributions among PU-plunges and the stiffest plunge produced the least homogeneous pressure distributions. The $mmax_{mid,FDM}$-plunge with a measured $mmax$ value close to the $mmax_{mid,PU}$-plunge does however not comply with this trend, it produced more homogeneous pressure distributions than any other plunge unit despite its average stiffness. A similar anomaly is seen in the foregoing experiment which further signifies that the tested FDM plunge units are insufficient representations of their geometric PU equivalents. On the other hand, the homogeneous distribution produced by FDM plunge units can in this case as well potentially be affirmed by the sensor pressure limit.

A physical explanation of the trend seen between PU plunges could be that softer plunge units are more capable of enclosing the protruded folds, resulting in an increased contact surface area, and hence a more evenly distributed expansion force. This capability should be reflected in the shore A hardness of the plunge units. However, the related plunge units were measured to $M_{sha}°$ - $D_{sha}/2°$ for the stiffest and softest PU plunge units, $M_{sha}°$ for the PU plunge unit with average stiffness, and $M_{sha}° + D_{sha}°$ for the FDM plunge unit. The proposition of enclosing-capability can therefore be questioned by this fact. However, as mentioned before, the shore A measurement test should be reviewed due to the violation of ISO standards for such tests.

The 4 different R-squared values signifies a reasonably good fit of the model and therefore significance in the experiment treatments. However not as good as in the factor screening experiment. This probably has to do with the transverse carton folds that are assumed to have caused the many outliers visible in the boxplot in Figure 7.10.

As mentioned in section 4.5, this experiment was subject to several errors and experimental design violations such as not utilizing randomization. As seen in Figure 7.11b, external factors were seen to build up over time (test runs) and affected the R2 response. It is expected to have affected the R1 response and hence the model fit as well. In conclusion, the influencing factors of the experiment outcome is difficult to determine.

8.5 FEA Model

The element size experiment showed relatively random and small dispersion in contact pressure results dependent on element size. It is worth mentioning that the mesh in the plunge lip region was intact in all 4 experiment runs. It is possible that the computed pressure results are subject to substantial singularity-related error and that the plunge lip mesh needs to be further refined to reflect the real pressure values and to be successfully used as a response variable in the RSM optimization. An alternative interpretation could be that the contact pressure values from the simulation with 1 mm element size are the most accurate. To find out, further experimental runs, with overall smaller element sizes, should be able to produce more converged contact pressure results that could be used for comparison.

It is remarkable how the element count suddenly grows with smaller element sizes in the element size experiment, the same goes for the computation time. It is also noticeable how the reaction force $max4 * R_y$ steadily grows before converging for element size 2 mm and 1 mm. Accuracy in results can hence be concluded to be a trade-off to computation time in this case. 2 mm was finally considered to be an appropriate global element size.

Finding a well-functioning mesh has to large extent been a trial and error procedure and the chosen meshing method is by no mean an optimal one. Further study in mesh methodologies to obtain even better results is encouraged.

The coefficient of friction experiment was successful in assessing how the coefficient of friction (μ) value impacts plunge lip contact pressure. The pressure generally decreases with higher μ-values and does not affect the pressure variance significantly. These results cohere with increased friction stresses for simulations with higher μ-values and hence resisted radial expansion of the plunge. It can therefore be concluded that an approximated and potentially inaccurate value on μ is not devastating for the purpose of this FEA.

Lastly, the choice of hyperelastic constitutive model was seen to not significantly affect the results considering the objectives of this FEA. Consequently, the 2-parameter Mooney-Rivlin model randomly chosen to be used in further simulations. It was however observed that the linear elastic model generated completely different results. Linear models should therefore be avoided for modeling elastomer plunges in the future.

8.5.1 FEA Validation

The comparison of FEA and experimental pressure distributions have several visual similarities as mentioned in section 7.4.4. The differences in pressure amplitude are however remarkable. Factors that are believed to be responsible for these differences are:

- The sensor pressure limit of 1.93 MPa suppressed the actual pressure distribution peaks and thus caused lower average pressures.
- The uniaxial material test data does not describe the actual material properties enough. Further experiments, for instance related to shear and compression stresses, since the FEA is subject to these deformation modes to a large degree, could enhance the accuracy of the constitutive model.
- The available material test data are inadequately representing the actual material properties of the PU in the plunge units tested.
- The carton and tape layers in the physical experiments act as cushioning and distributes the contact pressure over a larger area than the plunge lip itself. As a result, the average pressure is decreased and the pressure peaks are lowered.
- The CAD and the real plunge geometries vary in dimensional features such as deviating surfaces and edges not considered. Hence, the simulation deformation of the plunge differs from the actual.

The nonexistent correlation between measured Mecmesin force reaction and FEA vertical force reaction is also remarkable. The FEA force reaction has shown no sign of being subject to substantial numerical error in other experiments (see Tables 7.10 and 7.9). In this FEA experiment however, the values differentiate with almost 450 N. The differences are suggested to be caused mainly by how the geometric deviations were implemented in the CAD model and how the CAD model in general differs from the real plunge geometries.

The adequacy in terms of modeling pressure distributions has always been more important than modelling correct pressure magnitudes. The overall adequacy of the FEA model should be assessed dependent on what use case it is purposed for. In the following section, the model adequacy in terms of adapting plunge tools will be assessed.

8.6 Indent Optimization

The 4 RSM configurations produced similar response surfaces with slightly varying prediction capability in terms of RMSE. The choice of experimental design and response surface model is therefore seen as important.

Figure 7.18 contains predicted versus observed response-charts for the 4 RSM configurations. The CCD and BBD experimental designs with 2^{nd}-order polynomial response surfaces have good prediction capability for lower response values but less so for higher response values. The OSF design used together with a Kriging response surface model managed to model the system with better prediction capability in the entirety of the design space.

It is worth mention that the goodness of fit for the OSF model is relatively low however, the prediction errors for some of the design points are high. Whether the errors are too high is difficult to address without more testing in real-life applications. It can be assumed that a model has reached a sufficient level of adequacy when it can generate well-functioning plunge designs for several different package formats.

The accuracy of modeling the system and hence the prediction capability, is expected to increase for all 4 RSM configurations if more design points are used in the DoE. This will increase the resolution of the system response. It is unclear whether the 2^{nd}-order polynomial response surfaces will be capable of modeling the potentially more complex curvature of the system. The Kriging interpolation model, however, should perform better in this task.

A noticeable difference between the 4 optimized designs exists in design parameter values but also in contact pressure variance. However, all of them had the lowest contact pressure variance together with the v3 design which is a good sign of optimization relevancy.

One strength of the contact pressure variance variable is its independence to the average contact pressure magnitude. The variation in magnitude between measured and computed magnitude mentioned in the foregoing section and in section 7.4.4 is therefore seen as immaterial. At least for the purpose of minimizing contact pressure homogeneity.

The pressure distributions of the optimized designs in Figure 7.19 are however not so homogeneous as one might have hoped for. The contact pressure variance, and consequently the response variable, are to, a large degree, affected by the pressure peak regions on the upper and lower edges of the plunge lip. These peaks are also

expected to have caused relatively flat response surface optima.

A new less skewed response variable that avoids the inclusion of pressure peaks in the variance calculation (if possible) could result in optimized more homogeneous pressure distributions. Such a response variable could in addition generate a more expressed optimum that facilitates the decision of optimal indentation values. More than that, the objective of minimizing contact pressure variance is seen as adequate.

An alternative approach to reduce the influence of pressure peaks on plunge lip edges could be to model the plunge lip with a blunt radius of 20 mm or so. It would not significantly differentiate the CAD model from the real plunge tool but probably even out the pressure peaks over the vertical middle of the plunge lip.

The second optimization objective of minimizing average friction stress in the plunge lip contact is seen as helpful. A single objective function of minimizing the pressure variance was found to converge to the highest possible indentation values in initial RSMs which caused unwanted substantial vertical lip movement.

The implementation of RSM to optimize the indentation design parameters is considered promising for future plunge tool development. With relatively small designed experiments (15 or 13 design points), the methodology was successful in finding indentation values for 3 design parameters.

The OSF design used together with an interpolation response surface model such as Kriging, has shown the best system modeling capability. Proposed methodology adjustments that can enhance the stability and usability of the RSM configuration are:

- Developing a slightly different response variable with better capability of indicating useful homogeneous pressure distribution.
- Adding a slight radius over the entire plunge lip with an estimated radius of 20 mm in the CAD model. It can potentially even out contact pressure peaks near the plunge lip edges that are noticed to confuse the current contact pressure variance response variable.
- Increasing the number of design points in the experimental design.

9 Conclusions

An alternative plunge tool adaptation framework has been developed and reached a proof-of-concept state in this thesis. It is intended to be transferable to any new package format and be adjustable to alternative use cases. It has been built with the functions in ANSYS Workbench 2020 R1 but should be implementable on other FEM software packages in combination with a statistical programming language such as R. The setup time for such a tool has been estimated by ARPS to one week but it depends on many factors such as: which software to be used, available resources, and competence. This thesis covers many of the obstacles encountered when developing such a tool and will hopefully at least be of much help to anyone who proceeds with the same development.

A purpose-built FEA model serves as the core of the framework. It has proven to produce plunge lip pressure distribution results at a level of detail previously not available. However, the magnitude of the simulated contact pressure is far-off but this fact is expected to have little importance to the framework use-case.

Physical experiments have been conducted to validate the model. The model showed promising performance for the purpose of the FEA although further validation and model adjustments are needed in terms of other results. The significance of some model uncertainties such as element size, coefficient of friction, and choice of constitutive model, have been assessed by testing multiple configurations. In both systems, high pressures in the transition zone between plunge lip corner and sides were detected.

A regression analysis based on experimental design theory has been performed on FEA model-equivalent physical experiments. It has objectively identified the plunge design as the most influential factor, contributing to the plunge pressure distribution, followed by plunge height and lip width. Other system factors such as plunge stiffness and hardness had little influence on pressure distribution but probably more on transverse carton folds. The regression analysis has therefore been useful for mainly three things: Firstly, to confirm that the plunge pressure distribution effectively can

be adjusted with the use of plunge lip indentation. Secondly, that most system factors can be neglected in the framework but that deviations in plunge height and lip width should be paid attention to.

Thirdly, large differences between the pressure distribution of FDM manufactured and PU plunge units have been identified. The differences are likely not dependent on the experiments themselves. The use of FDM prototyping in its current state to examine the performance of prospected PU plunge designs is therefore questionable. However possible with a couple of suggested adjustments to the AM method. The suggested adjustments are: bonding the FDM body to the aluminum plunge tool adaptor. Using a solid core structure instead of infill. Explore alternative AM methods with higher geometric preservation and more isotropic material properties.

RSM was used together with the FEA model to optimize the plunge tool's three indentation design parameters after a hypothetical objective function. Four different RSM configurations have been verified and compared. An optimal space-filling experimental design used together with a Kriging interpolation response surface was most capable of modeling the FEA response.

An optimized plunge design can this way be obtained in roughly 24 hours using 4-cores of an average desktop computer from 2013. This framework has thus the potential to enable high performance in the first plunge tool design iteration. In contrast, the existing iterative design process often requires up to 3 iterations. Further validation and adjustment to ensure that the optimized plunge design actually performs well for multiple package formats is however recommended. The most recommended adjustment is to choose a more relevant response variable from the FEA and if needed, more design points in the experimental design could ease for higher optimization algorithm decisiveness.

The engineering tools presented in this report are encouraged to be used in other process improving applications as well. Some of them are cheaper and quicker to implement if data is available, such as regression analysis to trace responses to influential factors and to increase the understanding of any system. Setting up a functioning FEA and RSM environment requires more resources but if implemented, large savings on development cost and time can be made in addition to enhancing the plunge performance.

10 Recommendations for Further Research

These are ideas and insights for further research that have been brought to mind during the project course. They are listed in a random order and it is up to ARPS to decide what points are appropriate to address.

- Further development of the plunge design.
  - Flodberg, Eriksson et al. (n.d.[a]) found that the variable cross-section of the plunge is causing less plunge lip pressure in the corners. A constant or near-constant cross-section could be realized by radially extending the aluminum part of the plunge. Currently, the cross-section is more extended in the corners. An optimal radius of the aluminum part of the plunge could be obtained by setting this dimension as an input factor in an RSM optimization. The plunge lip pressure distribution could that way potentially be further homogenized.
  - Both experimental and FEA data indicates increased plunge lip pressures in the transition zones between corner and sides. A redesigned plunge circumference profile could eliminate these pressure peak zones and produce more pressure in the corners.
- Further research on transverse carton component folds.
  - How they can be avoided.
  - Inspect them more closely using a microscope to understand how they can be treated.
  - How they are affected by increased/decreased pressure and shear friction (the plunge design). What is an optimal plunge design that resolves issues with base carton folds, maybe not homogeneous pressure distribution?
  - Conduct experiments with an objective to determine optimal plunge lip stiffness and contact pressure.

  - Further research in whether $mmax$ (Mecmesin stiffness) is the most influencing factor in treatment of transverse carton folds. Statistical analysis could potentially reduce the amount of discarded plunge units.

- Further explore AM technologies. Use Hagelqvist (2018) and other AM knowledge in ARPS as a basis.
  - In the use of producing prototypes. FDM-plunges should be printed solid to resemble the PU-plunge properties more. Glue FDM-printed plunge onto aluminum part of a plunge for instance.
  - In the use of producing PU fabrication molds.
  - To replace PU plunges.

- Verify the quality control, its noise factors (durometer, Mecmesin equipment, operator errors, etc...), and its objective. Vieira et al. (2020) gives an evaluation of uncertainty on Shore hardness measurements that potentially could be of good use.

- Explore new measurement methods used in quality control such as touch-trigger probes or 3D-scanners that can be used to compare manufactured plunges with CAD-model. Detect deviating edges and surfaces. Use statistical analysis to relate tolerance avoidance to plunge performance and manufacturing causes.

- Conduct more pressure distribution experiments.
  - Create a Cause-and-Effect diagram together with all involved personnel. The effect (response) should ultimately be package weld quality but can alternatively be contact pressure distribution such as in this report. Discuss the impact of each cause. Choose new factors to study and conduct designed experiments to obtain objective insights on process improvement. For example, use the guideline in Coleman and Montgomery (1993).
  - More replications and fully randomized experiments to assess the effect of base carton folds on the pressure distribution.
  - Using sensors that has a sufficient cutoff sensing limit for the experiments (10 MPa). Further, diminish noise factors.
  - With more material data (plunge units) and possibly more factors (elaborate on expansion length, AM plunges, etc.), factor levels, and replications to more thoroughly identify significant system factors. Although it is possible that the plunge design factor on its own can make the package welding process robust.

- Apply more thoroughly methods of validating the structural FEA.

  - Conduct FEA and experimentation on a simpler geometry that has fewer error factors (basic cylinder or similar). Assess the need for further or improved material tests and test data. Create comparison graphs in system responses.
  - For example, such methods that use Bayesian statistical methodology and likelihood methodology as proposed by Bayarri et al. (2007).
  - Consider changing friction coefficient between plunge and inductor wall. It is currently 0.1, almost frictionless which leads to sliding and leveling of the contact pressure distribution. In reality, base cartons might be restricting vertical movement.

Further studies in optimization methodologies of structural FEAs.

- Other types of experimental designs or improved designs used in this report.
- Other types of response surfaces or predictive methods such as sparse-grid or neural networks.
- Use of generative design algorithms.

Explore the possibilities of adjusting induction heat distribution.

- Is it possible to increase heat in corners to increase melting of PE and increase seal quality?
- Conduct designed experiments to optimize induction heat parameters.

Bibliography

Ali, A., Hosseini, M. & Sahari, B. (2010). A review of constitutive models for rubber-like materials. *American Journal of Engineering and Applied Sciences*, *3*, 232–239.

ANSYS Inc. (2017). Mechanical apdl theory reference [Online; accessed November 7, 2021]. https://www.mm.bme.hu/~gyebro/files/ans_help_v182/ans_thry/ans_thry.html

Arora, J. (2017). *Introduction to optimum design*. Academic Press is an imprint of Elsevier.

Austrell, P. (1997). *Modeling of elasticity and damping for filled elastomers* (Doctoral dissertation) [Defence details Date: 1997-04-10 Time: 10:15 Place: John Ericssons vag 1, V:C External reviewer(s) Name: Hibbitt, David Title: Professor Affiliation: HKS Inc., 1080 Main Street, Pawtucket, RI 02860 —]. Structural Mechanics. Structural Mechanics, Lund University.

Bayarri, M. J., Berger, J. O., Paulo, R., Sacks, J., Cafeo, J. A., Cavendish, J., Lin, C.-H. & Tu, J. (2007). A framework for validation of computer models. *Technometrics*, *49*(2), 138–154. https://doi.org/10.1198/004017007000000092

Coleman, D. E. & Montgomery, D. C. (1993). A systematic approach to planning for a designed industrial experiment. *Technometrics*, *35*(1), 1–12. http://www.jstor.org/stable/1269280

Dahlin, R. (1987). *Expanderbar plunge för ändförslutning* (SE457946). https://tc.prv.se/spd/p/patent?token=03AGdBq25NdA2ZFITa0CLdqc9ZNDR2uJFRvtloy5_9c7Eb1TP8gcYJw_DIZlVJJqQ-ysFkxCTQ6oxT6uk2hXqRYCQCnGph9DM1inYRDwzQTkG-ZJWS2W-9GM9HiXEfdCO0J08vggF7DQxExmpXfI9WRO9_JeomXncw0By323KP_xTPU_YJ_7BOeUWouo4DOMS46IReTfy91CYlgUr9llBu6-hsE-ldv_OI-gRLIHizFdFRmVj8iJqUZVzPR1UE__5aTlX-8po4K1HwTRIpLpssIyAMiz14rvYG1LvO233sU4j8makxTLqBKy-Qp2rXJjar4VvOj-CmgPQM_vY8XKX8_FG0rGMJDPTuGR2sBP57dTWPNhBDvn-0XZ1IRfUj6YkGO6BHs81N7V65xyAvNReQ6zHtnnu5DvvEkYUTvAZ9dOG9CmN6xsRbBAP_d&p1=gfNhDf51M4t7eM42P9NdVA&p2=dkzDqaPsPQY&content=plunge&lang=en&tab=1&hits=true&hitsstart=0&start=0

Designxplorer user's guide (2020 R1). (2020). ANSYS, Inc. Winston-Salem, NC, USA.

Flodberg, G., Eriksson, M., Friberg, I. & Nilsson, S.-B. (n.d.[a]). *Delrapport 19:1.* [internal document].

Flodberg, G., Eriksson, M., Friberg, I. & Nilsson, S.-B. (n.d.[b]). *Delrapport 19:3.* [internal document].

Flodberg, G., Eriksson, M., Friberg, I. & Nilsson, S.-B. (n.d.[c]). *Delrapport 19:4. tryckmätning med olika plunschar mot olika förhöjda kopparplattor* [internal document].

Flodberg, G., Friberg, I. & Nilsson, S.-B. (n.d.[a]). *Delrapport 7. uppmätning av tryck från plunsch mot cekacan burkens vägg* [internal document].

Flodberg, G., Friberg, I. & Nilsson, S.-B. (n.d.[b]). *Preliminär delrapport 4. tryckoptimering.* [internal document].

Hagelqvist, P. (2018). *Framtagning av plungar med hjälp av 3d-printing för tillverkning av förpackningsprover* [internal document].

Harrell, F. (2015). *Regression modeling strategies : With applications to linear models, logistic and ordinal regression, and survival analysis*. Springer.

Jones, B. & Johnson, R. (2009). Design and analysis for the gaussian process model. *Quality and Reliability Eng. Int.*, *25*, 515–524. https://doi.org/10.1002/qre.1043

Joseph, V. R. (2016). Space-filling designs for computer experiments: A review. *Quality Engineering*, *28*(1), 28–35.

Marckmann, G. & Verron, E. (2005). Efficiency of hyperelastic models for rubber-like materials.

Minitab. (n.d.). Ways to identify outliers in regression and ANOVA [Online; accessed November 24, 2021]. https://support.minitab.com/en-us/minitab/18/help-and-how-to/modeling-statistics/regression/supporting-topics/model-assumptions/ways-to-identify-outliers/

Montgomery, D. C. (2013). *Design and analysis of experiments: International student version*. John Wiley; Sons.

Myers, R. H., Montgomery, D. C., Vining, G. G., Borror, C. M. & Kowalski, S. M. (2004). Response surface methodology: A retrospective and literature survey. *Journal of Quality Technology*, *36*(1), 53–77. https://doi.org/10.1080/00224065.2004.11980252

Tekscan. (n.d.). Sensor construction image [Online; accessed November 7, 2021]. https://www.tekscan.com/sites/default/files/SensorConstructionImg.png

Vieira, T., Lundberg, J. & Eriksson, O. (2020). Evaluation of uncertainty on shore hardness measurements of tyre treads and implications to tyre/road noise measurements with the close proximity method. *Measurement*, *162*, 107882. https://doi.org/https://doi.org/10.1016/j.measurement.2020.107882

Wu, C. F. J. (2015). Post-fisherian experimentation: From physical to virtual. *Journal of the American Statistical Association*, *110*(510), 612–620. https://doi.org/10.1080/01621459.2014.914441

A Appendix A

A.1 Initial Activity List

- Attain adequate material properties of the polyurethane material used for the plunge tools.
- Develop a FEA of the plunge expansion mechanism. Assess the significance of model simplifications in interest of saving computational and experimental resources, and software independency.
- Validate the FEA-model by conducting appropriate experiments with attention to induced pressure distribution between plunge and package components during the welding mechanism.
- Use the FEA to optimize a plunge design in terms of 4 design parameters in the CAD model.
- Literature review of AM technologies and materials with the goal to find alternatives that meet the requirements for plunge tools. The considered requirements are related to attributes such as fatigue strength, stiffness, surface finish, manufacturing time, and cost.
- Use the FEA and manufactured prototypes to explore the potential use of AM plunge tools.

B Appendix B

B.1 Pilot Experiment

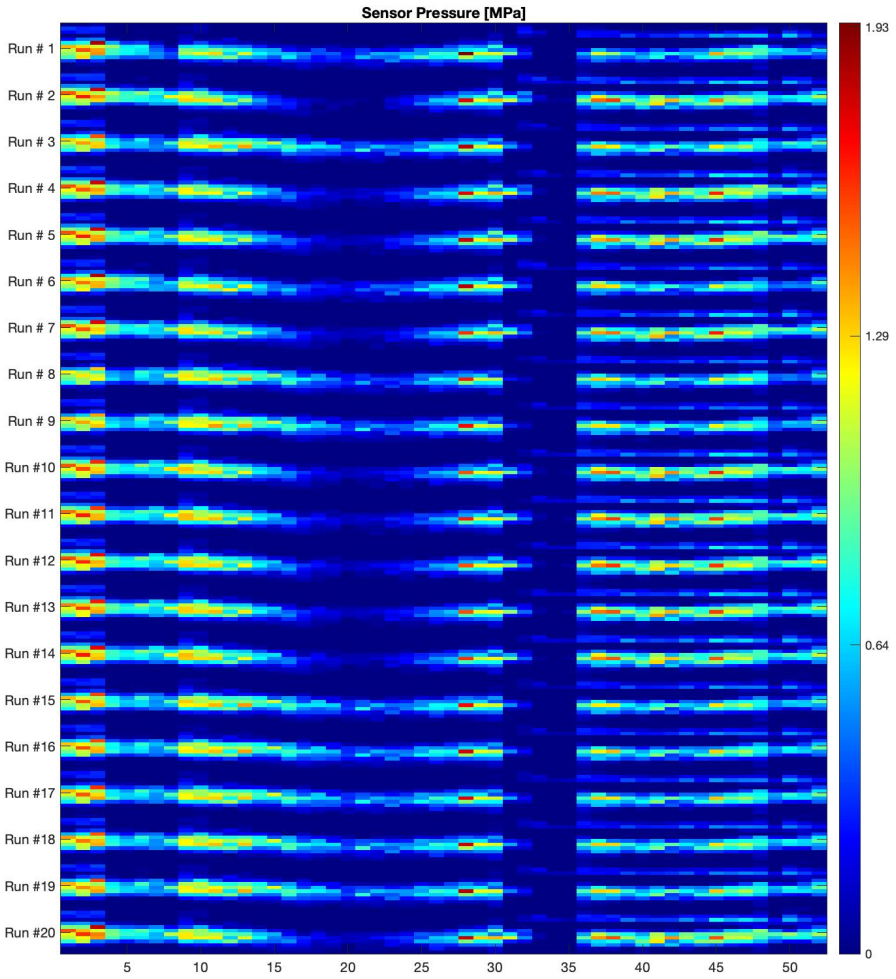

Figure B.1: Pressure distribution images from the pilot experiment. A v3 design plunge unit (*EP2021-04-26#111*) and a v1 design plunge unit (*WaM 201201#40*) being tested in random order. The v3 plunge is tested at run 1, 3, 6, 8, 9, and 15-19.

B.2 Factor Screening Experiment

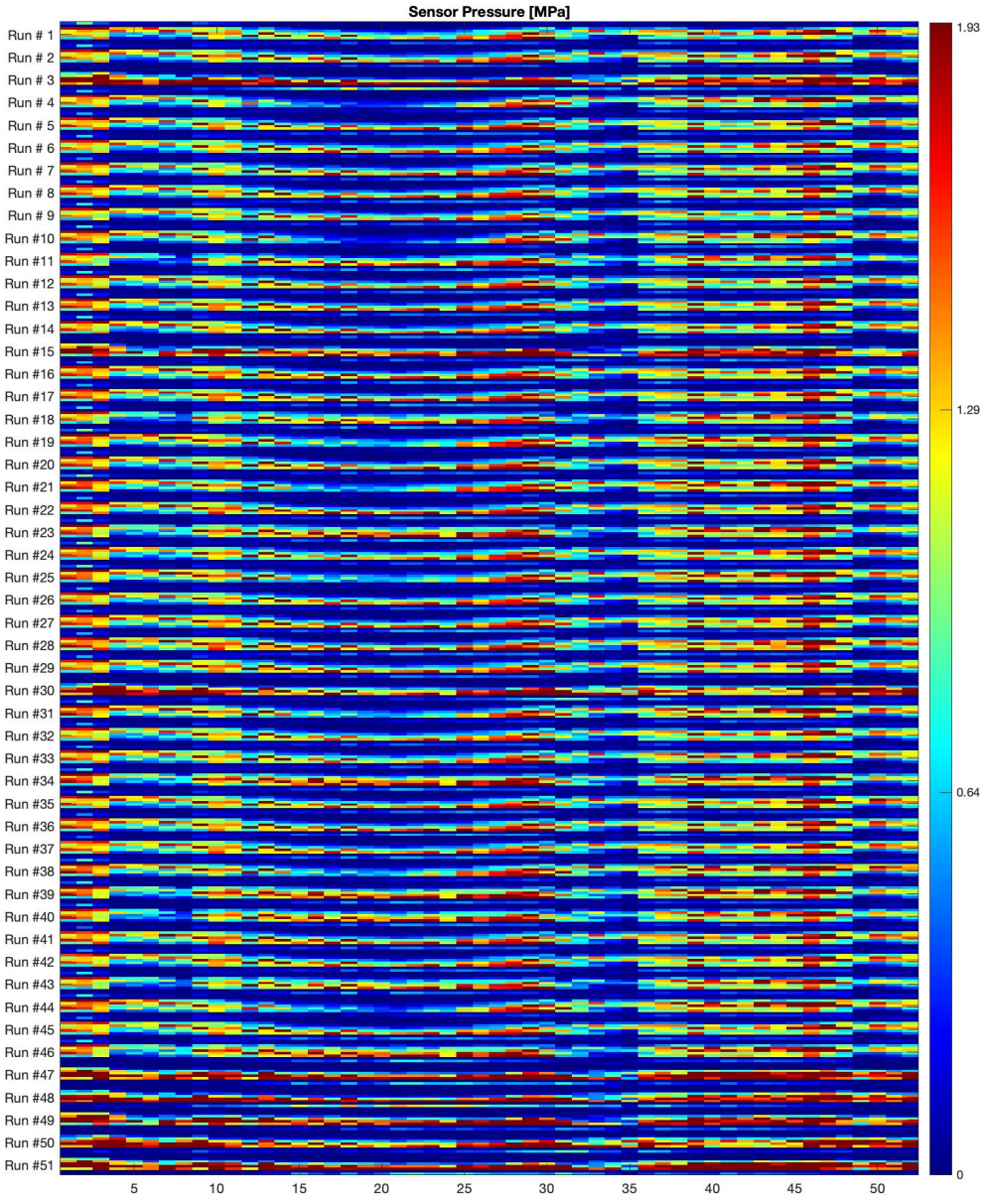

Figure B.2: Pressure distribution images from the factor screening experiment.

expansion #	Plunge Serial	Design
1	EP2021-04-26#111	v3
2	EP 2021-04-26#106	v3
3	3D 1	v2
4	WaM 201201#40	v1
5	EP 2021-04-26#049	v3
6	EP2021-04-26#110	v3
7	EP2021-04-26#119	v3
8	EP 2021-04-26#062	v3
9	EP 2021-04-26#077	v3
10	WaM 201201#13	v1
11	WaM 201201#34	v2
12	EP 2021-04-26#075	v3
13	EP 2021-04-26#034	v3
14	EP2021-04-26#120	v3
15	3D 3	v3
16	EP 2021-04-26#093	v3
17	EP 2021-04-26#058	v3
18	WaM 201201#35	v2
19	WaM 201201#07	v1
20	EP 2021-04-26#061	v3
21	WaM 201201#24	v1
22	EP 2021-04-26#045	v3
23	WaM 201201#25	v2
24	EP2021-04-26#112	v3
25	WaM 201201#07	v1
26	EP2021-04-26#118	v3
27	EP 2021-04-26#092	v3
28	EP 2021-04-26#012	v3
29	EP 2021-04-26#073	v3
30	3D 2	v4
31	WaM 201201#13	v1
32	EP 2021-04-26#070	v3
33	EP2021-04-26#111	v3
34	WaM 201201#22	v2
35	EP2021-04-26#123	v3
36	EP 2021-04-26#048	v3
37	EP 2021-04-26#055	v3
38	WaM 201201#24	v1
39	WaM 201201#22	v2
40	WaM 201201#34	v2
41	EP 2021-04-26#047	v3
42	EP 2021-04-26#114	v3
43	WaM 201201#35	v2
44	WaM 201201#40	v1
45	EP 2021-04-26#076	v3
46	WaM 201201#25	v2
47	3D 4	v1
48	3D 1	v2
49	3D 3	v3
50	3D 2	v4
51	3D 4	v1

Table B.1: Plunge units used in each respective expansion in the factor screening experiment.

B.3 Experiment With Transverse Carton Components

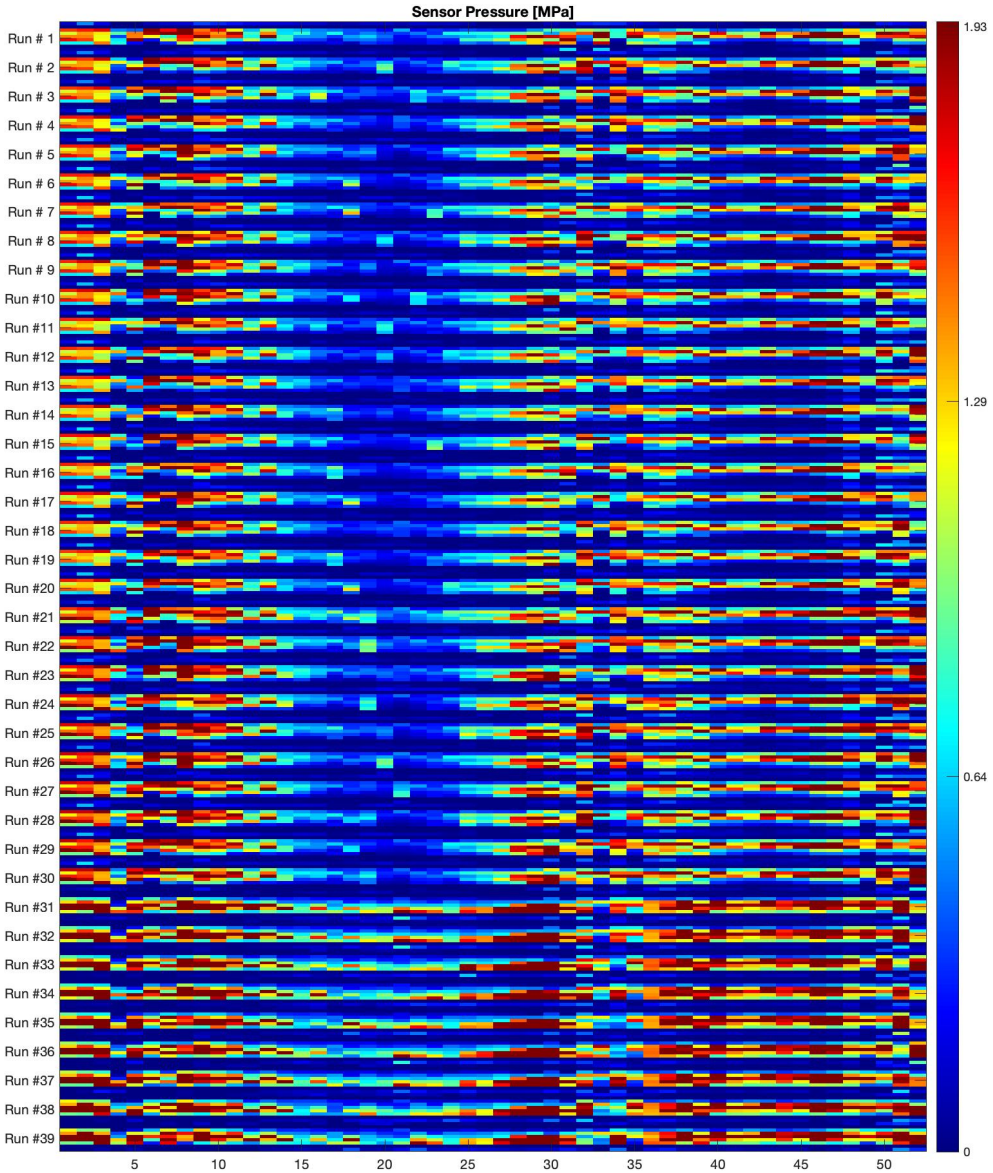

Figure B.3: Pressure distribution images from the experiment with transverse carton components.

B.4 Experiment 6

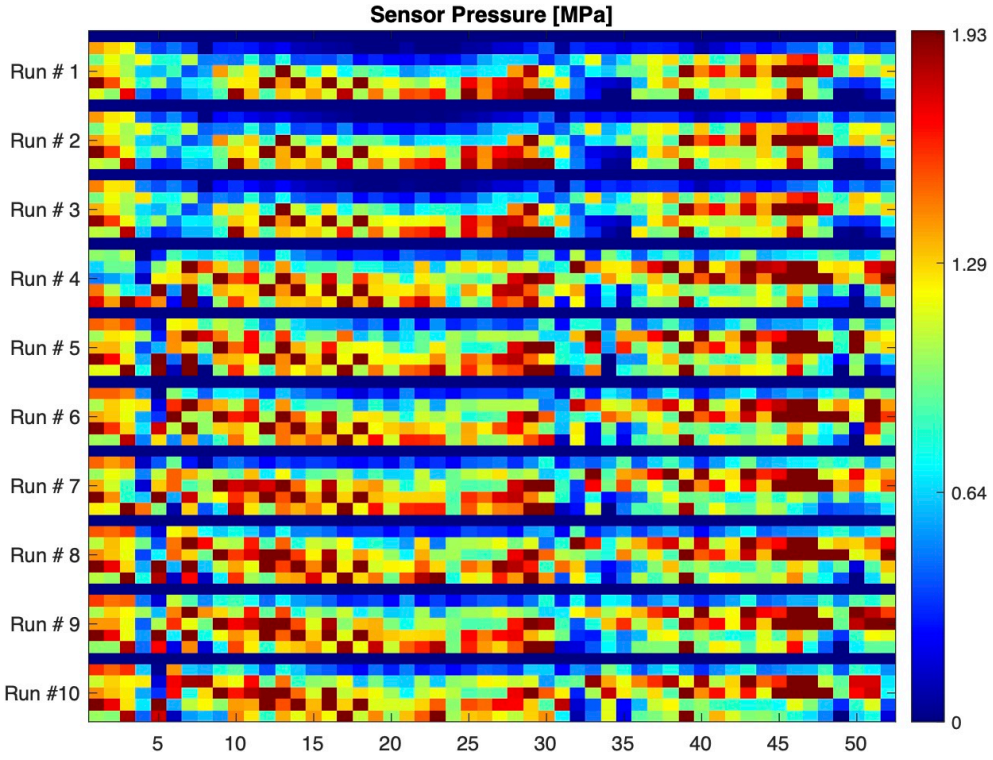

Figure B.4: Pressure distribution images from the sixth experiment. Plunge *EP 2021-04-26#012* is being tested three times without a transverse carton component and then seven times with.

B.5 Experiment 7

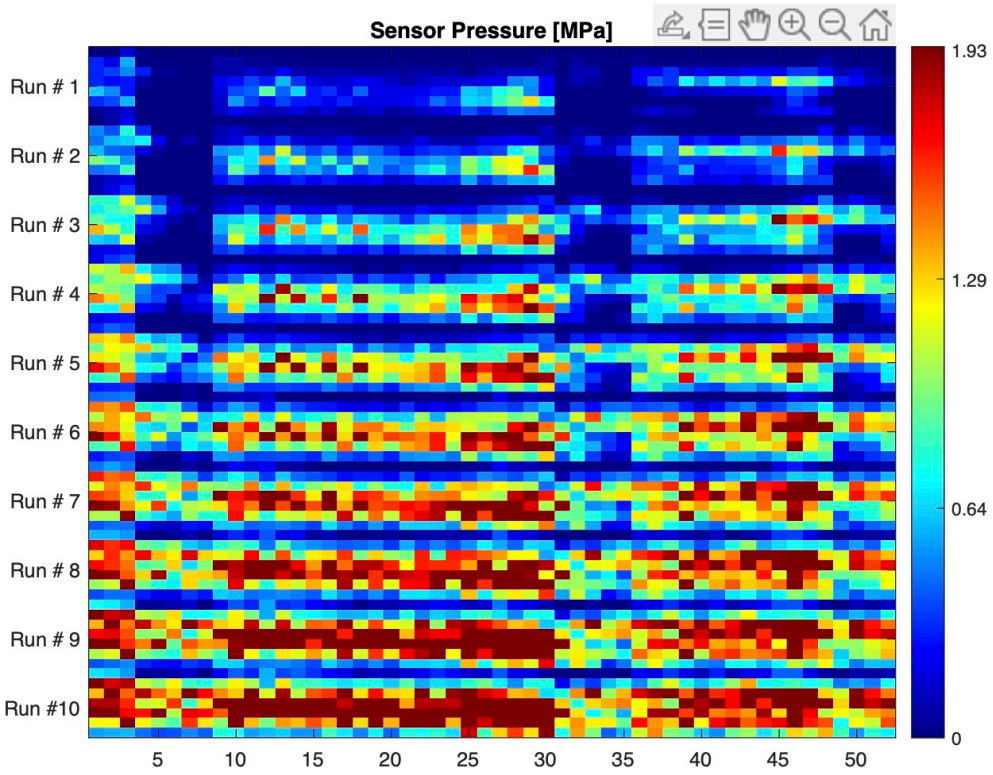

Figure B.5: Pressure distribution images from the seventh experiment. Plunge *EP 2021-04-26#012* is being tested without a transverse carton component at different expansion lengths. Starting with 5.5 mm, then increased with 0.5 mm for every run up to 9.5 mm.

C Appendix C

C.1 ANSYS Mechanical APDL Script for Computing Vertical Force Reaction

```
FINISH
/post1

! (s − select a new set) (NAME − name of component or assembly to be selected)
nsel,all
cmsel,s,bc_displacement

!select those elements connected to the selected nodes, 1=only elements with all nodes in the selected
set.
esln,s
nlist

*get,my_min_noden,node,,num,min
*get,my_SB,active,0,set,sbst !saving the number of substeps in quasi static tension test
*dim,RESULTS,TABLE,my_SB,3,,TIME !the table storing the results

!the loop for storing the _time_
*do,i,1,my_SB
set,2,i
*get,tt,active,0,set,time
RESULTS(i,1)=tt !saving the _time_ to the first column in the table
RESULTS(i,3)=UY(my_min_noden)
*enddo

!(nnum − the name of the resulting parameter) (ELEM − entity keyword) (0,count − number of nodes
in the selected set)
*get,my_nnum,node,0,count

*do,i,1,my_SB
    set,2,i !loadstep 2, substep i
    tsum=0.0
    tnoden=0
    *do,j,1,my_nnum
        tnoden=ndnext(tnoden)
        temp=0.0
        *get,temp,NODE,tnoden,rf,fy
        tsum=tsum + temp
    *enddo
```

```
      RESULTS(i,2)=tsum
*enddo

! write results to file
filen='..\..\freac'
filen=strcat(filen,chrval(tsum))
*cfopen,filen,'csv'
*vwrite,'Time', 'ForceY', 'DispY'
%C, %C, %C
*vwrite,RESULTS(1,1),RESULTS(1,2),RESULTS(1,3)
%G, %G, %G
*cfclos
```